

EXPERIMENTAL EVIDENCE FOR A C-PEPTIDE COMPLEX RECEPTOR ON RED
BLOOD CELLS

By

Morgan Geiger

A DISSERTATION

Submitted to
Michigan State University
in partial fulfillment of the requirements
for the degree of

Chemistry-Doctor of Philosophy

2021

ABSTRACT

EXPERIMENTAL EVIDENCE FOR A C-PEPTIDE COMPLEX RECEPTOR ON RED BLOOD CELLS

By

Morgan Geiger

Pancreatic β -cells secrete insulin and C-peptide, a 31-amino acid peptide, in a 1:1 mole ratio. People with type 1 diabetes (T1D) require exogenous insulin to survive due to damaged or destroyed β -cells. However, even with regular insulin treatments, patients develop complications such as retinopathy, neuropathy, and nephropathy, and it has been proposed that poor blood flow could be causing these complications. Prior research has shown that C-peptide increases microvascular blood flow, therefore, it could be a useful therapy to prevent these complications. The unknown C-peptide receptor and mechanism has been a major roadblock in utilizing C-peptide as a therapeutic. Our group has reported that approximately 1,800 C-peptide molecules bind per red blood cell (RBC) in the presence of albumin, while there was no detectable C-peptide binding per RBC without albumin. Thus, it is hypothesized here that C-peptide binds to RBCs through an albumin/C-peptide complex receptor, as opposed to binding to the RBC alone.

The work in this dissertation focuses on analyzing the binding of bovine serum albumin (BSA) to RBCs using a radiolabeling method to attach technetium-99m (Tc^{99m}) to BSA for gamma decay detection. A binding saturation experiment was conducted to examine the BSA specific binding to RBCs with and without C-peptide. The specific binding curves revealed that albumin saturates at 14,021 ($\pm 1,489$) BSA molecules/RBC with a K_d of $1.14 (\pm 0.07) \times 10^{-7}$ M. Whereas, in the presence of C-peptide and Zn^{2+} , albumin saturates at 16,695 ($\pm 1,479$) BSA molecules/RBC with a K_d of $2.00 (\pm 0.05) \times 10^{-7}$

M. At saturation, the additional 2,700 BSA molecules/RBC in the presence of C-peptide and Zn^{2+} indicates that not only does an albumin receptor exist on RBCs, but also a separate receptor for an albumin/C-peptide complex.

Due to its role in the delivery of C-peptide, the molecular state of albumin may be critical. Albumin is more glycated in individuals with T1D in comparison to healthy controls. This dissertation utilizes the radiolabeling saturation experiment to analyze the effects of glycation on BSA binding to RBCs. Varying percentage of glycation (11-48%) were analyzed with and without C-peptide and Zn^{2+} . As the glycation percentage increased, the number of BSA molecules binding per RBC increased; however, the difference between samples containing C-peptide to those without C-peptide decreased. In fact, at the higher glycation levels, there is more albumin binding in the absence of C-peptide. Importantly, the amount of RBC C-peptide uptake decreased when carried by glycated BSA compared to normal BSA.

Abnormal albumin delivery may not only be a determinant of disease in people with T1D. Albumin delivery of C-peptide was also examined in people with multiple sclerosis (MS, an autoimmune disease). When comparing BSA binding to MS RBCs to healthy control RBCs, more BSA molecules bound per MS RBC. Previous research in our lab has shown that MS RBCs binds more C-peptide and release higher concentrations of ATP than healthy controls. This suggests that in unhealthy conditions, the albumin/C-peptide/ Zn^{2+} complex is binding differently than in healthy conditions, which results in abnormal downstream effects.

ACKNOWLEDGMENTS

First, I would like to thank Michigan State University and the National Institutes of Health for the funding that made all this work possible. I would also like to thank my guidance committee, Dr. Liangliang Sun, Dr. Kurt Zinn, Dr. John Frost, and Dr. Karen Draths. Their questions and advice over the years helped to shape my research. In addition, I have really enjoyed my collaboration with Dr. Zinn on the radiolabeling projects. His unending willingness to help me learn and his true interest in my projects were extremely helpful and encouraging throughout my last several years.

My advisor, Dr. Dana Spence, has also been an important role in my accomplishments in graduate school. He created an environment where his students are treated as family and it is possible to maintain a balance between work and life. Not only did he always have his door open for research questions, but also for discussions about life and future goals. I believe that the overall environment of his lab is what allowed me to survive graduate school.

In addition, my time at MSU was made better by the past and present members of the Spence group who I consider all to be my friends. Dr. Cody Pinger played a key role in answering my questions about graduate school and eventually ended up encouraging me to enroll at the university. Not only was he helpful during the decision process, but also throughout my remaining years in graduate school, especially for the flow cytometry troubleshooting and the cell secretion/bead project. His expertise was missed after his graduation. I would also like to thank Dr. Suzanne Summers for her assistance with C-peptide data and her willingness to help. I am especially grateful for her attention to

detail throughout my dissertation editing process. All my commas in this dissertation would be messed up without her watchful eye. The glycated albumin data here would not have been possible without Monica Jacobs and her never ending dedication to her research. Taneisha Griggs and I began the albumin bead project during her summer program here, so I would like to thank her for her determination in starting the project. I would also like to thank all other current Spence lab members for their encouragement: Lisa Meints, Marcus Bunn, Nathan Redman, Amelie Moyna Lobel, Logan Soule, Lauren Skrajewski, and Stephen Branch. I would also like to thank the Zinn lab members for their willingness to share their lab space and instrumentation with me. Nate Kauffman was a huge help training me on the radiolabeling process.

I would also like to thank my undergraduate advisor, Dr. Tami Sivy, for her guidance and advice through my undergraduate honors thesis. She helped me to understand its ok if the project doesn't work right away, but to just keep trying. Her continuous support and willingness to help bettered me as a researcher and that drove me through graduate school. In addition, I would like to thank Dr. David Karpovich, without him I can truly say I would not be at MSU.

Finally, I would like to thank all of my friends and family for their continued love and support. My parents, Rob and Teresa, encouraged me from the beginning especially as I struggled through my second year. My nieces Olivia, Adelyn, and Charlotte were constant motivation to keep going and be a good role model. I would especially like to thank my friends Becca Boyea, Jessica Betz, and Katarina Keel. Without their open ears and friendship, I would not have made it this far. My husband, Travis, was my rock throughout this process as he listened to my concerns and never doubted me. He was

especially great during my second year when he helped with whatever he could to keep me going. Lastly, I would like to thank my fur babies, Barry and Thea. Their smiles and love brought me so much joy over my last two years of graduate school. All praise be to God.

TABLE OF CONTENTS

LIST OF TABLES.....	xi
LIST OF FIGURES.....	xii
Chapter 1- Introduction.....	1
1.1 Diabetes Mellitus	1
1.2 Diabetic Complications	2
1.3 Proinsulin	4
1.3.1 Insulin	7
1.3.2 C-peptide	9
1.4 Red Blood Cells	10
1.4.1 C-peptide and Red Blood Cells	12
1.4.2 C-peptide Receptor	15
1.5 Albumin, C-peptide, and Red Blood Cells.....	17
REFERENCES.....	21
Chapter 2- Albumin Binding to Red Blood Cells	30
2.1 Introduction.....	30
2.1.1 Background	30
2.1.2 An Introduction to Binding.....	31
2.1.3 Albumin Binding.....	33
2.1.4 Difference between Human Serum Albumin and Bovine Serum Albumin ..	34
2.2 Methods.....	36
2.2.1 Flow Cytometry Troubleshooting.....	36
2.2.2. Isolation and Purification of RBCs for BSA-FITC Samples.....	44
2.2.3. BSA-FITC Sample Preparation.....	45
2.2.4 Technetium Labeling of Albumin	46
2.2.4.a HYNIC Kit Preparation	47
2.2.4.b Tricine/Tin Kit Preparation.....	48
2.2.4.c BSA-HYNIC Conjugation.....	48
2.2.4.d SEC Preparation	49
2.2.4.e Lowry Assay.....	49
2.2.5 BSA- ^{99m} Tc Sample Preparation.....	50
2.2.5.a C-peptide Purification.....	52
2.2.6. BSA- ^{99m} Tc Gamma Counter Troubleshooting.....	53
2.2.7 BSA- ^{99m} Tc and C-peptide Binding	54
2.3 Results.....	56
2.3.1 PVDF Retention.....	56
2.3.2 BSA-FITC Equilibrium Dialysis	56
2.3.3 BSA-FITC/RBC Samples.....	57
2.3.4 BSA- ^{99m} Tc Binding to RBCs	59
2.3.5 BSA- ^{99m} Tc and C-peptide Binding to RBCs.....	60

2.3.6 BSA- ^{99m} Tc and C-peptide Binding	63
2.4 Discussion	64
REFERENCES.....	68
 Chapter 3- Binding of Albumin in Diseased States.....	 73
3.1. Introduction.....	73
3.1.1 Glycated Albumin in T1D	73
3.1.1.a Glycated Albumin Binding to Zn ²⁺ and C-peptide	75
3.1.2 Multiple Sclerosis.....	77
3.1.2.a Multiple Sclerosis Diagnosis.....	81
3.1.2.b Multiple Sclerosis Treatments	83
3.1.2.c Multiple Sclerosis and RBCs	84
3.2 Methods.....	85
3.2.1 BSA Enrichment	85
3.2.2 Bicinchoninic Acid Assay on Isolated BSA	86
3.2.3 Mass Spectrometry Identification of Isolated BSA	87
3.2.4 Isolation and Purification of RBCs for nBSA and gBSA Samples	87
3.2.5 nBSA and gBSA Sample Preparation.....	88
3.2.6 C-peptide Uptake on RBCs for nBSA and gBSA	89
3.2.7 MS Sample Preparation.....	89
3.3. Results.....	90
3.3.1 Mass Spectrometry Spectra for Isolated BSA.....	90
3.3.2 Binding of gBSA versus nBSA to RBCs.....	91
3.3.2.a Binding of gBSA at Varying Glycation Percentages	92
3.3.3 C-peptide Uptake to RBCs	96
3.3.4. Binding of BSA to MS RBCs.....	97
3.4. Discussion	99
REFERENCES.....	103
 Chapter 4- Albumin/C-peptide Receptor Isolation	 108
4.1 Introduction.....	108
4.1.1 Receptors	108
4.1.1.a G-Protein-Coupled Receptors	109
4.1.2 Receptor Identification Methods	112
4.1.2.a Co-immunoprecipitation	114
4.1.3 C-peptide Receptor	116
4.1.4 Insulin Secreting Cells	118
4.2 Methods.....	120
4.2.1 C-peptide Bead Preparation	120
4.2.2 ELISA on Prepared CC34 Beads	121
4.2.3 Dynamic Cell 3D-Printed Device	122
4.2.4 Troubleshooting of Beads on 3D-Printed Device.....	123
4.2.5 INS-1 Cell Growth.....	126
4.2.6 INS-1 Cell Secretion Collection	127
4.2.7 INS-1 Cell Secretions and CC34 Beads	128
4.2.8 Preparation of Carboxylic Acid Albumin Dynabeads®	130

4.2.9 Bicinchoninic Acid Assay: Measuring Albumin Total Concentration	132
4.2.10 BSA Bead Samples	133
4.2.11 Rat/Mouse C-peptide ELISA.....	133
4.3 Results.....	134
4.3.1 C-peptide binding to CC34 Beads	134
4.3.2 ELISA Analysis of the C-peptide in 3D-Printed Device/Beads.....	135
4.3.3 ELISA Analysis of INS-1 Cell Secretions and Beads.....	137
4.3.4 Carboxylic Acid Albumin Beads.....	142
4.4 Discussion	143
REFERENCES.....	147
Chapter 5- Conclusions and Future Directions.....	153
5.1 Conclusions	153
5.1.1 Albumin Binding to RBCs	154
5.1.2 Albumin Binding in Diseased States.....	155
5.1.3 Receptor Isolation.....	157
5.2 Future Studies on Albumin Beads for Receptor Identification.....	158
5.3 Future Studies on C-peptide Binding to RBCs.....	159
5.3.1 Fluorescent Tag.....	159
5.3.2 Radiolabeled C-peptide	161
5.4 GLUT1 Aggregation Studies.....	163
5.5 Future Albumin Binding Studies.....	165
REFERENCES.....	167

LIST OF TABLES

Table 2.1. C-peptide Purification HPLC Gradient Method. Solvent A: 0.1% HPLC-grade trifluoroacetic acid (TFA; EMD Millipore, Burlington, MA) in HPLC-grade water (Sigma Aldrich). Solvent B: 0.089% TFA/60% HPLC-grade acetonitrile (Sigma Aldrich) in HPLC-grade water. 52

Table 4.1: Sample Preparation of CC34 Beads and INS-1 Cell Secretions. The volumes of CC34 beads, 1,600 pM rat C-peptide stock, INS-1 cell secretions, and buffer added for the four samples used in this experiment. *Sample was volume adjusted in final calculation. 130

Table 4.2: Results for Static 3D-Printed Device Experiment. The concentrations of C-peptide (pM) in each of the three devices used: control beads, CC34 beads, and no beads. The C-peptide concentrations were reported for the membrane insert, the bead solution, and the buffer well. The total C-peptide concentration for the device was then calculated and compared to the added 1,600 pM C-peptide concentration. *The total C-peptide concentration was not able to be comparably calculated for device one since there was not any solution in the buffer well (n=1, error=standard deviation for ELISA well duplicates). 137

Table 5.1: Free ^{99m}Tc of SEC C-peptide fractions. A) TLC was used to determine the free ^{99m}Tc for fraction 4 and 5 of C-peptide-^{99m}Tc separated by SEC. B) Fraction 4 from A) was run back through the column to analyze whether additional free ^{99m}Tc could be removed. Fractions 4-6 from the second column were analyzed using TLC. All fractions were selected based on their activities determined by the dose calorimeter or gamma counter. 162

Table 5.2: Free ^{99m}Tc of SEC C-peptide fractions and HPLC collection. TLC was used to determine the free ^{99m}Tc for fractions 4-6 of C-peptide-^{99m}Tc separated by SEC, as well as the collection from HPLC. 163

LIST OF FIGURES

Figure 1.1: Healthy Eye Compared to an Eye with Retinopathy. Poor blood flow associated with diabetes results in damage to the blood vessels of the retina. As new weakened vessels grow, the vitreous becomes clouded resulting in poor eyesight or even blindness.	3
Figure 1.2: Proinsulin Cleavage. C-peptide allows for the interchain disulfide bridge formation of insulin. The peptide is then cleaved from insulin resulting in separate molecules that are secreted into the circulation in equimolar amounts.	5
Figure 1.3: C-peptide and Insulin Release from the Pancreatic β -cell. As blood glucose levels increase, glucose is transported into the β -cell through the GLUT2 transporter found on the membrane. Glucose undergoes glycolysis, and the ratio of ATP/ADP increases, resulting in the closing of the K_{ATP} channel. The channel closure depolarizes the cell to open the Ca^{2+} channel. The influx of Ca^{2+} results in the exocytosis of the granules and subsequent release of C-peptide, insulin, and Zn^{2+}	7
Figure 1.4: Red Blood Cell Receptors and Transporters. A depiction of an RBC with several known receptors/transporters and the proposed C-peptide/albumin complex receptor (in blue), which will be discussed in subsequent sections.	11
Figure 1.5: Release of ATP and Subsequent NO. Proposed mechanism of C-peptide/albumin complex binding to an RBC receptor. An intracellular signaling mechanism results in ATP release from the RBC, which binds to a P2Y receptor on the endothelial cell. ATP binding generates an intracellular signaling pathway that leads to the production of NO, which results in vasorelaxation in smooth muscle cells.	14
Figure 1.6: Human Serum Albumin Representations. A) Serum albumin, a globular protein, is shown with bound fatty acids in white and red. B) The structure of human serum albumin with Sudlow's Site I and II depicted in Subdomains IIA and IIIA, respectively. Images borrowed from Protein Data Bank and Chuang, V. & Otagiri, M.	18
Figure 2.1: Binding Representations. A. A binding curve representing the total binding, saturable specific binding, and linear nonspecific binding. B. A Scatchard plot demonstrating that the slope of bound/free ligand versus bound ligand is equal to the negative inverse of K_d and the x-intercept is equal to B_{max}	32
Figure 2.2: Crystal Structures of HSA and BSA. The differences in the tryptophan (Trp) residues, in green, between human and bovine serum albumin. Image borrowed from Belatik et al.	34
Figure 2.3: Comparison of BSA and HSA C-peptide Uptake. The C-peptide uptake to 7% RBCs in the presence of either BSA or HSA. $n=3$, error=SEM, $p=0.08$	35

Figure 2.4: Depiction of Flow Cytometry. An internal look at the sample entering the flow cytometer sample injection port before the cells are individually lined up to be analyzed by the laser. The highlighted box demonstrates the flow cell containing the sample core and sheath fluid as seen from above..... 37

Figure 2.5: Flow Cytometry Gating Steps. A. Gate depicting selected RBC population. B. Population from Gate A (P1) where only fluorescence above the blank was selected. C. The population in Gate B (P2 in P1) where the cell aggregates were deselected. D. The population from Gate C (P3 in (P2 in P1)) again selected for only fluorescence above the blank..... 39

Figure 2.6: Flow cytometry dot plots depicting the difference in background with and without filtering solutions prior to sample incubation. Prior to filtering the solutions (A), only 48.4% of particles were used, after filtering the solutions (B), 89.7% of the particles were used..... 40

Figure 2.7: Image of BD CS&T Beads Corrections. Adjustments were made to dim and mid+bright regions of the fluorescence plots. Once changes were made, a quality control report was generated to tell the user if FSC, SSC, and all detectors (FL1-FL4) passed parameter testing. 42

Figure 2.8: 3D-Printed Equilibrium Dialysis Device. BSA-FITC was placed in the sample compartment, and the free FITC traveled through the membrane to the buffer compartment for detection..... 44

Figure 2.9: Isolation of RBCs and Sample Preparation. Whole blood was drawn from consenting donors and centrifuged/washed to separate plasma, buffy coat, and RBCs. Samples were prepared with isolated RBCs, BSA-^{99m}Tc, PSS, Zn²⁺, and C-peptide before a 2 h incubation at 37 °C. Samples were centrifuged, the supernatant was removed, and cells were washed with AF-PSS five times before the gamma decay was detected on the gamma counter. 51

Figure 2.10: Ultrafiltration Device Manufacturing. A representation of the 3D-printed device used to separate the free C-peptide from C-peptide bound to BSA-^{99m}Tc. Figure adapted from Jacobs et al. 55

Figure 2.11: BSA molecules bound per RBC in response to BSA molecules added per RBC sample. A. The binding of BSA-FITC to RBC without IgG. B. The binding of BSA-FITC to RBC with IgG to act as a blocking agent. n=4, error=SEM. 58

Figure 2.12: Increasing BSA-FITC Concentrations added to RBCs. Relative fluorescence units (RFU) as a function of increasing BSA-FITC concentrations (μM) added to RBC samples. An equation is displayed with a trendline fitted to the points. n=4, error=SEM. 59

Figure 2.13: BSA-^{99m}Tc binding to RBCs. A saturation experiment conducted to determine the specific binding of BSA (circle) to RBCs. This was completed by preparing two sample types of BSA-^{99m}Tc with RBCs and subtracting the resulting data. One sample set was

prepared in AF-PSS to represent total binding (triangle), and the other sample set was prepared in PSS so the excess unlabeled BSA could act as a blocking agent to demonstrate nonspecific binding (square). n=6, error=SEM. 60

Figure 2.14: BSA-^{99m}Tc binding to RBCs with C-peptide and Zn²⁺. A saturation experiment conducted to determine the specific binding of BSA (circle) to RBC in the presence of C-peptide and Zn²⁺. This was completed by preparing two sample types of BSA-^{99m}Tc with RBCs and subtracting the resulting data. One sample set was prepared in AF-PSS to represent total binding (triangle), and the other sample set was prepared in PSS so the excess unlabeled BSA could act as a blocking agent to demonstrate nonspecific binding (square). n≥4, error=SEM..... 61

Figure 2.15: Specific Binding of BSA-^{99m}Tc to RBCs with and without C-peptide and Zn²⁺. The specific binding of BSA without C-peptide or Zn²⁺ (black) in comparison to the specific binding of BSA with C-peptide and Zn²⁺ (white) extracted from Figures 2.13 and 2.14. n≥4, error=SEM, *p<0.05. 62

Figure 2.16: Specific Binding of BSA-^{99m}Tc to RBCs with or without C-peptide on the same donor RBCs. The specific binding of BSA without C-peptide (grey) in comparison to the specific binding of BSA with C-peptide (black). This experimental set up was conducted on the same day to compare the difference in BSA binding on the same donor cells. The albumin binding difference between with and without C-peptide is significantly different than zero (p<0.01). n=5, error=SEM.4 63

Figure 2.17: The binding of C-peptide to BSA-^{99m}Tc and BSA. A bar graph representing the binding of C-peptide to labeled (^{99m}Tc) and unlabeled BSA. BSA-^{99m}Tc bound 18.8 (±0.3) nM C-peptide with nK_a'=4.56 (±1.04) x 10⁶ M⁻¹, whereas BSA bound 19.3 (±0.2) nM with nK_a'= 6.25 (±1.08) x 10⁶ M⁻¹. Values demonstrated no significant difference. n=6, error=SEM, p>0.1..... 64

Figure 3.1: The Maillard Reaction. The mechanism of albumin glycation showing the Schiff base and Amadori product intermediates and the final advanced glycated end product (AGE). 73

Figure 3.2: Normal or Glycated Albumin Binding to Zn²⁺. The percentage of free Zn²⁺ was analyzed for normal HSA (n=3), normal HSA in a glucose environment (n=5), and glycated HSA (n=5). The gHSA sample was statistically higher than nHSA. *p<0.05, error=standard deviation. Image borrowed from Pinger, C., 2018..... 75

Figure 3.3: Normal or Glycated Albumin Binding to C-peptide. The percentage of free C-peptide was analyzed for normal HSA and glycated HSA. There was not a statistical difference. n=3, error=standard deviation. Image borrowed from Pinger, C., 2018..... 77

Figure 3.4: Depiction of a neuron. The neuron consists of the cell body, axon, myelin sheath, and axon terminal. In MS, demyelination (damage to the myelin sheath) occurs. 79

Figure 3.5: Four Types of Multiple Sclerosis. RRMS is characterized by attacks and periods of remission. SPMS is similar to RRMS but becomes a gradual deterioration without attacks. PPMS is characterized by steady deterioration without attacks. PRMS is characterized by steady deterioration with attacks. 81

Figure 3.6: MS Lesion Change. The change in MS lesions over time can be viewed using the subtraction method. A. Baseline MRI scan. B. Follow-up MRI scan after 3 years with new lesion formation (arrow). C. Subtraction of image A from image B to demonstrate lesion formation (arrow). Image borrowed from Bakshi et al. 83

Figure 3.7: Control versus MS RBC ATP Release. ATP released from control RBCs (black bar) was 138 (± 21) nM ATP. ATP released from MS RBCs (grey bar) was 375 (± 51) nM ATP. $n \geq 11$, error=SEM. Figure borrowed from Letourneau et al. 85

Figure 3.8: Mass Spectra of nBSA and gBSA. The spectra of isolated nBSA and gBSA with insets demonstrating percent glucose (Glc; +162 Da), cysteine (Cys; +119 Da), sodium (Na; +23 Da), acetonitrile (A; +41 Da), and normal (Norm). On this day, the nBSA was 13% glycosylated, and the gBSA was 47% glycosylated. 91

Figure 3.9: Binding of nBSA and gBSA to RBC. The binding of normal BSA (11%; triangles) and glycosylated BSA (48%; circles) to RBCs in the presence of C-peptide and Zn^{2+} . $n \geq 4$, error=SEM, * $p < 0.05$, ** $p = 0.05$ 92

Figure 3.10: Binding of >45% Glycosylated BSA to RBC. The binding of gBSA to RBCs with (48%; closed circles) and without (45%; open circles) C-peptide and Zn^{2+} . $n = 4$, error=SEM, * $p < 0.05$, ** $p = 0.05$ 93

Figure 3.11: Binding of 23% Glycosylated BSA to RBC. The binding of gBSA to RBCs with (closed circles) and without (open circles) C-peptide and Zn^{2+} . There is no significant difference between the two curves ($p > 0.25$). $n = 4$, error=SEM. 94

Figure 3.12: Binding of 17% Glycosylated BSA to RBC. The binding of gBSA to RBCs with (closed circles) and without (open circles) C-peptide and Zn^{2+} . $n = 4$, error=SEM, * $p < 0.05$ 95

Figure 3.13: Binding of BSA to RBC at Varying Glycosylation Percentages. A) The specific binding of BSA to RBCs with (dark grey) and without (white) C-peptide and Zn^{2+} at saturation. Shown here are 11, 14, 17, 23, 45, and 48% glycosylation. $n \geq 4$, error=SEM. B) The difference in BSA binding to RBCs with or without C-peptide and Zn^{2+} . BSA molecules/RBC bound values for data without C-peptide and Zn^{2+} was subtracted from BSA molecules/RBC bound values for data with C-peptide and Zn^{2+} . Values are at saturation and represent approximate differences. $n \geq 4$ 96

Figure 3.14: RBC C-peptide Uptake with nBSA or gBSA. The uptake of C-peptide (in nM) by RBC in the presence of Zn^{2+} and nBSA (12% glycosylation; dark grey bar) or gBSA (46% glycosylation; light grey bar). There is significantly less RBC C-peptide uptake when carried by gBSA compared to nBSA. $n = 4$, error=SEM, * $p < 0.05$ 97

Figure 3.15: Binding of nBSA to MS RBCs. The binding of nBSA to RBCs from patients with MS with (closed circles) and without (open circles) C-peptide and Zn²⁺. n=3 (except n=2 for the fourth point at 255,935 BSA molecules/RBC Added without C-peptide and Zn²⁺), error=SEM. 98

Figure 3.16: Binding of nBSA to MS and Control RBCs. The binding of nBSA to RBCs from patients with MS (red circles) compared to control RBCs (black triangles) when C-peptide and Zn²⁺ were present. n≥3, error=SEM, *p<0.05. 99

Figure 4.1: G-Protein Activation. Ligand binding to a GPCR results in a conformation change that allows it to bind to the GDP bound Gα subunit. The Gα subunit releases GDP and binds to GTP, resulting in separate activated Gα and Gβγ subunits that cause subsequent signaling mechanisms. (Adapted from Alberts et al.) 110

Figure 4.2: Co-immunoprecipitation Procedure. Antibody bound beads are added to a protein solution, and after an incubation period, the beads are pulled down (through centrifugation or magnetic interactions) to remove the proteins that are specific to the antibodies on the beads. 115

Figure 4.3: 3D-Printed Dynamic Cell Device. An image of the 3D-printed dynamic cell device from the .stl file. Outer circles are for peristaltic pump tubing connection. Inner circles were covered with membranes, and membrane inserts were placed in the wells. 123

Figure 4.4: Priming Set-Up for the Dynamic Cell 3D-Printed Device. The tubing connected to the first pump (light grey) introduced PBS into the device. The tubing connected to the second pump (dark grey) removed the PBS from the device and out to waste. This set-up was maintained until the system was purged, and the device could be set up in a continuous flow without the PBS or waste tubes. 125

Figure 4.5: Carboxylic Acid Bead Interaction with Albumin. The carboxylic acid bead is linked to the primary amine of albumin (BSA) through an EDC crosslinker. 131

Figure 4.6: Free C-peptide in CC34 Bead Supernatant. The striped bar represents C-peptide stock without beads, while the grey bar represents C-peptide stock with CC34 beads. This indicates that the CC34 beads were successful in binding to the rat C-peptide stock. (n≥2 (ELISA duplicate), error=standard deviation, *p<0.05). 135

Figure 4.7: Increasing CC34 Bead Volumes in INS-1 Cell Secretions. The striped bar represents the C-peptide concentration in the diluted cell secretions without beads, while the grey bars represent the free C-peptide concentrations from cell secretions with CC34 beads (n≥2 (ELISA duplicate), error=standard deviation, #p>0.05). 139

Figure 4.8: The Comparison of CC34 Beads in Storage Buffer or PBS with Cell Secretions. The C-peptide concentration of the control sample (striped), which consisted of INS-1 cell secretions and PBS without beads. The grey bars represent the free C-peptide concentration from the CC34 beads, in either PBS/Tween®-20/PBS or PBS, with INS-1 cell secretions (n≥2 (ELISA duplicate), error=standard deviation, #p=0.29). 140

Figure 4.9: BSA Concentration during Bead Preparation. The difference between the concentration of BSA added to the beads and the concentration of BSA found in the supernatant after bead coupling (n=1 stock, n=2 supernatant, error=standard deviation). 142

Figure 4.10: C-peptide Concentrations after BSA Bead Interaction. A) The comparison of the control (without BSA beads) and the sample (with BSA beads) at higher C-peptide stock concentrations (n=2, error=standard deviation, p>0.05). B) The repetition of the experiment in figure A, but with a diluted C-peptide stock (n=1). 143

Figure 4.11: 3D-Printed y-shaped Microfluidic Device. A) Micro-CT (X-ray imaging technique) image of the y-shaped device to visualize the device channel (PerkinElmer QuantumGX micro-CT, Waltham, MA). B) An image of the device showing the buffer inlet, RBC inlet that contains a 75 μm inner diameter silica capillary to mimic RBC shear stress in microvascular blood vessels, and the outlet. The flowing of 7% RBC in buffer mixing with a flowing reagent solution (luciferin/luciferase). The luciferin/luciferase reacts with RBC-derived ATP to produce a chemiluminescent signal that is detected through a PMT in a black-box. 145

Figure 5.1: Total binding of C-peptide-FITC molecules bound per RBC. C-peptide-FITC was added to albumin containing RBC samples and analyzed using flow cytometry. The number of bound C-peptide molecules/RBC was then calculated..... 160

Figure 5.2: GLUT Imaging on CHO Cells. The clustering of GLUT1 (labeled with eGFP) and GLUT4 (labeled with mCherry) on CHO cells prior to the addition of albumin, C-peptide, and Zn²⁺. Picture from Geiger et al. 164

Chapter 1- Introduction

1.1 Diabetes Mellitus

In 2018, diabetes was listed as the seventh leading cause of death in the United States and costs the United States \$327 billion in healthcare costs in 2017.^{1,2} The Centers for Disease Control and Prevention (CDC) reported that 34.2 million people, or 10.2% of the U.S. population, have diabetes.³ Of these 34.2 million, 7.3 million adults have diabetes, but are undiagnosed.³ This number continues to increase, as every 21 seconds an adult in the United States is diagnosed with diabetes.⁴ Overall, the number of patients with diabetes is expected to nearly double by 2030, in comparison to 2008.⁵ In addition, an estimated 88 million adults in the United States have prediabetes.³

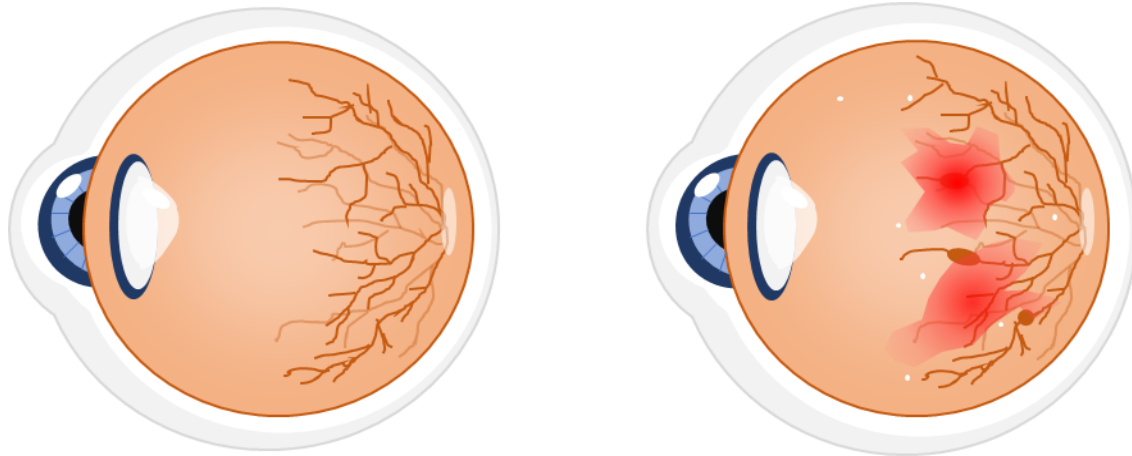
Diabetes is characterized by chronic hyperglycemia, or high blood glucose levels.⁵ There are two main types of diabetes, namely type 1 and type 2. If hyperglycemia is caused by an insulin deficiency this is considered type 1 diabetes (T1D), whereas type 2 diabetes (T2D) is caused by an insulin resistance, or insulin not effectively working in the body.⁵ T1D is caused by insulin deficiency because the pancreas either lacks or has defective pancreatic β -cells, therefore, patients are not producing insulin.⁶ In these cases, β -cells are thought to have been destroyed by an autoimmune response.⁶ T2D is considered a result of insulin resistance because the body still produces insulin; however, cells do not respond to the hormone.⁶ Of the 34.2 million people with diabetes, 5% of cases are T1D.³ This type requires an injection of exogenous insulin to maintain healthy blood glucose levels. After fasting, a healthy individual will have a blood glucose level less than 5.5 mM, whereas a person with diabetes will have blood glucose levels higher

than 7.0 mM.⁷ Other types of diabetes include gestational diabetes, maturity-onset diabetes of the young (MODY), type A insulin resistance, and drug/chemical induced diabetes.⁶

1.2 Diabetic Complications

Even with treatment to control blood glucose levels, patients with diabetes develop a variety of such complications as retinopathy, neuropathy, nephropathy, and cardiovascular disease.⁵ These organs and tissues, including kidneys, eyes, and nerves, are most vulnerable to complications because they lack the ability to autoregulate the excess glucose uptake.⁸ The Diabetes Control and Complications Trial (DCCT) found that for patients who received normal therapy for diabetes, the incidence of complications in patients after 30 years was still 50% for retinopathy, 25% for nephropathy, and 14% for cardiovascular disease.⁹ These data suggest there are other factors when treating diabetic complications than just the normal therapy for diabetes (controlled glucose levels). A possible associated factor may be microvascular blood flow dilemmas, which are common in chronic diabetic complications.⁵

The most common microvascular complication of diabetes is retinopathy.¹⁰ Overall, one of the major causes of visual impairment is diabetic retinopathy.^{11,12} Blood vessels within the retina of a patient with diabetes are damaged, and the oxygen supply is impaired as shown in Figure 1.1.^{10,11} As a result, a vascular endothelial growth factor mechanism will cause the retinal cells to form new vessels (in a process called angiogenesis), that are malformed, leading to clouding of the vitreous.^{10,13–15} It is the clouding of the vitreous that often leads to increased visual impairment.



Healthy Eye

Retinopathy Eye

Figure 1.1: Healthy Eye Compared to an Eye with Retinopathy. Poor blood flow associated with diabetes results in damage to the blood vessels of the retina. As new weakened vessels grow, the vitreous becomes clouded resulting in poor eyesight or even blindness.

In the kidney, required substances are returned to the vasculature through the tubule, while waste is removed through urine, and the glomerular basement membrane separates the urinary space from the vasculature to maintain the filtration barrier.^{16,17} In nephropathy, the tubules and glomerular basement membrane are affected.^{5,18,19} The glomerular filtration rate (GFR) initially increases on average 40% above normal.^{15,20} As GFR decreases, proteinuria (increased protein levels in urine) develops, and blood hydrostatic pressure increases due to the lower osmotic pressure.^{18,20-23} High blood pressure results in artery damage that affects artery elasticity, which decreases blood flow.²⁴ Eventually this GFR decrease results in uremia (or increased levels of urea and waste products in the blood), which is fatal if left untreated.^{18,20} Nephropathy is a major cause of end-stage renal failure.^{5,25}

Neuropathy, a result of nerve damage, is caused by poor blood flow that results in endoneurial hypoxia.²⁶ Endoneurial blood flow is reduced due to the impairment of endothelial nitric oxide synthase (eNOS) and decreased levels of nitric oxide (NO), which results in the reduction of acute nerve conduction.^{27,28} Hypoxia-inducible factor 1 (HIF-1) is responsible for regulating the hypoxia responses throughout the body.²⁹ However, HIF-1 activation is impaired in diabetes.²⁹ More than half of patients with diabetes develop neuropathy and a 15% risk of a lower extremity amputation.⁵ I hypothesize that improving blood flow will decrease these diabetes complications.

1.3 Proinsulin

The islets of Langerhans are cell clusters within the pancreas that produce and release hormones related to glucose level regulation.³⁰ One example of such cell clusters are β -cells, which are responsible for the production and release of insulin and C-peptide.³⁰ Proinsulin, consisting of C-peptide and insulin, assembles within the endoplasmic reticulum.^{31,32} C-peptide links insulin, which allows for protein folding for the formation of disulfide bonds between the A and B chains of insulin.^{31,33} C-peptide connects to the N-terminus of the insulin A chain and the C-terminus of the insulin B chain as shown in Figure 1.2.³² The N and C terminal helices of the A chain form 2 disulfide bonds with the central helix of the B chain.³² Proinsulin moves to the β -cell Golgi region to initiate cleavage to form insulin and C-peptide.^{31,34} There are 2 Ca^{2+} -dependent endopeptidases that can cleave proinsulin into insulin.³⁵ The optimum pH for both type 1 and type 2 endopeptidase is ~ 5.5 , which corresponds with the pH inside of the β -cell granule.³⁵ Type 1 and type 2 endopeptidases are prohormone convertases, PC2 and PC1/3, that cleave paired basic amino acid sequences, specifically, Lys-Arg at the

A-chain junction and Arg-Arg at the B-chain junction.^{31,34} Cleavage ensues by the removal of the C-terminal basic amino acids exposed by the endopeptidases through carboxypeptidase-E.³¹ Insulin and soluble C-peptide are then stored within the β -cell granules until release.³¹ Insulin is stored in a crystalline hexamer unit with two Zn^{2+} ions and is insoluble below pH 7.0.^{36,37} Therefore, the slightly acidic pH (5.5) inside of the β -cell granule helps maintain the packing and storage of insulin in association with Zn^{2+} .^{36,37} At the acidic pH of the granule, C-peptide is protonated and does not bind to Zn^{2+} .³⁸

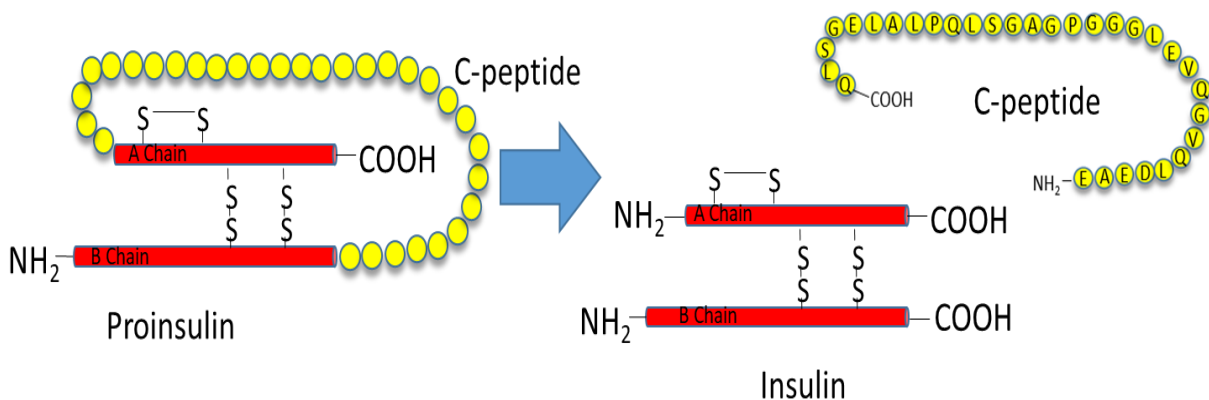


Figure 1.2: Proinsulin Cleavage. C-peptide allows for the interchain disulfide bridge formation of insulin. The peptide is then cleaved from insulin resulting in separate molecules that are secreted into the circulation in equimolar amounts.

At resting state, the low glucose concentration results in low levels of adenosine triphosphate (ATP) within the β -cell.³⁹ As a result, the K_{ATP} channel remains open and the cell membrane is hyperpolarized, which keeps the Ca^{2+} channel closed and prevents insulin release.³⁹ After consumption, blood glucose levels rise and glucose enters the pancreatic β -cell through the glucose transporter found on the β -cell, GLUT2, as shown in Figure 1.3.³⁹ This process occurs when blood glucose approach and exceed values higher than 7 mM.⁴⁰ Through glycolysis, ATP is formed and the ratio of ATP to adenosine

diphosphate (ADP) increases, which blocks K^+ efflux through the K_{ATP} channel.³⁹ The closed channel results in a depolarization of the β -cell, which opens the voltage-gated Ca^{2+} channel.³⁹ The opening of the channel results in an influx of Ca^{2+} , and subsequent exocytosis of insulin secretory granules.³⁹ The granules contain C-peptide, as well as the hexamers containing insulin and Zn^{2+} that were discussed above.³² The granules fuse to the plasma membrane, which opens the granule interior to the extracellular space.³⁹ Insulin and C-peptide are released from the β -cell into the bloodstream in equimolar amounts. Once the granule is exposed to the slightly basic pH of the circulation (7.4), Zn^{2+} and insulin dissociate in less than 40 ms.³⁶

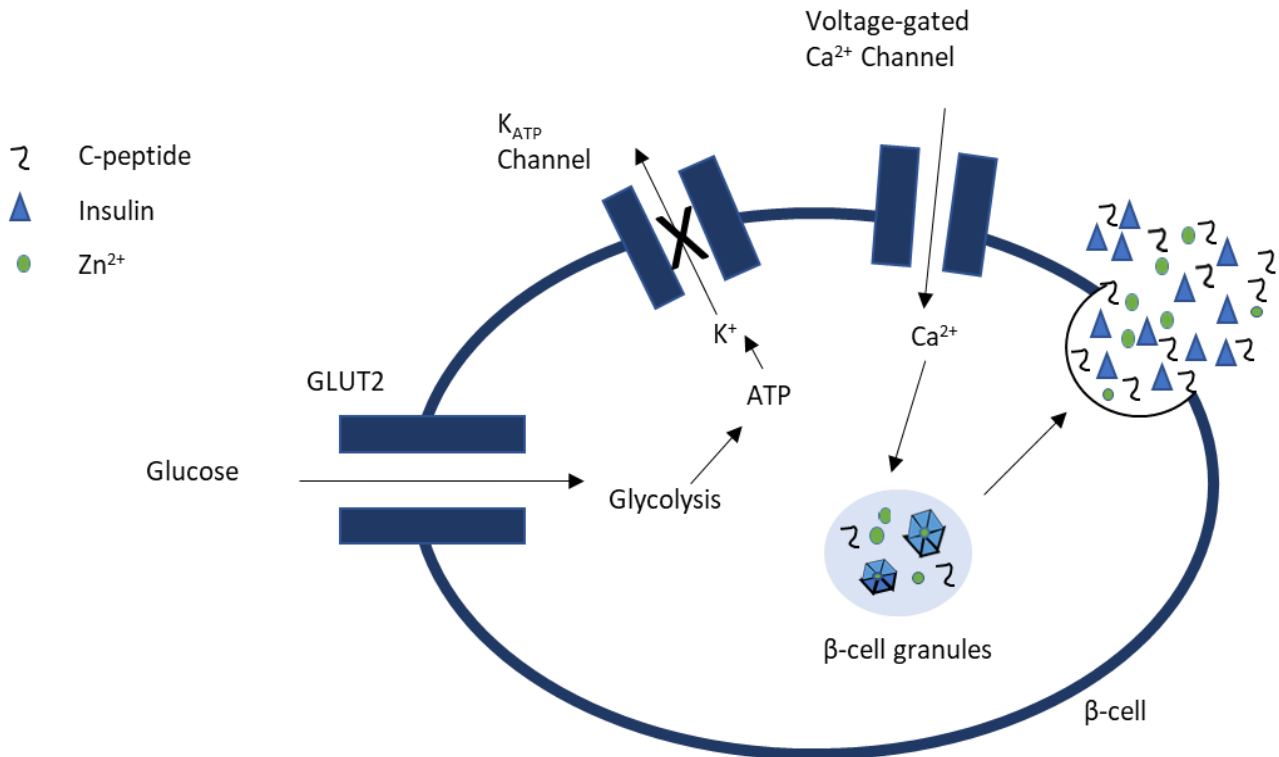


Figure 1.3: C-peptide and Insulin Release from the Pancreatic β -cell. As blood glucose levels increase, glucose is transported into the β -cell through the GLUT2 transporter found on the membrane. Glucose undergoes glycolysis, and the ratio of ATP/ADP increases, resulting in the closing of the K_{ATP} channel. The channel closure depolarizes the cell to open the Ca^{2+} channel. The influx of Ca^{2+} results in the exocytosis of the granules and subsequent release of C-peptide, insulin, and Zn^{2+} .

1.3.1 Insulin

Insulin is a 5,802 Da hormone consisting of 51 amino acids, where the A chain consists of 21 amino acids, and the B chain consists of 30 amino acids.³² For the first two decades of the 20th century, several groups attempted to extract molecules from the pancreas.⁴¹ Studies of the pancreatic extracts were successful in lowering blood sugar concentrations in animals; however, due to the impurities and toxic reactions, the extracts were not used in humans with diabetes.⁴¹ In 1921, Frederick G. Banting and Charles Best were given laboratory space by J.J.R. Macleod to investigate why previous pancreatic

extractions were unsuccessful.⁴¹ Banting and Best were successful in extracting insulin from the pancreas.⁴¹ Insulin was injected into the first patient on January 11, 1922.⁴¹ This patient was Leonard Thompson, who even at 14 years old, only weighed 65 pounds when admitted the previous month.⁴¹ However, slight impurities resulted in an abscess at the injection site. Even though his blood sugar levels decreased, it was not considered significant enough to continue the injections. On January 23, 1922, Thompson received another dose, but this time with insulin purified by J.B. Collip using 90% alcohol.⁴¹ This was the first visibly successful clinical test for diabetes, as Thompson's blood glucose levels significantly decreased, he felt better, become more active, and his overall appearance improved. By June 1922, the Eli Lilly company began to work on insulin production, and as early as August, shipments were being sent to hospitals.⁴¹

Over the next few decades, research focused mainly on discovering insulin's cellular mechanisms. The insulin receptor, a receptor tyrosine kinase, was characterized in 1971.^{32,42} Upon entering the bloodstream from the pancreatic β -cell, 60% of insulin is removed by the liver.³² The remaining insulin travels to insulin receptors found on such GLUT4 containing cells as adipocytes and myocytes, to increase glucose uptake and decrease blood glucose levels.⁴³ The half-life of insulin in the bloodstream is shorter than C-peptide, 3 minutes versus 30 minutes, because of the insulin receptor-mediated uptake that results in lysosomal degradation.^{31,34} While insulin functions to facilitate glucose uptake into GLUT4 containing cells, the function of C-peptide after secretion is not fully understood.

1.3.2 C-peptide

In 1967, Don Steiner and Philip Oyer discovered a polypeptide between the chains of insulin.^{44,45} The following year, Chance et al. was able to isolate and characterize a connecting peptide, which confirmed Steiner's findings.^{45,46} Human C-peptide has a molecular mass of 3,020 Da and consists of 31 amino acids, with five acidic residues, but no basic or aromatic amino acids.^{31,47} This results in a negatively charged peptide with a hydrophilic nature.⁸ The glycine-rich central region of C-peptide is hypothesized to allow flexibility for bending in a hairpin structure when connected to the insulin chains in proinsulin.³¹

C-peptide has long been considered, by most scientists, to be an inactive biological molecule.^{48,49} However, a surge of reports in the early 1990s stimulated a renewed interest in C-peptide as a possible missing component alongside insulin replacement therapy. Numerous reports describe beneficial effects of exogenous C-peptide replacement therapy in studies using rat models of T1D and in humans with T1D.⁵⁰⁻⁵⁹ There are also many reports involving C-peptide's beneficial effects on cells, *in vitro*.^{8,25,60-65} The last five amino acids on the C-terminus (residues EGSLQ) are thought to be important for membrane interactions and signaling.³³ This region demonstrated 75% of C-peptide's activity and is strictly conserved among mammals.^{33,66} Position 27, a glutamic acid residue, is required for C-peptide interaction with cells. When E27 was mutated to alanine, its ability to bind albumin was nonexistent.¹³ Due to C-peptide's longer half-life, C-peptide concentrations in the bloodstream are greater than those of insulin.⁶⁷ The life-span of C-peptide is 30 minutes in circulation and the physiological concentration is 0.6 nM.^{31,61} Therefore, C-peptide is a useful tool to monitor the course of diabetes.⁶⁸

1.4 Red Blood Cells

On average, a healthy adult has 5 L of whole blood in their body, which is composed of red blood cells (RBCs, 45%), plasma (55%), white blood cells, and platelets.⁶⁹ RBCs average 8.0 μm in diameter and 83 fL in volume.⁷⁰ RBCs lack a nucleus and internal organelles, which provides additional space for hemoglobin within the cell.⁶⁹ Hemoglobin, an iron-containing protein, is responsible for binding and releasing of carbon dioxide and oxygen.⁷¹ The spectrin membrane skeleton provides the cell with its elasticity and flexibility.⁷¹ The deformability of the biconcave shaped cell allows it to squeeze into small capillaries to transport and exchange gases throughout the body.^{72,73} RBCs have a life span of approximately 120 days and worn cells are removed from the vascular system by macrophages.^{69,71} Due to the short life span, cells are constantly replaced by bone marrow through a process called hematopoiesis or more specifically, when referring to RBCs, erythropoiesis.⁶⁹

The RBCs' membranes act as their load-bearing component due to the lack of organelles.⁷² The membrane consists of lipids and proteins arranged as a lipid bilayer with proteins attached or penetrating.⁷² Overall, the cell membrane proteins are hydrophobic.⁷² Palma et al. identified 275 proteins in an RBC and upon determining localization, 29% of these were membrane proteins and 20% were from the cytoskeleton.⁷² However, Pasini et al. detected 340 membrane proteins.⁷⁴ Kakhniashvili et al. identified 181 RBC proteins, of which 91 were membrane proteins and 43 were unidentified proteins.⁷¹ These studies demonstrate that the RBC membrane is composed of several proteins, which have not been agreed upon.

The many membrane proteins also consist of receptors and transporters found on the RBC as shown in Figure 1.4. Examples of these include band 3 for anion exchange, aquaporin 1 for water transport, Kidd antigen protein for urea transport, β -adrenergic to bind epinephrine and norepinephrine, Rhesus-associated glycoprotein (RhAG) for carbon dioxide transport, cystic fibrosis transmembrane conductance regulator (CFTR) for anion import, and pannexin 1 for ATP release.^{75–80} Glucose transporter, GLUT1, makes up 10% of the total integral membrane protein.⁴³ This correlates to more than 200,000 GLUT1 molecules per RBC.⁸¹ The large number of GLUT1 molecules, along with the high affinity for glucose, maximizes the uptake of glucose into the cell.^{43,82}

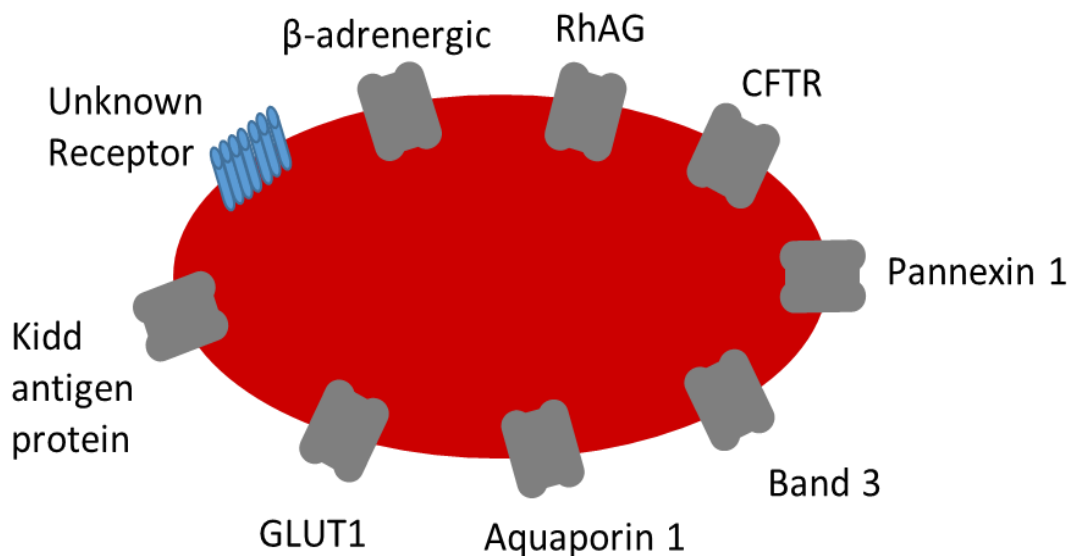


Figure 1.4: Red Blood Cell Receptors and Transporters. A depiction of an RBC with several known receptors/transporters and the proposed C-peptide/albumin complex receptor (in blue), which will be discussed in subsequent sections.

1.4.1 C-peptide and Red Blood Cells

C-peptide specifically binds to fibroblasts, venous endothelial cells, and human renal tubular cells, and the Spence lab found that C-peptide binds specifically to RBCs saturating at approximately 2 picomoles, corresponding to 1,800 molecules of C-peptide per cell.^{13,83} All binding sites are expected to be occupied at physiological concentrations of C-peptide, therefore, healthy patients do not experience a response after C-peptide administration.⁶⁸

People with T1D that have low, but present, C-peptide plasma concentrations are less prone to develop long term complications than those who are completely C-peptide deficient.^{50,66} Our group's research, as well as others, has shown that C-peptide improves the ability of RBCs to release ATP, which stimulates the vessel dilator nitric oxide (NO) in the bloodstream.^{27,80,84} This is believed to improve blood flow, thus decreasing diabetic complication severity.

It was originally believed that C-peptide required a metal to interact with RBCs since an RBC-derived ATP increase did not occur solely with C-peptide, but required a metal.⁸⁵ In literature, C-peptide is prepared in different purities for experiments, and many groups undervalue the importance of a 2% impurity.⁸⁶ Pinger et al. discussed that even at 98% purity, the C-peptide is contaminated with a 1:1 ratio of Fe²⁺. This contaminant led to the belief that C-peptide activity only occurred when Cr³⁺ or Fe²⁺ were present.⁸⁵ Due to its presence in the pancreatic β -cell granules, Zn²⁺ was suggested as a possibility for cellular activity.¹³ It was found that C-peptide binds to RBCs with or without Zn²⁺, however, Zn²⁺ does not bind to RBCs without C-peptide.¹³ Additionally, previous data do not show

any specific binding between C-peptide and Zn^{2+} .¹³ Therefore, it was determined that C-peptide does not require a metal to interact with RBCs.

RBCs incubated with albumin, C-peptide, and Zn^{2+} resulted in significantly higher ATP release (319.8 (\pm 15.2) nM) than cells without C-peptide or Zn^{2+} ((194.9 (\pm 19.7) nM, $p < 0.005$).¹³ An increase in ATP release required the addition of Zn^{2+} to the RBCs along with C-peptide.³⁸ Also, Zn^{2+} without C-peptide did not exhibit any biological effects.³⁸ Samples that contained C-peptide and Zn^{2+} but lacked albumin did not show a significant increase in ATP release.¹³ Sprague et al. showed that the ATP release from RBCs is dependent on the Zn^{2+} and C-peptide ratio for samples incubated with C-peptide and insulin.^{62,67,84}

It is suggested that C-peptide binding to RBCs results in the activation of heterotrimeric G protein (G_s), which triggers adenylyl cyclase (AC) to produce cyclic adenosine monophosphate (cAMP), that phosphorylates and thus activates phosphokinase A (PKA) as shown in Figure 1.5. PKA activation results in the opening of the CFTR, which allows for the import of anions.⁸⁰ This influx of anions allows for the maintenance of RBC ionic balance when ATP is released through Pannexin 1.⁸⁰ C-peptide binding to RBCs also results in an increase of glucose uptake, thus an increase in ATP release.⁶⁸

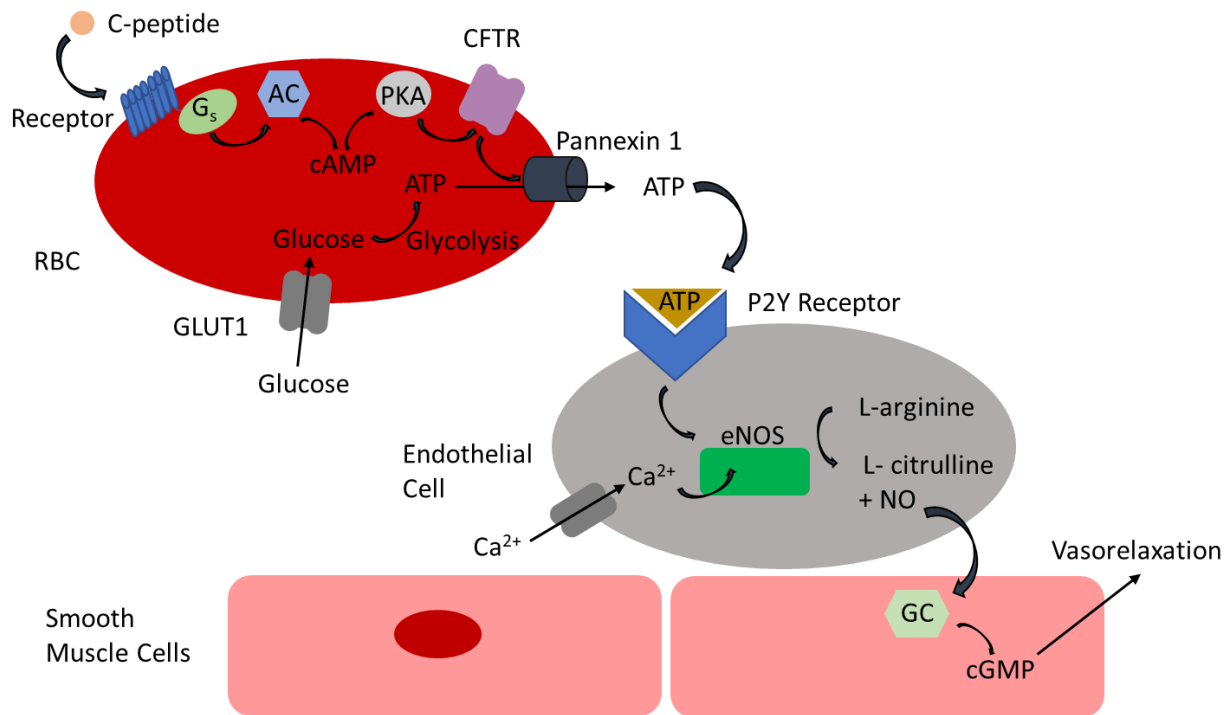


Figure 1.5: Release of ATP and Subsequent NO. Proposed mechanism of C-peptide/albumin complex binding to an RBC receptor. An intracellular signaling mechanism results in ATP release from the RBC, which binds to a P2Y receptor on the endothelial cell. ATP binding generates an intracellular signaling pathway that leads to the production of NO, which results in vasorelaxation in smooth muscle cells.

The released ATP binds to the P2Y receptor on endothelial cells, which increases the activity of eNOS by increasing Ca²⁺ uptake, resulting in the production of NO as a byproduct during the conversion of L-arginine to L-citrulline.^{61,68,80,87} NO diffuses into the bloodstream and then to the vascular smooth muscle cells, where it activates guanylate cyclase (GC), which increases cyclic guanosine monophosphate (cGMP), resulting in vasorelaxation caused by smooth muscle myosin filaments.^{61,68,87} The gaseous nature of NO allows it to diffuse rapidly and it does not require a carrier to move across membranes.⁸⁸ Robert Furchgott, Louis Ignarro, and Ferid Murad received the 1998 Nobel Prize in Physiology or Medicine for the importance of NO in the cardiovascular system.⁸⁹

RBCs of people with T1D exhibit abnormal qualities including decreased deformability and increased aggregation.⁶⁴ Deformability is important for RBCs to travel through capillaries, therefore, reduced deformability results in reduced blood flow.^{61,64} C-peptide has been shown to increase RBC deformability and tissue blood flow to improve circulation by increasing the function of endothelial cells, and improved renal function by normalizing glomerular hyperfiltration, thus reducing urinary albumin excretion.^{64,90} Therefore, an administration of C-peptide improves the deformability of RBCs in people with T1D.⁶⁴ The Spence lab hypothesizes that reintroducing C-peptide into the body along with insulin will result in a decrease in diabetic complication severity.

1.4.2 C-peptide Receptor

Since C-peptide's discovery in the late 1960s, many studies have been conducted in an attempt to implement a C-peptide/insulin therapy in hopes of reducing diabetic complications.^{51,60,61,63,64,91,92} These studies demonstrated that C-peptide along with insulin reduced complications when examined *in vitro* and *in vivo*. However, a 12-month phase 2b clinical trial at Cebix found that C-peptide did not statistically affect neuropathy in comparison to the placebo group.⁹¹ In this study, a pegylated form of C-peptide was utilized because the longer half-life is better for patient convenience and C-peptide exposure.⁹¹ Whereas, the half-life of C-peptide is 30 minutes, PEG-C-peptide has a 6-7 day half-life.⁹¹ The polyethylene glycol (PEG) molecule, with a molecular weight of 40 kDa, was covalently bound at the N-terminus of C-peptide.⁹¹ *In vitro* studies showed that PEG-C-peptide maintained the peptide's bioactivity.⁹¹ In addition, they only used C-peptide as opposed to our proposed C-peptide, Zn²⁺, and albumin complex that will be discussed later.

A major roadblock in the use of C-peptide as a therapy for T1D is the lack of a known receptor mechanism. It is proposed that the C-peptide receptor is a G protein-coupled receptor (GPCR) due to the intracellular signaling cascades that are activated by the peptide.^{68,93} Pertussis toxin results in an inhibition of C-peptide binding and intracellular signaling, which also suggests a GPCR.^{68,90} Of the 136 orphan GPCR suggested by Sharman et al., Yosten et al. narrowed this to 24 GPCRs because they were expressed in the three cell lines analyzed: KATOIII, HEK293, and TF-1.⁹³ However, not all 24 GPCRs were analyzed. GPR160, GPR146, and GPR107 were knocked down in KATOIII cells using siRNA.⁹³ The ability of C-peptide to stimulate c-Fos expression was blocked in GPR146 and unaffected in GPR107 or GPR160.⁹³ However, a direct physical interaction between C-peptide and GPR146 has not been determined.⁹³

It is also possible that GPR146 is promiscuous and interacts with multiple ligands or could be a co-receptor rather than the receptor itself.^{11,93} Yosten et al. only investigated orphan GPCRs, however, due to GPCR promiscuity, it is possible that a GPCR with a known ligand may also interact with C-peptide.¹¹ Since evidence for a direct interaction between C-peptide and GPR146 has not been demonstrated, further experiments are necessary such as co-immunoprecipitation and radioligand binding studies.⁹³ Also, evidence has suggested that C-peptide interacts with the membrane through a receptor complex, which could be a GPCR coupled to an integrin, adapter protein, receptor activity modifying protein (RAMP), or another receptor.¹¹ There is also the possibility that the receptor is a glutamate receptor coupled to a ligand-gated ion channel because free glutamic acid can partly displace C-peptide from cell membranes.⁶⁶

1.5 Albumin, C-peptide, and Red Blood Cells

Albumin, a simple protein shown in Figure 1.6A, is the most abundant blood plasma protein and acts as a carrier for endogenous molecules, exogenous compounds, ions, and toxic waste.^{94–98} In addition to acting as a carrier, albumin is responsible for 80% of blood's colloid osmotic pressure.⁹⁵ Human serum albumin has a molecular mass of 66,348 Da and consists of 585 amino acids.^{94,95} The human liver synthesizes approximately 13.9 g of human serum albumin per day, and synthesis is inversely related to colloid osmotic pressure.^{95,99} After synthesis, albumin leaves the hepatocyte to the circulation system, where it enters the extracellular space through pores of fenestrated endothelium.⁹⁵ Both the extravascular and intravascular spaces contain albumin where its physiological concentration is 600 μM and its half-life is 19 days.^{95,100} The protein consists of three homologous domains: I, II, and III, which are divided into subdomains A and B.^{94,95} Two main ligand binding sites, called Sudlow's Site I and II, are present in subdomain IIA and IIIA as shown in Figure 1.6B.^{95,101}

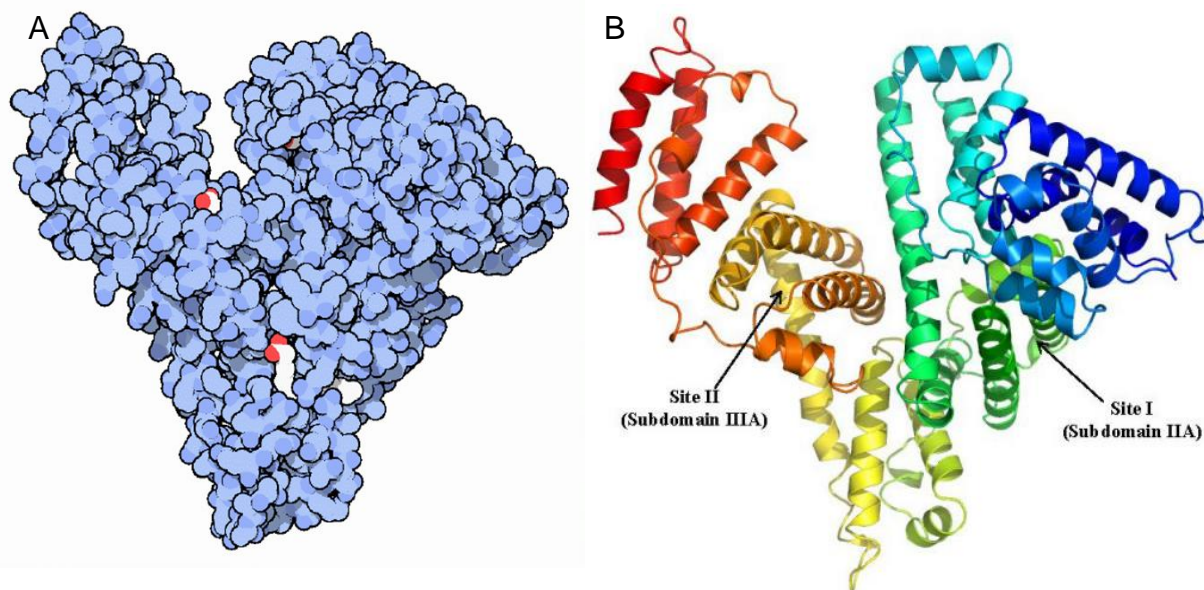


Figure 1.6: Human Serum Albumin Representations. A) Serum albumin, a globular protein, is shown with bound fatty acids in white and red. B) The structure of human serum albumin with Sudlow's Site I and II depicted in Subdomains IIA and IIIA, respectively. Images borrowed from Protein Data Bank and Chuang, V. & Otagiri, M.

Previous research has found that albumin specifically binds C-peptide, with an affinity of $1.75 (\pm 0.64) \times 10^5 \text{ M}^{-1}$ and a binding stoichiometry of $0.53 (\pm 0.003)$, which indicates that two C-peptide molecules bind per albumin molecule.¹³ In order to analyze the C-peptide uptake onto RBCs, an ELISA measurement was conducted. Results demonstrated that C-peptide binding to the cell occurred in the presence of albumin, but that C-peptide binding was absent in albumin-free samples.¹³ Due to the protein's conformational adaptability, albumin is able to bind Zn^{2+} and C-peptide.^{13,102} As a two-site binding event, albumin can bind Zn^{2+} with an affinity of $5.08 (\pm 0.98) \times 10^7 \text{ M}^{-1}$ and C-peptide with an affinity of $2.66 (\pm 0.25) \times 10^5 \text{ M}^{-1}$.¹³ It is believed that albumin binds around 75-80% of the Zn^{2+} in the plasma and is the major Zn^{2+} transporter.^{100,103} There is only one high-affinity site for Zn^{2+} on albumin and it is located at the domain I and II interface.^{100,103} There is also evidence to suggest one or two secondary binding sites that

have a significant, yet weaker, affinity for Zn^{2+} .¹⁰³ However, only 2% of albumin molecules carry one Zn^{2+} ion at a time.¹⁰⁰

While the C-peptide receptor remains elusive, there have been several membrane-associated albumin-binding proteins discovered: albondin/glycoprotein 60 (gp60), glycoprotein 18 (gp18), glycoprotein 30 (gp30), neonatal Fc receptor (FcRn), heterogeneous nuclear ribonucleoproteins (hnRNPs), calreticulin, cubilin, megalin, and secreted protein acidic and rich in cysteine (SPARC).^{95,99} 50% of albumin leaves the capillary lumen through albondin, a transporter found on the plasma membrane of continuous endothelium, that increases capillary permeability.⁹⁵ Native albumin does not interact with gp18 and gp30, but rather, they interact with conformationally-modified albumin for degradation.^{95,99} Both glycoproteins are found on many cell types, such as fibroblasts, macrophages, and endothelial cells.⁹⁵ FcRn is found in the gut, kidneys, lungs, and blood-brain-barrier, as well as the endothelium and antigen-presenting cells.⁹⁵ It binds native albumin to protect the protein from degradation in acidic endosomes.⁹⁵ Both calreticulin and hnRNPs bind native albumin and are found on tumor cell lines.⁹⁵ Cubilin, a multi-ligand receptor, is found in absorptive intestinal cells and kidney proximal tubule cells and is involved in endocytosis of many ligands, such as albumin.^{95,99} Megalin, a transmembrane protein, is found in a plethora of cells and tissues such as kidney proximal tubule cells, absorptive intestinal cells, thyrocytes, lungs, and others.⁹⁵ Megalin in the proximal tubule acts as the receptor for albumin endocytosis.^{99,104} Cubilin and megalin are bound with high affinity, suggesting that megalin assists in the cubilin-ligand complex internalization.⁹⁵ SPARC interacts with albumin in a manner similar to albondin and is found on tumor cells, pancreatic, testicular, ovarian, myocytes, and endothelial cells.⁹⁵

However, the specific binding of albumin to RBCs has not been categorized into a receptor type. Our group hypothesizes that the C-peptide receptor has not been discovered because it is an albumin/C-peptide receptor separate from an albumin receptor. This dissertation focuses on the binding of albumin to healthy and diseased state RBCs, with or without C-peptide. Method development for the isolation of the albumin/C-peptide receptor utilizing magnetic beads is also reported.

REFERENCES

REFERENCES

- (1) Center for Disease Control and Prevention. Underlying Cause of Death 1999-2016 <https://wonder.cdc.gov/ucd-icd10.html> (accessed Mar 20, 2020).
- (2) American Diabetes Association. Economic Costs of Diabetes in the U.S. in 2017. *Diabetes Care* **2018**, *41* (5), 917–928.
- (3) Center for Disease Control and Prevention. *National Diabetes Statistics Report: Estimates of Diabetes and Its Burden in the United States; 2020*.
- (4) American Diabetes Association. *Fast Facts Data and Statistics about Diabetes*; Arlington, 2017.
- (5) Forbes, J. M.; Cooper, M. E. Mechanisms of Diabetic Complications. *Physiol. Rev.* **2013**, *93* (1), 137–188.
- (6) American Diabetes Association. Diagnosis and Classification of Diabetes Mellitus. *Diabetes Care* **2008**, *32* (SUPPL. 1), S62–S67.
- (7) Mayo Clinic Health System. Diabetes www.mayoclinic.org (accessed Mar 16, 2021).
- (8) Al-isawi, Z. J. Role of C-Peptide in the Vasculature, University of Leicester, 2019.
- (9) Nathan, D. M.; Zinman, B.; Cleary, P. A.; Backlund, J.-Y. C.; Genuth, S.; Miller, R.; Orchard, T. J. Modern-Day Clinical Course of Type 1 Diabetes Mellitus After 30 Years' Duration: The Diabetes Control and Complications Trial/Epidemiology of Diabetes Interventions and Pittsburgh Epidemiology of Diabetes Complications Experience (1983-2005). *Arch. Intern. Med.* **2009**, *169* (14), 1307–1316.
- (10) Fong, D. S.; Aiello, L. P.; Ferris, F. L.; Klein, R. Diabetic Retinopathy. *Diabetes Care* **2004**, *27* (10), 2540–2553.
- (11) Kolar, G. R.; Grote, S. M.; Yosten, G. L. C. Targeting Orphan G Protein-Coupled Receptors for the Treatment of Diabetes and Its Complications: C-Peptide and GPR146. *J. Intern. Med.* **2017**, *281* (1), 25–40.
- (12) Fong, D. S.; Ferris, F. L.; Davis, M. D.; Chew, E. Y. Causes of Severe Visual Loss in the Early Treatment Diabetic Retinopathy Study: ETDRS Report No. 24. *Am. J. Ophthalmol.* **1999**, *127* (2), 137–141.
- (13) Liu, Y.; Chen, C.; Summers, S.; Medawala, W.; Spence, D. M. C-Peptide and Zinc Delivery to Erythrocytes Requires the Presence of Albumin: Implications in Diabetes Explored with a 3D-Printed Fluidic Device. *Integr. Biol.* **2015**, *7*, 534–543.

- (14) Pierce, E. A.; Averyt, R. L.; Foley, E. D.; Aiellot, L. P.; Smith, L. E. H.; Deluca, H. F. Vascular Endothelial Growth Factor/Vascular Permeability Factor Expression in a Mouse Model of Retinal Neovascularization. *Proc. Natl. Acad. Sci.* **1995**, *92* (3), 905–909.
- (15) Martin, A.; Komada, M. R.; Sane, D. C. Abnormal Angiogenesis in Diabetes Mellitus. *Med. Res. Rev.* **2003**, *23* (2), 117–145.
- (16) Miner, J. H. The Glomerular Basement Membrane. *Exp Cell Res* **2013**, *318* (9), 973–978.
- (17) Diseases, N. I. of D. and D. and K. Your Kidneys & How They Work.
- (18) Cooper, M. E. Pathogenesis, Prevention, and Treatment of Diabetic Nephropathy. *Lancet* **1998**, *352* (9123), 213–219.
- (19) Hills, C. E.; Brunskill, N. J.; Squires, P. E. C-Peptide as a Therapeutic Tool in Diabetic Nephropathy. *Am. J. Nephrol.* **2010**, *31* (5), 389–397.
- (20) Mogensen, C. E.; Christensen, C. K.; Vittinghus, E. The Stages in Diabetic Renal Disease With Emphasis on the Stage of Incipient Diabetic Nephropathy. *Diabetes* **1983**, *32* (Supl 2), 64–78.
- (21) Peters, T. Clinical Aspects: Albumin in Medicine. In *All About Albumin*; Academic Press: New York, 1995; pp 251–284.
- (22) Rice University. The Cardiovascular System: Blood Vessels and Circulation. In *Anatomy and Physiology*; OpenStax: Houston, 2020.
- (23) Cleveland Clinic. Proteinuria.
- (24) Center for Disease Control and Prevention. About High Blood Pressure.
- (25) Hills, C. E.; Al-Rasheed, N.; Al-Rasheed, N.; Willars, G. B.; Brunskill, N. J. C-Peptide Reverses TGF-B1-Induced Changes in Renal Proximal Tubular Cells: Implications for Treatment of Diabetic Nephropathy. *Am. J. Physiol. - Ren. Physiol.* **2009**, *296* (3), 614–621.
- (26) Low, P. A.; Schmelzer, J. D.; Ward, K. K.; Curran, G. L.; Poduslo, J. F. Effect of Hyperbaric Oxygenation on Normal and Chronic Streptozotocin Diabetic Peripheral Nerves. *Exp Neurol* **1988**, *99* (1), 201–212.
- (27) Giebink, A. W.; Vogel, P. A.; Medawala, W.; Spence, D. M. C-Peptide-Stimulated Nitric Oxide Production in a Cultured Pulmonary Artery Endothelium Is Erythrocyte Mediated and Requires Zn²⁺. *Diabetes. Metab. Res. Rev.* **2013**, *29* (1), 44–52.
- (28) Stevens, M. J.; Zhang, W.; Li, F.; Sima, A. A. F. C-Peptide Corrects Endoneurial Blood Flow but Not Oxidative Stress in Type 1 BB/W or Rats. *Am. J. Physiol.* -

Endocrinol. Metab. **2004**, 287, 497–505.

(29) Cerychova, R.; Pavlinkova, G. HIF-1, Metabolism, and Diabetes in the Embryonic and Adult Heart. *Front. Endocrinol. (Lausanne)*. **2018**, 9 (AUG), 1–14.

(30) Krull, D. L.; Peterson, R. A. Preclinical Applications of Quantitative Imaging Cytometry to Support Drug Discovery. In *Methods in Cell Biology*; Darzynkiewicz, Z., Holden, E., Orfao, A., Telford, W., Wlodkowic, D., Eds.; Elsevier Inc.: NWalham, 2011; Vol. 102, pp 291–308.

(31) Steiner, D. F. The Proinsulin C-Peptide - a Multirole Model. *Exp. Diabesity Res.* **2004**, 5 (1), 7–14.

(32) Wilcox, G. Insulin and Insulin Resistance. *Clin. Biochem. Rev.* **2005**, 26 (2), 19–39.

(33) Hills, C. E.; Brunskill, N. J. Cellular and Physiological Effects of C-Peptide. *Clin. Sci.* **2009**, 116 (7), 565–574.

(34) Yosten, G. L. C.; Kolar, G. R. The Physiology of Proinsulin C-Peptide: Unanswered Questions and a Proposed Model. *Physiology* **2015**, 30 (4), 327–332.

(35) Hutton, J. C. Insulin Secretory Granule Biogenesis and the Proinsulin-Processing Endopeptidases. *Diabetologia* **1994**, 37 (Suppl 2), 48–56.

(36) Kennedy, R. T.; Huang, L.; Aspinwall, C. A. Extracellular PH Is Required for Rapid Release of Insulin from Zn - Insulin Precipitates in β -Cell Secretory Vesicles during Exocytosis. *J. Am. Chem. Soc.* **1996**, 118 (7), 1795–1796.

(37) Li, Y. V. Zinc and Insulin in Pancreatic Beta-Cells. *Endocrine* **2014**, 45 (2), 178–189.

(38) Meyer, J. a; Subasinghe, W.; Sima, A. a F.; Keltner, Z.; Reid, G. E.; Daleke, D.; Spence, D. M. Zinc-Activated C-Peptide Resistance to the Type 2 Diabetic Erythrocyte Is Associated with Hyperglycemia-Induced Phosphatidylserine Externalization and Reversed by Metformin. *Mol. Biosyst.* **2009**, 5 (10), 1157–1162.

(39) Martin, G. M.; Chen, P. C.; Devaraneni, P.; Shyng, S. L. Pharmacological Rescue of Trafficking-Impaired ATP-Sensitive Potassium Channels. *Front. Physiol.* **2013**, 4 (386), 1–16.

(40) Skelin, M.; Rupnik, M.; Cencic, A. Pancreatic Beta Cell Lines and Their Applications in Diabetes Mellitus Research. *ALTEX* **2010**, 27 (2), 105–113.

(41) Rosenfeld, L. Insulin: Discovery and Controversy. *Clin. Chem.* **2002**, 48 (12), 2270–2288.

(42) Lee, J.; Pilch, P. F. The Insulin Receptor: Structure, Function, and Signaling. *Am.*

Physiol. Soc. **1994**, 226 (2), 319–334.

(43) Mueckler, M.; Thorens, B. The SLC2 (GLUT) Family of Membrane Transporters. *Mol. Aspects Med.* **2013**, 34 (0), 121–138.

(44) Steiner, D.; Oyer, P. The Biosynthesis of Insulin and a Probable Precursor of Insulin by a Human Islet Cell Adenoma. *Proc. Natl. Acad. Sci. U.S.A.* **1967**, 57 (2), 473–4800.

(45) Brandenburg, D. History and Diagnostic Significance of C-Peptide. *Exp Diabetes Res.* **2008**, 1–7.

(46) Chance, R.; Ellis, R.; Bromer, W. Porcine Proinsulin : Characterization and Amino Acid Sequence. *Science (80-.)*. **1968**, 161 (3837), 165–167.

(47) Lind, J.; Lindahl, E.; Perálvarez-Marín, A.; Holmlund, A.; Jörnvall, H.; Mäler, L. Structural Features of Proinsulin C-Peptide Oligomeric and Amyloid States. *FEBS J.* **2010**, 277 (18), 3759–3768.

(48) Steiner, D. F. The Proinsulin C-Peptide - A Multirole Model. *Exp. Diabetes Res.* **2004**, 5 (1), 7–14.

(49) Henriksson, M.; Shafqat, J.; Liepinsh, E.; Tally, M.; Wahren, J.; Jörnvall, H.; Johansson, J. Unordered Structure of Proinsulin C-Peptide in Aqueous Solution and in the Presence of Lipid Vesicles. *Cell. Mol. Life Sci.* **2000**, 57 (2), 337–342.

(50) Sjöberg, S.; Gjötterberg, M.; Berglund, L.; Möller, E.; Östman, J. Residual C-Peptide Excretion Is Associated with a Better Long-Term Glycemic Control and Slower Progress of Retinopathy in Type I (Insulin-Dependent) Diabetes Mellitus. *J. Diabet. Complications* **1991**, 5, 18–22.

(51) Johansson, B. L.; Borg, K.; Fernqvist-Forbes, E.; Kernell, A.; Odergren, T.; Wahren, J. Beneficial Effects of C-Peptide on Incipient Nephropathy and Neuropathy in Patients with Type 1 Diabetes Mellitus. *Diabet. Med.* **2000**, 17, 181–189.

(52) Sjoquist, M.; Huang, W.; Johansson, B. L. Effects of C-Peptide on Renal Function at the Early Stage of Experimental Diabetes. *Kidney Int.* **1998**, 54 (3), 758–764.

(53) Samnegård, B.; Jacobson, S. H.; Jaremko, G.; Johansson, B. L.; Ekberg, K.; Isaksson, B.; Eriksson, L.; Wahren, J.; Sjöquist, M. C-Peptide Prevents Glomerular Hypertrophy and Mesangial Matrix Expansion in Diabetic Rats. *Nephrol. Dial. Transplant.* **2005**, 20 (3), 532–538.

(54) Pierson, C. R.; Zhang, W.; Sima, A. A. F. Proinsulin C-Peptide Replacement in Type 1 Diabetic BB/Wor-Rats Prevents Deficits in Nerve Fiber Regeneration. *J. Neuropathol. Exp. Neurol.* **2003**, 62 (7), 765–779.

- (55) Sima, A. A. F.; Zhang, W.; Sugimoto, K.; Henry, D.; Li, Z.; Wahren, J.; Grunberger, G. C-Peptide Prevents and Improves Chronic Type I Diabetic Polyneuropathy in the BB/Wor Rat. *Diabetologia* **2001**, *44* (7), 889–897.
- (56) Samnegaård, B.; Jacobson, S. H.; Jaremko, G.; Johansson, B. L.; Sjöquist, M. Effects of C-Peptide on Glomerular and Renal Size and Renal Function in Diabetic Rats. *Kidney Int.* **2001**, *60* (4), 1258–1265.
- (57) Sjöberg, S.; Gunnarsson, R.; Gjøtterberg, M.; Lefvert, A. K.; Persson, A.; Ostman, J. Residual Insulin Production, Glycaemic Control and Prevalence of Microvascular Lesions and Polyneuropathy in Long-Term Type 1 (Insulin-Dependent) Diabetes Mellitus. *Diabetologia* **1987**, *30*, 208–213.
- (58) Zerbini, G.; Mangili, R.; Luzi, L. Higher Post-Absorptive C-Peptide Levels in Type 1 Diabetic Patients without Renal Complications. *Diabet. Med.* **1999**, *16*, 1048–1049.
- (59) Johansson, B. L.; Sjöberg, S.; Wahren, J. The Influence of Human C-Peptide on Renal Function and Glucose Utilization in Type 1 (Insulin-Dependent) Diabetic Patients. *Diabetologia* **1992**, *35*, 121–128.
- (60) Wahren, J.; Ekberg, K.; Jörnvall, H. C-Peptide Is a Bioactive Peptide. *Diabetologia* **2007**, *50* (3), 503–509.
- (61) Forst, T.; Kunt, T. Effects of C-Peptide on Microvascular Blood Flow and Blood Hemorheology. *Exp. Diabetes Res.* **2004**, *5* (1), 51–64.
- (62) Richards, J. P.; Yosten, G. L. C.; Kolar, G. R.; Jones, C. W.; Stephenson, A. H.; Ellsworth, M. L.; Sprague, R. S. Low O₂-Induced ATP Release from Erythrocytes of Humans with Type 2 Diabetes Is Restored by Physiological Ratios of C-Peptide and Insulin. *Am. J. Physiol. Regul. Integr. Comp. Physiol.* **2014**, *307* (7), R862–R868.
- (63) Forst, T.; De La Tour, D. D.; Kunt, T.; Pfützner, A.; Goitom, K.; Pohlmann, T.; Schneider, S.; Johansson, B. L.; Wahren, J.; Löbig, M.; et al. Effects of Proinsulin C-Peptide on Nitric Oxide, Microvascular Blood Flow and Erythrocyte Na⁺,K⁺-ATPase Activity in Diabetes Mellitus Type I. *Clin. Sci.* **2000**, *98* (3), 283–290.
- (64) Kunt, T.; Schneider, S.; Pfützner, A.; Goitom, K.; Engelbach, M.; Schauf, B.; Beyer, J.; Forst, T. The Effect of Human Proinsulin C-Peptide on Erythrocyte Deformability in Patients with Type I Diabetes Mellitus. *Diabetologia* **1999**, *42* (4), 465–471.
- (65) Richards, J. P.; Stephenson, A. H.; Ellsworth, M. L.; Sprague, R. S. Synergistic Effects of C-Peptide and Insulin on Low O₂-Induced ATP Release from Human Erythrocytes. *Am. J. Physiol. - Regul. Integr. Comp. Physiol.* **2013**, *305*, 1331–1336.
- (66) Wahren, J.; Jörnvall, H. C-Peptide Makes a Comeback. *Diabetes. Metab. Res. Rev.* **2003**, *19* (5), 345–347.

- (67) Richards, J. P.; Bowles, E. A.; Ellsworth, M. L.; Stephenson, A. H.; Sprague, R. S. Signalling Mechanisms Involved in C-Peptide-Mediated Inhibition of Low O₂-Induced ATP Release from Human Erythrocytes. *ISBT Sci. Ser.* **2016**, *11* (Suppl. 1), 325–331.
- (68) Wahren, J.; Kallas, Å.; Sima, A. A. F. The Clinical Potential of C-Peptide Replacement in Type 1 Diabetes. *Diabetes* **2012**, *61* (4), 761–772.
- (69) Bergman, R. A.; Afifi, A. K.; Heidger, P. M. Anatomy Atlases: Atlas of Microscopic Anatomy: Section 4: Blood <http://www.anatomyatlases.org> (accessed Mar 19, 2020).
- (70) Manzone, T. A.; Dam, H. Q.; Soltis, D.; Sagar, V. V. Blood Volume Analysis: A New Technique and New Clinical Interest Reinvigorate a Classic Study. *J. Nucl. Med. Technol.* **2007**, *35* (2), 55–63.
- (71) Kakhniashvili, D. G.; Bulla, L. A.; Goodman, S. R. The Human Erythrocyte Proteome. *Mol. Cell. Proteomics* **2004**, *3* (5), 501–509.
- (72) De Palma, A.; Roveri, A.; Zaccarin, M.; Benazzi, L.; Daminelli, S.; Pantano, G.; Buttarello, M.; Ursini, F.; Gion, M.; Mauri, P. L. Extraction Methods of Red Blood Cell Membrane Proteins for Multidimensional Protein Identification Technology (MudPIT) Analysis. *J. Chromatogr. A* **2010**, *1217* (33), 5328–5336.
- (73) Shin, S.; Ku, Y.; Babu, N.; Singh, M. Erythrocyte Deformability and Its Variation in Diabetes Mellitus. *Indian J. Exp. Biol.* **2007**, *45* (1), 121–128.
- (74) Pasini, E. M. E.; Kirkegaard, M.; Mortensen, P.; Lutz, H. U.; Thomas, A. W.; Mann, M. In-Depth Analysis of the Membrane and Cytosolic Proteome of Red Blood Cells. *Blood* **2006**, *108* (3), 791–801.
- (75) Hamasaki, N. The Role of Band 3 Protein in Oxygen Delivery by Red Blood Cells. *Indian J. Clin. Biochem.* **1999**, *14* (1), 49–58.
- (76) Crisp, R. L.; Maltaner, R. E.; Vittori, D. C.; Solari, L.; Gammella, D.; Schwartzman, G.; García, E.; Rapetti, M. C.; Donato, H.; Nesse, A. Red Blood Cell Aquaporin-1 Expression Is Decreased in Hereditary Spherocytosis. *Ann. Hematol.* **2016**, *95* (10), 1595–1601.
- (77) Dean, L. The Kidd Blood Group. In *Blood Groups and Red Cell Antigens [Internet]*; Beck, B., Ed.; Bethesda (MD) National Center for Biotechnology Information, 2005; pp 1–6.
- (78) Tsukamoto, T.; Sonenberg, M. Catecholamine Regulation of Human Erythrocyte Membrane Protein Kinase. *J. Clin. Invest.* **1979**, *64* (2), 534–540.
- (79) Endeward, V.; Cartron, J.-P.; Ripoché, P.; Gros, G. RhAG Protein of the Rhesus Complex Is a CO₂ Channel in the Human Red Cell Membrane. *FASEB J.* **2008**, *22* (1), 64–73.

- (80) Ellsworth, M. L.; Sprague, R. S. Regulation of Blood Flow Distribution in Skeletal Muscle: Role of Erythrocyte-Released ATP. *J. Physiol.* **2012**, *590* (20), 4985–4991.
- (81) Montel-Hagen, A.; Blanc, L.; Boyer-Clavel, M.; Jacquet, C.; Vidal, M.; Sitbon, M.; Tylor, N. The GLUT1 and GLUT4 Glucose Transporters Are Differentially Expressed during Perinatal and Postnatal Erythropoiesis. *Blood* **2008**, *112* (12), 4729–4738.
- (82) Wonderlin, W. Just in Time Medicine justintimemedicine.com/cirriculumcontent (accessed May 1, 2021).
- (83) Rigler, R.; Pramanik, A.; Jonasson, P.; Kratz, G.; Jansson, O. T.; Nygren, P.-A.; Stahl, S.; Ekberg, K.; Johansson, B.-L.; Uhlen, S.; et al. Specific Binding of Proinsulin C-Peptide to Human Cell Membranes. *Proc. Natl. Acad. Sci.* **1999**, *96* (23), 13318–13323.
- (84) Richards, J. P.; Bowles, E. A.; Gordon, W. R.; Ellsworth, M. L.; Stephenson, A. H.; Sprague, R. S. Mechanisms of C-Peptide-Mediated Rescue of Low O₂-Induced ATP Release from Erythrocytes of Humans with Type 2 Diabetes. *Am. J. Physiol. Regul. Integr. Comp. Physiol.* **2015**, *308* (5), R411–R418.
- (85) Meyer, J. A.; Froelich, J. M.; Reid, G. E.; Karunarathne, W. K. A.; Spence, D. M. Metal-Activated C-Peptide Facilitates Glucose Clearance and the Release of a Nitric Oxide Stimulus via the GLUT1 Transporter. *Diabetologia* **2008**, *51* (1), 175–182.
- (86) Pinger, C. W.; Entwistle, K. E.; Bell, T. M.; Liu, Y.; Spence, D. M. C-Peptide Replacement Therapy in Type 1 Diabetes: Are We in the Trough of Disillusionment? *Mol. Biosyst.* **2017**, *13* (8), 1432–1437.
- (87) Forst, T.; Hach, T.; Kunt, T.; Weber, M. M.; Pfützner, A. Molecular Effects of C-Peptide in Microvascular Blood Flow Regulation. *Rev. Diabet. Stud.* **2009**, *6* (3), 159–167.
- (88) Domingos, P.; Prado, A. M.; Wong, A.; Gehring, C.; Feijo, J. A. Nitric Oxide: A Multitasked Signaling Gas in Plants. *Mol. Plant* **2015**, *8* (4), 506–520.
- (89) Zetterström, R. The 1998 Nobel Prize--Discovery of the Role of Nitric Oxide as a Signalling Molecule. *Acta Paediatr.* **2008**, *98* (3), 593–599.
- (90) Wahren, J. C-Peptide and the Pathophysiology of Microvascular Complications of Diabetes. *J. Intern. Med.* **2016**, *281* (1), 3–6.
- (91) Wahren, J.; Foyt, H.; Daniels, M.; Arezzo, J. C. Long-Acting C-Peptide and Neuropathy in Type 1 Diabetes: A 12-Month Clinical Trial. *Diabetes Care* **2016**, *39* (4), 596–602.
- (92) Johansson, B. L.; Kernell, A.; Sjöberg, S.; Wahren, J. Influence of Combined C-Peptide and Insulin Administration on Renal Function and Metabolic Control in Diabetes Type 1. *J. Clin. Endocrinol. Metab.* **1993**, *77* (4), 976–981.

- (93) Yosten, G. L. C.; Kolar, G. R.; Redlinger, L. J.; Samson, W. K. Evidence for an Interaction between Proinsulin C-Peptide and GPR146. *J. Endocrinol.* **2013**, *218* (2), B1–B8.
- (94) Peters, T. The Albumin Molecule: Its Structure and Chemical Properties. In *All About Albumin*; Academic Press: New York, 1995; pp 9–75.
- (95) Merlot, A. M.; Kalinowski, D. S.; Richardson, D. R. Unraveling the Mysteries of Serum Albumin—More than Just a Serum Protein. *Front. Physiol.* **2014**, *5* (299), 1–7.
- (96) Curry, S.; Brick, P.; Franks, N. P. Fatty Acid Binding to Human Serum Albumin: New Insights from Crystallographic Studies. *Biochim. Biophys. Acta - Mol. Cell Biol. Lipids* **1999**, *1441* (2–3), 131–140.
- (97) Goodsell, D. Serum Albumin.
- (98) Peters, T. Ligand Binding by Albumin. In *All About Albumin*; Academic Press: New Jersey, 1995; pp 76–132.
- (99) Bern, M.; Sand, K. M. K.; Nilsen, J.; Sandlie, I.; Andersen, J. T. The Role of Albumin Receptors in Regulation of Albumin Homeostasis: Implications for Drug Delivery. *J. Control. Release* **2015**, *211*, 144–162.
- (100) Lu, J.; Stewart, A. J.; Sadler, P. J.; Pinheiro, T. J. T.; Blindauer, C. A. Albumin as a Zinc Carrier: Properties of Its High-Affinity Zinc-Binding Site. *Biochem. Soc. Trans.* **2008**, *36* (6), 1317–1321.
- (101) Chuang, V. T. G.; Otagiri, M. Photoaffinity Labeling of Plasma Proteins. *Molecules* **2013**, *18* (11), 13831–13859.
- (102) Weisiger, R. A. Functions of the Liver. In *Textbook of Hepatology: From Basic Science to Clinical Practice*; Rodes, J., Benhamou, J.-P., Blei, A., Reichen, J., Rizzetto, M., Eds.; Blackwell Publishing: Malden, 2007; pp 250–255.
- (103) Handing, K. B.; Shabalina, I. G.; Kassar, O.; Khazaipoul, S.; Blindauer, C. A.; Stewart, A. J.; Chruszcz, M.; Minor, W. Circulatory Zinc Transport Is Controlled by Distinct Interdomain Sites on Mammalian Albumins. *Chem. Sci.* **2016**, *7* (11), 6635–6648.
- (104) Tojo, A.; Kinugasa, S. Mechanisms of Glomerular Albumin Filtration and Tubular Reabsorption. *Int. J. Nephrol.* **2012**, *2012*, 1–9.

Chapter 2- Albumin Binding to Red Blood Cells

2.1 Introduction

2.1.1 Background

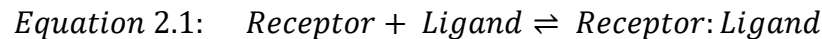
In chapter 1, the concept of the elusive C-peptide receptor and the debate over the idea that the receptor is a G-protein-coupled receptor (GPCR) was discussed. Since pertussis toxin inhibited C-peptide binding (indicating a GPCR) and GPR146 blocked C-peptide's ability to stimulate c-Fos expression in KATOIII cells, GPR146 was selected as the C-peptide receptor by Yosten et al.¹ However, a direct physical interaction between GPR146 and C-peptide was not established. Lindors et al. and members of the Willars lab provide evidence against GPR146 being the C-peptide receptor.^{2,3} This will be discussed in further detail in chapter 4. Due to a lack of understanding of C-peptide's receptor and mechanism, C-peptide is not being utilized as part of the type 1 diabetes (T1D) therapy.

For over a decade, the Spence lab has focused on C-peptide binding to red blood cells (RBCs). Initial data from 2008 demonstrated that C-peptide caused an increase in RBC-derived ATP when a metal was present.⁴ Following research focused on C-peptide binding to RBCs in the presence of Zn^{2+} because it is also secreted from pancreatic β -cell. A 2015 publication from our group released data demonstrating that C-peptide and Zn^{2+} required albumin to bind to RBCs.⁵ Zn^{2+} also required C-peptide to bind to RBCs, but C-peptide did not require Zn^{2+} to bind to RBCs.⁵ Isothermal titration calorimetry (ITC) data demonstrated that C-peptide and Zn^{2+} do not specifically bind to each other, but that albumin specifically binds C-peptide and Zn^{2+} .⁵ Since C-peptide does not bind to RBCs

on its own accord, the C-peptide receptor concept needed to be revisited. I hypothesize that the C-peptide receptor is not solely for C-peptide, but rather for an albumin/C-peptide complex receptor.

2.1.2 An Introduction to Binding

According to Clark's Theory, the physical constants that define classical interactions between ligand and receptor are dependent on several assumptions: the interaction is reversible, the receptor molecules are all equivalent and independent, the occupied receptor site number is proportional to the biological response, the interaction is measured after equilibrium is reached, and the ligand only exists in either bound or unbound forms to the receptor.⁶ When all of the assumptions are made, the following equation results at equilibrium:^{6,7}



Affinity, or the strength of the ligand binding to the receptor, is judged by either the equilibrium association constant, K_a , or the equilibrium dissociation constant, K_d .⁷ At equilibrium,

$$\text{Equation 2.2: } \frac{[RL]}{[R][L]} = K_a$$

$$\text{Equation 2.3: } \frac{[R][L]}{[RL]} = K_d$$

where $[R]$ =free receptor, $[L]$ =free ligand, and $[RL]$ =bound ligand.⁷ The equilibrium dissociation constant is the concentration of ligand that results in half of the receptors

being occupied at equilibrium.⁸ If K_d is small, then the receptor has a high affinity for the ligand, whereas, a large K_d represents that the receptor's affinity for the ligand is low.⁸

Not all detected binding, known as total binding, represents data that is relevant to the ligand/receptor interaction. For example, specific binding refers to saturable binding with a finite number of receptors that is of interest when analyzing ligand/receptor interactions.⁸ However, nonspecific binding is nonsaturable and not of interest to the desired receptor.⁸ Rather, nonspecific binding occurs due to chemical properties, charge, and hydrophobicity of the ligand and cell membrane.⁸ In contrast to specific binding, which is saturable and results in a saturation binding curve, nonspecific binding results in a linear relationship with increasing ligand concentrations as shown in Figure 2.1A.⁸ Collectively, the specific and nonspecific binding result in the total binding.

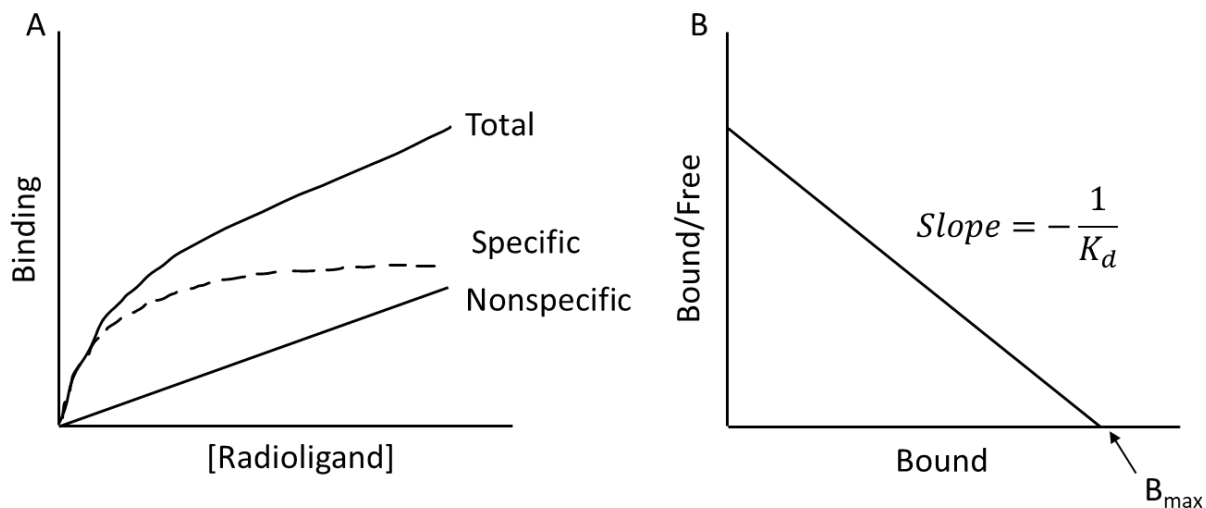


Figure 2.1: Binding Representations. A. A binding curve representing the total binding, saturable specific binding, and linear nonspecific binding. B. A Scatchard plot demonstrating that the slope of bound/free ligand versus bound ligand is equal to the negative inverse of K_d and the x-intercept is equal to B_{max} .

The traditional method used to linearize binding data is Scatchard plot analysis as shown in Figure 2.1B. The x-axis is the specifically bound ligand concentration, and the y-axis is the ratio of specifically bound ligand concentration to the free ligand concentration. Once a trendline is fit to the data, the slope of the line is equal to the negative inverse of K_d , also known as negative K_a , and the x-intercept is the B_{max} . An estimate of the number of binding sites on the cell can be given by B_{max} .⁹

2.1.3 Albumin Binding

A 1983 study at the University of California, San Francisco demonstrated that albumin-ligand complexes interact specifically with RBCs.¹⁰ Even though the methods by which the data were gathered were not described, a discussion with Dr. Weisiger (one of the authors) revealed that the methods of this study followed closely with their other studies of albumin binding to hepatocytes. Wright et al. utilized human serum albumin (HSA) labeled with ^{125}I for gamma decay detection to examine binding of the protein to the RBC.¹¹ It was estimated that the K_d value was on the order of 10^{-6} M, and the number of sites per RBC was approximately 10^4 .¹⁰ Also, it was estimated that less than 1% of the RBC surface was occupied by albumin, suggesting that albumin is interacting at a limited number of sites rather than coating the cell surface nonspecifically. Data was evaluated through a single saturable binding process and a nonsaturable process, but it was found that including a second saturable process did not improve the quality of the fit.¹¹ The quality of fit indicates that albumin alone only binds to one receptor, rather than two binding sites with different affinities.¹² In a second study by the same group, the apparent K_d was reported to be 208 (± 143) nM with the number of sites per cell being 21 (± 20) $\times 10^3$.¹¹

2.1.4 Difference between Human Serum Albumin and Bovine Serum Albumin

The structural differences between HSA and bovine serum albumin (BSA) are very limited. There is one tryptophan (Trp) difference between the amino acid sequences. Whereas, HSA has one Trp, BSA has two as shown in Figure 2.2.^{13,14} In BSA, Trp-134 is located on the surface of the molecule in the first domain, while Trp-212 is located in a hydrophobic binding pocket in the first domain.¹⁴ The location of Trp-214 in HSA is similar to that of Trp-212 in BSA. This does result in a slight difference in the fluorescence emission spectrum between the two proteins, as HSA's one Trp has three-quarters the emission as the average Trp of BSA.¹³ In addition, HSA has 45 valine residues compared to 35 in BSA.¹³ HSA exists in one unfolded state, while BSA exists in two unfolded states between pH 4.8-5.6. However, this is not relevant for our RBC studies since physiological pH (7.40) is outside of this range.¹³

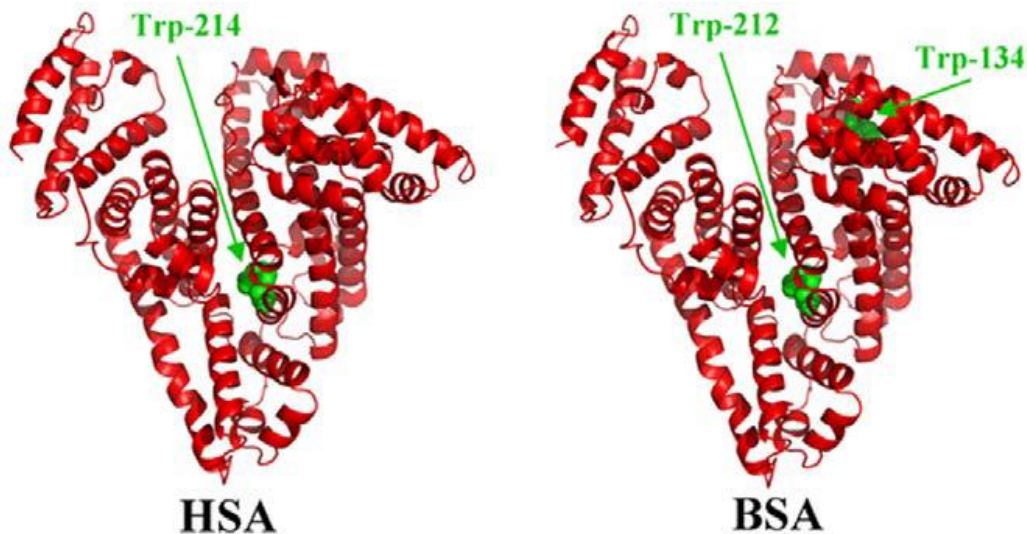


Figure 2.2: Crystal Structures of HSA and BSA. The differences in the tryptophan (Trp) residues, in green, between human and bovine serum albumin. Image borrowed from Belatik et al.

Previous unpublished data from our lab demonstrate that there is not a significant difference (two-sample assuming equal variances two-tailed t-test) in C-peptide uptake by RBCs between BSA and HSA. BSA resulted in C-peptide uptake of 1.75 (± 0.13) nM, whereas HSA resulted in C-peptide uptake of 1.36 (± 0.10) nM as shown in Figure 2.3. The p value equaled 0.08, which indicates that the null hypothesis (that there is not a difference between the means) should be accepted. Due to the overall cost savings, BSA was chosen for method development and analysis.

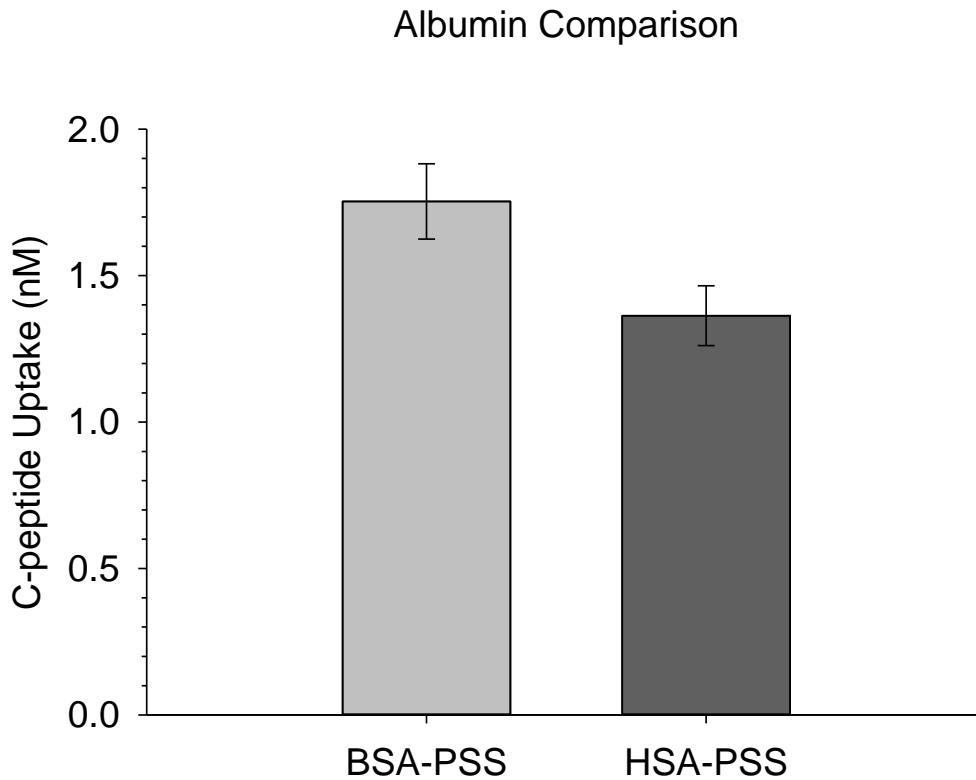


Figure 2.3: Comparison of BSA and HSA C-peptide Uptake. The C-peptide uptake to 7% RBCs in the presence of either BSA or HSA. $n=3$, error=SEM, $p=0.08$.

2.2 Methods

2.2.1 Flow Cytometry Troubleshooting

Due to the single cell analysis ability of flow cytometry, this technique was selected for analyzing albumin binding to RBCs. In flow cytometry, the sample is introduced into the instrument through a sample injection port (SIP). The sample core is surrounded by sheath fluid within a flow cell where the cells are aligned in a single file due to the surrounding flow and are excited by a laser as shown in Figure 2.4.¹⁵ After laser interaction, the light scatters and is detected through photodiodes and photomultiplier tubes (PMTs). The sheath fluid and sample fluid remain separate due to the sample core exerting a greater pressure.¹⁵ This pressure can be controlled by the user and is important for determining the diameter of the sample core. Increasing the flow rate accelerates more cell per unit time by the PMTs, thus requiring faster data acquisition; however, the diameter of the sample core is increased and more than one cell could cross in front of the laser at a time.¹⁵ To decrease this likelihood, samples can be analyzed at a slower flow rate (14 $\mu\text{L}/\text{min}$; 10 μm core).¹⁶

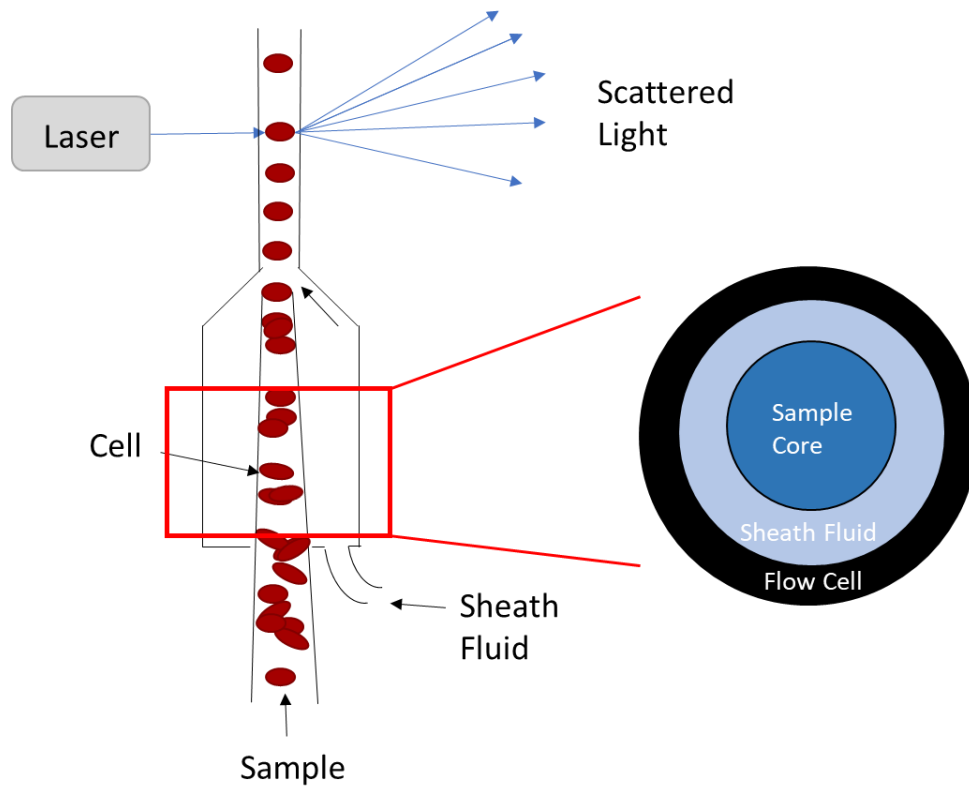


Figure 2.4: Depiction of Flow Cytometry. An internal look at the sample entering the flow cytometer sample injection port before the cells are individually lined up to be analyzed by the laser. The highlighted box demonstrates the flow cell containing the sample core and sheath fluid as seen from above.

Another important parameter to set is the acquisition limits, which in this case, were event counts. The instrument (Accuri™ C6 Plus; BD BioSciences, Franklin Lakes, NJ) can count how many events, or cells/particles, pass in front of the laser during the run time. By setting the desired event count, the samples can be equally compared by the number of cells analyzed. Event counts ranging from 5,000-50,000 were tested to determine optimal counts for analysis. The number of events did not affect results, therefore 10,000 was selected for event counts moving forward.

Several parameters can be evaluated after detection. Photodiodes are used to detect the forward scatter (FSC) and side scatter (SSC) of light interacting with the flowing

cells, which can provide unique information about the passing cell. For example, FSC represents the size of the cell, whereas SSC represents the cell's internal complexity and granularity.¹⁷ In addition, several PMTs are housed within the instrument to detect fluorescence of multiple emission wavelengths, which correspond to the desired fluorophore. After data acquisition, event counts can be plotted as SSC versus FSC to differentiate between debris and varying cell types (e.g., platelets, neutrophils, RBCs, etc.). In Figure 2.5A, gating of the RBC population is depicted. Next, events are plotted as fluorescein isothiocyanate (FITC; a fluorophore) versus FSC as shown in Figure 2.5B. This allows for the RBC population from Figure 2.5A to be further gated to remove background fluorescence. This reduced population was then replotted as shown in Figure 2.5C as FSC versus FSC. All events that fall within the line are single cells, however, any events that fall outside of this line are cell aggregates that were discarded. The final fluorescence after the gating steps could then be determined by plotting FITC versus FSC of the single cell population as shown in Figure 2.5D.

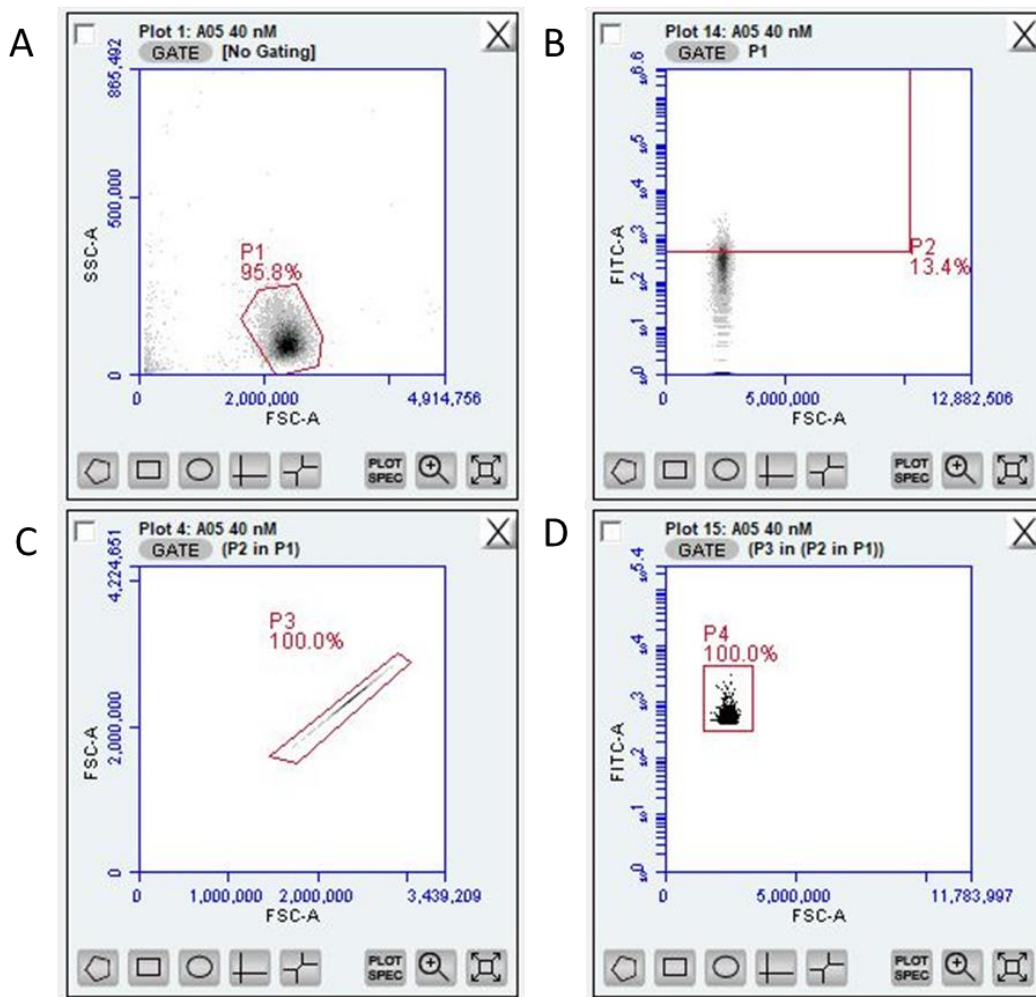


Figure 2.5: Flow Cytometry Gating Steps. A. Gate depicting selected RBC population. B. Population from Gate A (P1) where only fluorescence above the blank was selected. C. The population in Gate B (P2 in P1) where the cell aggregates were deselected. D. The population from Gate C (P3 in (P2 in P1)) again selected for only fluorescence above the blank.

All solutions were filtered through a 0.22 μm Millex Durapore® polyvinylidene difluoride (PVDF) membrane syringe filter (Millipore, Burlington, MA) to remove any particles. Prior to PVDF solution filtering, an abundance of particles were visible in the bottom left of the graph as shown in Figure 2.6A. After PVDF filtering, fewer particles were visible outside of the interested cell area, as shown in Figure 2.6B. Removing unnecessary particles was important for analysis because an increased percentage of

the 10,000 events counted were the RBCs of interest rather than debris outside of the cell area. In using PVDF solution filtering, it was important to ensure the BSA-FITC (Sigma Aldrich, St. Louis, MO) was not retained in the membrane, therefore affecting the protein concentration of the stock solution. A 3 μM BSA-FITC stock solution was prepared and divided into two 1 mL samples. One sample was filtered and both samples were analyzed on a FlexStation-3 spectrophotometer (Molecular Devices LCC, Sunnyvale, CA) at 485 nm excitation and 515 nm emission wavelengths. Also, it was determined that filtering the incubated sample through 48 μm nylon mesh (Sefar Nitex[®], Buffalo, NY) prior to flow cytometry analysis removed further unwanted particles. It is common practice to filter samples through a nylon mesh prior to analysis in order to prevent clogging of the instrument fluidics.¹⁸

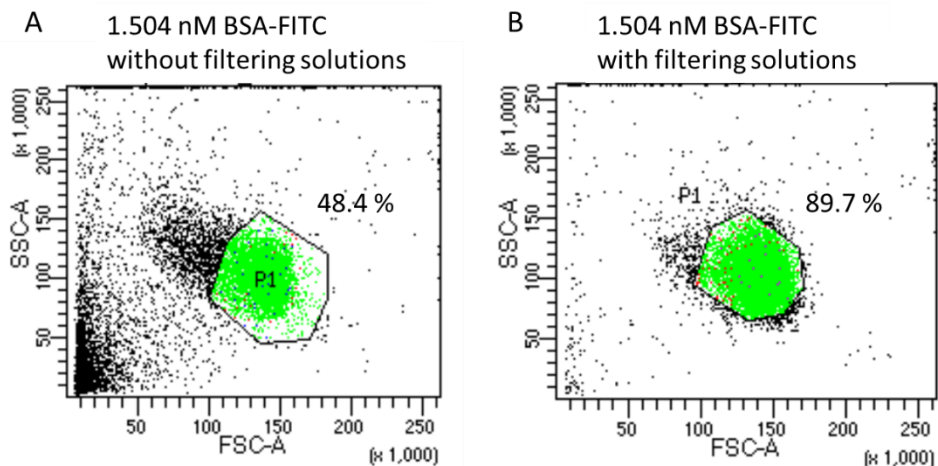


Figure 2.6: Flow cytometry dot plots depicting the difference in background with and without filtering solutions prior to sample incubation. Prior to filtering the solutions (A), only 48.4% of particles were used, after filtering the solutions (B), 89.7% of the particles were used.

In addition to sample filtering, sample run orders were analyzed. The concern was that cells would aggregate at the bottom of the vials prior to analysis and results would be altered based on timing of the measurement. Therefore, samples were run in order

from the blank to the highest BSA-FITC concentration and then again in reverse. Results show a slight difference in two of the samples' fluorescence corresponding to run order once the samples were gated. Therefore, it was determined that samples needed to be run in the same order each time to limit day-to-day variations. Also, a BD Accuri™ C6 Plus (BD BioSciences) was purchased because of its autosampler option that agitates the samples between runs to prevent the aggregation previously seen.

Once samples were running successfully on the flow cytometer, a calibration method was developed. Quantum™ FITC-5 molecules of equivalent soluble fluorochrome (MESF) beads were purchased from Bangs Laboratories, Inc. (Fishers, IN). The bead MESF values were known and could be plotted in relation to the resulting instrument fluorescence. The different bead preparation methods tested included filtering, running individually or collectively, and buffer compositions. It was determined that additional filtering of the bead solutions was not necessary. Running the beads collectively did work in most instances, but on one experimental day, three of the beads were undistinguishable and a calibration curve could not be created. Therefore, it was determined that it was best to prepare the beads separately to avoid wasted experiments. Beads were prepared in the respective buffers (physiological salt solution (PSS) or albumin free-PSS (AF-PSS) for the samples they would represent. AF-PSS consists of 4.7 mM KCl (Fisher Scientific, Waltham, MA), 2.0 mM CaCl₂ (Fisher Scientific), 140.5 mM NaCl (Sigma Aldrich), 12.0 mM MgSO₄ (Fisher Scientific), 21.0 mM tris(hydroxymethyl) aminomethane (Tris; Invitrogen, Carlsbad, CA), and 5.5 mM dextrose (Sigma Aldrich) at pH 7.4). PSS is essentially a solution of salts that is isotonic with the blood serum, and it contains all reagents of AF-PSS plus 0.5% BSA (Sigma Aldrich) at pH 7.4. In addition to

validation beads, instrument quality control beads (BD CS&T Beads; BD BioSciences) were purchased to assure that the instrument was correctly aligned for each experiment. This procedure limits instrumental variations in experiments from day-to-day. The dim and mid+bright regions of the detectors were adjusted as shown in Figure 2.7.

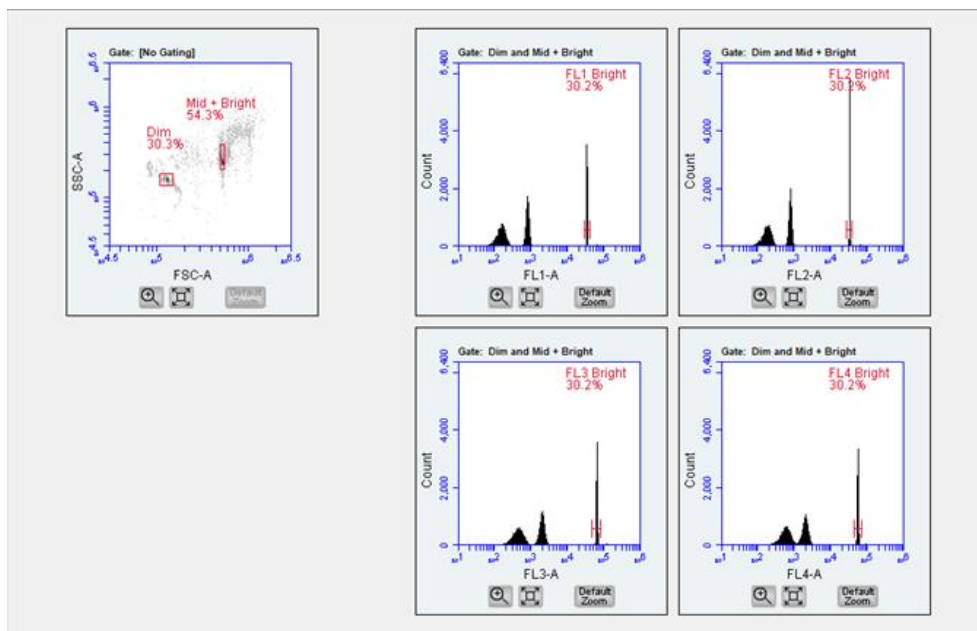


Figure 2.7: Image of BD CS&T Beads Corrections. Adjustments were made to dim and mid+bright regions of the fluorescence plots. Once changes were made, a quality control report was generated to tell the user if FSC, SSC, and all detectors (FL1-FL4) passed parameter testing.

3D-printed equilibrium dialysis devices, as shown in Figure 2.8, were utilized to determine if all FITC was bound to the BSA. An equilibrium dialysis base plate was printed using a Stratasys J750 3D-printer (Stratasys, Eden Prairie, MN) in VeroClear with TangoBlack lined wells to provide a seal and prevent leaking between the buffer and sample compartments.¹⁹ A print-pause-print method was utilized to integrate the 3.5 kDa membrane in a membrane device that could be placed within the base plate. TangoBlack was utilized to create a seal, and VeroWhite was utilized for device structure.¹⁹ After the bottom half of the membrane device was printed, the operation was paused, and the

membrane was placed over the bottom half of the membrane device. Printing then resumed to seal the membrane into the device. The membrane device was placed perpendicularly inside of the equilibrium dialysis base plate for the experiment. 1 mL of 75 μ M BSA-FITC (prepared in AF-PSS) was added to the sample compartment on the right, and 1 mL of AF-PSS was added to the left buffer compartment. Incubation time was characterized previously and determined to be 6 h on a shaker incubator (37 °C) for this device.¹⁹ Following incubation, the solution was removed from the sample and buffer compartments and placed into separate vials. The sample compartment, buffer compartment, and BSA-FITC standards (0, 30, 45, and 75 μ M; prepared in AF-PSS) were diluted 1:100 and placed in triplicate into an opaque 96-well plate. Sample fluorescence was determined using a FlexStation-3 spectrophotometer (Molecular Devices LCC) at 485 nm excitation and 515 nm emission wavelengths.

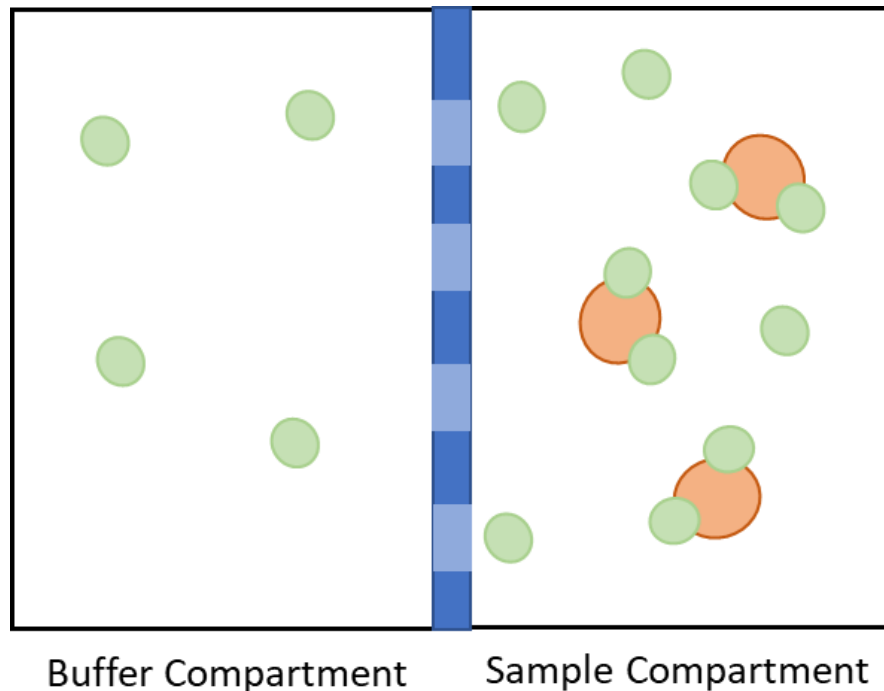


Figure 2.8: 3D-Printed Equilibrium Dialysis Device. BSA-FITC was placed in the sample compartment, and the free FITC traveled through the membrane to the buffer compartment for detection.

2.2.2. Isolation and Purification of RBCs for BSA-FITC Samples

Whole blood was collected from healthy donors by venipuncture into heparinized tubes (Fisher Scientific). The blood was centrifuged at 500 xg for 10 minutes at room temperature. The plasma and buffy coat were discarded through aspiration, and RBCs were washed by resuspending in normal PSS, while other RBCs were washed in AF-PSS. The RBCs were re-centrifuged, the buffer was removed by aspiration, and new buffer was added for a total of three washes. The hematocrit was determined utilizing a StatSpin® CritSpin™ microhematocrit centrifuge (Beckman Coulter, Brea, CA) and digital hematocrit reader (StatSpin® CritSpin™; Beckman Coulter). This quantitative value for the hematocrit could then be used to prepare dilutions for the RBC samples.

2.2.3. BSA-FITC Sample Preparation

A 30 μM BSA-FITC stock solution was prepared by dissolving BSA-FITC in AF-PSS. Since BSA does not fluoresce within the visible spectrum, a fluorophore (such as FITC) was required for detection. BSA-FITC was selected due to its commercial availability and its common use in fluorescent studies.^{20–23} Also, the fluorescence emission of FITC (515 nm) falls within one of the flow cytometer detectors (533 ± 30 nm).¹⁶ This stock was filtered through a 0.22 μm Millex Durapore® PVDF syringe filter (Millipore) and then diluted 1:10 with AF-PSS twice to obtain stocks 1-3. Stocks 2 and 3 were used to obtain the desired BSA-FITC concentrations (0, 90, 150, 200, 260, 300, 340, 380, and 500 nM). Samples were prepared containing 0.01% RBCs, increasing concentrations of BSA-FITC, and AF-PSS. Matching samples were made with the addition of 0.01% Immunoglobulin G (IgG; Sigma Aldrich) to act as a blocking agent for nonspecifically bound molecules. IgG is a common blocking agent and is the most common antibody *in vivo*.^{24,25} The sample vials were incubated at 37 °C for 2 h prior to nylon filtration for analysis on the flow cytometer. Validation beads were made with or without IgG and analyzed per manufacturer's protocol. Attempts were made to obtain lower BSA-FITC concentrations (0, 0.1, 0.5, 1, 1.5, 2, 3, 4, 4.5, 15, and 30 nM) to obtain lower BSA molecules/RBC ratios. The resulting fluorescence on the cells gated without aggregates was too low to be distinguished from the blank (calculated limit of detection was approximately 1,600 fluorescent events). The number of events that fell within those parameters were less than 20 events (if not zero), which was not significant in comparison to 10,000 events for calculations. Prior to these experiments, samples were also prepared with 0.05% RBC and increasing BSA-FITC concentrations (0, 75, 150, 300, and

450 μM), and AF-PSS to determine the level of BSA-FITC concentrations that would saturate the cell. However, FITC experiments were discontinued due to the linear increase in fluorescence with additional BSA-FITC rather than saturation. Therefore, a radiolabeling method was utilized to allow for direct albumin detection on the RBC by detecting gamma decay.

2.2.4 Technetium Labeling of Albumin

BSA was incubated with a 99.6 nM succinimidyl 6-hydrazinonicotinate (HYNIC; provided by Dr. Gary Bridger, AnorMED, Inc., Langley, British Columbia, Canada) kit for 1 h (all times were provided during training with the Zinn lab) where the conjugation occurred through the 1' amine groups on the BSA, which contains 59 lysine residues.^{26–28} The BSA-HYNIC was placed into a Slide-A-Lyzer™ 10K MWCO dialysis cassette (Thermo Scientific, Rockford, IL) to remove excess HYNIC. The dialysis cassette was placed into phosphate buffered saline (PBS; 10.1 mM Na_2HPO_4 (Sigma Aldrich), 2.7 mM KCl (Fisher Scientific), 136.9 mM NaCl (Sigma Aldrich), and 1.8 mM KH_2PO_4 (Sigma Aldrich) at pH 7.40) at 4 °C for 2 h before the PBS was replaced with new PBS and left overnight at 4 °C. The following morning, sodium pertechnetate (TcO_4^- , Cardinal Health, Swartz Creek, MI) was incubated with a previously prepared 0.25 mM SnCl_2 (Acros Organics, Geel, Belgium)/0.21 M tricine (Sigma Aldrich) kit for 15 minutes. The tin reduced the TcO_4^- , and the tricine acted as a co-ligand reagent to stabilize the complex with HYNIC.²⁹ A portion of this solution (150 μL ; determined by final sample activity because 200 μL resulted in samples that were too hot to obtain gamma decay values within the instrument's linear range) was then added to the BSA-HYNIC complex and incubated for an additional 30 minutes. After incubation, 1 mL of the solution was added

to a 10 mL 6K Pierce™ polyacrylamide desalting column (Thermo Scientific) to separate free ^{99m}Tc from BSA- ^{99m}Tc . The column was washed with 1 mL of PBS eight times, and the activity of each collected fraction was measured utilizing a CRC-25R dose calibrator (Capintec Inc., Florham Park, NJ). The first fraction with the highest activity was tested for free and colloidal ^{99m}Tc by thin layer chromatography (TLC) using Tec-control ^{99m}Tc chromatography strips (Biodex, Shirley, NY). The fraction was spotted (2 μL) onto two Tec-control dark green chromatography strips and placed into either PBS or methyl ethyl ketone (MEK; Acros Organics). After the solution reached the top of the strip, the top portion was cut off and both portions were analyzed using a 2480 WIZARD² automatic gamma counter (Perkin Elmer, Waltham, MA). The TLC strip in PBS provided the percentage of free ^{99m}Tc , as the smaller ^{99m}Tc traveled up the strip faster than the labeled BSA. The strip in MEK provided the percentage of colloidal ^{99m}Tc , as only TcO_4^- moved up the MEK solvent front.³⁰ MEK can separate TcO_4^- from other ^{99m}Tc phosphorous compounds like the insoluble TcO_2 , therefore, it demonstrated the ^{99m}Tc reduction was successful.³¹ In addition, a Lowry assay was completed for the selected fraction to determine the concentration of labeled BSA. Colorimetric assays, such as the Lowry assay, work by a color change proportional to the protein concentration.⁷

2.2.4.a HYNIC Kit Preparation

1.2 mg of HYNIC was diluted with 1 mL dimethylformamide (DMF; Acros Organics). For BSA-HYNIC kits, 23.8 μL of the prepared solution was required for a 1:1 mole ratio of BSA to HYNIC. The solution was pipetted into a 5 mL lyophilization vial (Wheaton, Millville, NJ), and the septum was loosely placed on top (Fisher Scientific). The vials were placed into the freeze-dryer (VirTis AdVantage, Gardiner, NY) that was

precooled to -80 °C. The vacuum (Leybold, Cologne, Germany) was set for 10 seconds and then freeze was selected for 45 minutes. The condenser was turned on, and after it reached -90 °C, the freezer was turned off, and the vacuum was turned on. The heat was turned to -70 °C, and the vials were left overnight. In the morning, the heat was set to 10 °C for 1 h. An air pump (Craftsman; Stanley Black and Decker, New Britain, CT) was attached to the freeze dryer, and the air valve was opened. The stopper was engaged three times to close the septa on the vials. Caps were screwed onto the vials and they were stored at -20 °C until required.

2.2.4.b Tricine/Tin Kit Preparation

3.6 mg of tricine (Sigma Aldrich) were placed in a beaker with 98 mL of 18.2 MΩ water. The pH was adjusted to 7.1 with NaOH while stirring. The solution was transferred to a vacuum flask prior to degassing the solution using a sonicator (Branson, Danbury, CT) and vacuum. Next, 80 mg of SnCl₂ (Acros Organics) were added to 1.7 mL of 100% ethanol (Decon Labs, Inc., King of Prussia, PA). After the tricine was completely degassed, 100 μL of SnCl₂ solution were added to the tricine and mixed. The solution was pipetted as 1 mL aliquots in 5 mL lyophilization vials (Wheaton). The freezer method from section 2.2.4.a. was followed to freeze dry these kits with a maximum of 30 vials prepared during a single lyophilization.

2.2.4.c BSA-HYNIC Conjugation

A 75 μM BSA stock was prepared in PBS. It is important to note that PSS or AF-PSS cannot be used because tris competes against BSA lysine groups during the HYNIC conjugation.³² 200 μL of the BSA stock and 600 μL of 0.15 M Na₂PO₄ buffer (pH

7.8) were added to the prepared HYNIC kit. After mixing, the vial was covered with aluminum foil and placed on a rocker (Thermo Scientific) for 1 h. The BSA-HYNIC was placed into a Slide-A-Lyzer™ 10K MWCO dialysis cassette (Thermo Scientific) using a 22 g 1.5” needle (BD Biosciences) and 5 mL syringe (BD Biosciences). The excess air was removed from the cassette. The dialysis cassette was placed into 400 mL of PBS at 4 °C for 2 h before the PBS was replaced with new PBS and left overnight at 4 °C. In the morning, the BSA-HYNIC was removed from the dialysis cassette utilizing a 22 g 1.5” needle and 1 mL syringe by injecting air prior to removing the sample.

2.2.4.d SEC Preparation

Polyacrylamide desalting columns (10 mL 6K Pierce™) were ordered from Thermo Scientific. Columns were visually checked for air bubbles, and these were removed using inversion, if necessary. Utilizing a column funnel, 10 mL of PBS were added to the open column. This process was repeated to further pack down the resin. The column bottom was then capped, excess resin was removed, and a fret was placed securely into the column mouth. The column was then capped and left overnight for next day labeling. If labeling would not occur the following day, the column was stored at 4 °C until needed.

2.2.4.e Lowry Assay

Reagents A-D were prepared: Reagent A (2% Na₂CO₃ (Jade Scientific, Canton, MI) in 0.1 N NaOH (Macron Fine Chemicals™; Avantor, Center Valley, PA), Reagent B (0.5% CuSO₄ · 5 H₂O (EMD, Gibbstown, NJ) in 1% potassium sodium tartrate (Alfa Aesar, Haverhill, MA)), Reagent C (50 mL Reagent A and 1 mL Reagent B), and Reagent D (Folin reagent (MP Biomedicals, Irvine, CA) diluted 1:1 with water). Reagents A-C could

be prepared prior to experiments, but Reagent D must be prepared on the day of the experiment. Approximately 25.0 mg BSA (recorded correctly and exactly) was placed in a 50 mL volumetric flask and diluted to mark with 18.2 Ω M water. This stock was used to prepare 6 vials of BSA Lowry standards (0, 20, 75, 150, 300, 500, and 600 μ L), which were all diluted to 700 μ L with 18.2 Ω M water. In addition, two samples were prepared from the desired BSA-^{99m}Tc fraction (50 and 75 μ L diluted to 700 μ L with 18.2 Ω M water). All standards and samples were prepared in 5 mL macrocentrifuge vials (VWR, Radnor, PA). 3.0 mL of Reagent C was pipetted into each vial and left for 10 minutes before adding 0.3 mL of Reagent D to each vial. Then each vial was inverted and incubated at room temperature for 30 minutes. Solution aliquots were transferred to 1.5 mL polystyrene cuvettes (DOT Scientific, Burton, MI), and absorbance values were read at 750 nm using a NanoDrop One spectrophotometer (Thermo Fisher). Standard absorbance values were plotted versus BSA mass (μ g), and sample BSA mass was determined by averaging the values given by the standard curve.

2.2.5 BSA-^{99m}Tc Sample Preparation

Once the concentration of BSA was determined through a Lowry assay, stocks were created between 4,000-6,000 nM in either AF-PSS or PSS (depending on the sample set; later decreased to 3,200 nM to conserve albumin). Samples were prepared with the desired amount of BSA-^{99m}Tc (0, 50, 100, 340, 775, 1,000, 1,600, and 2,700 nM), 7% RBCs (utilizing section 2.2.2 for 7% RBC due to microvasculature RBC concentration), and PSS (or AF-PSS). The samples were incubated for 2 h at 37 °C. Half of the samples were prepared with excess unlabeled BSA (PSS) to block BSA-^{99m}Tc binding, which demonstrates nonspecific binding, while the other half prepared without

excess unlabeled BSA (AF-PSS) to demonstrate total binding. In this way, the specific binding of BSA to RBCs could be calculated by subtracting the nonspecific binding of BSA from the total binding of BSA. In addition, BSA binding to the RBCs was analyzed with or without C-peptide or Zn^{2+} . After incubation, cells were centrifuged (750 xg for 1 minute) to allow for the supernatant to be removed, and AF-PSS was added. Cells were centrifuged again and washed five times with AF-PSS to remove loosely adsorbed proteins. Five washes were selected based on minimal changes in supernatant CPM between the fourth and fifth washes. Samples were then measured using a 2480 WIZARD² automatic gamma counter utilizing the ^{99m}Tc (140 KeV) method that measured samples for 20 seconds each. This process is depicted in Figure 2.9.

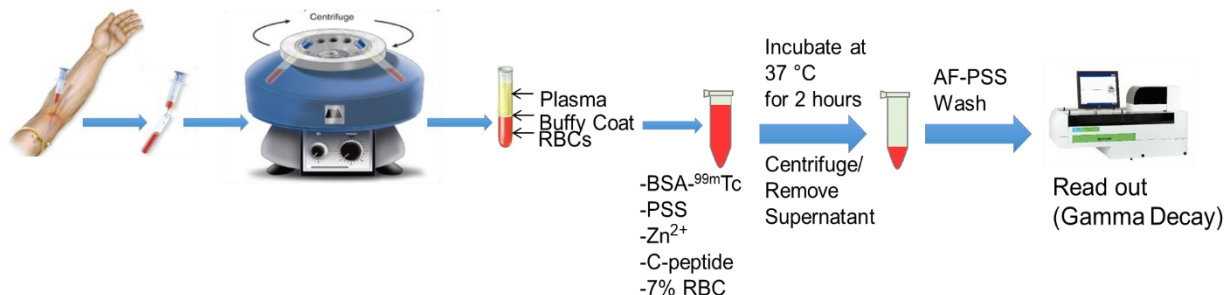


Figure 2.9: Isolation of RBCs and Sample Preparation. Whole blood was drawn from consenting donors and centrifuged/washed to separate plasma, buffy coat, and RBCs. Samples were prepared with isolated RBCs, BSA-^{99m}Tc, PSS, Zn²⁺, and C-peptide before a 2 h incubation at 37 °C. Samples were centrifuged, the supernatant was removed, and cells were washed with AF-PSS five times before the gamma decay was detected on the gamma counter.

Since the samples with and without C-peptide and Zn²⁺ were prepared on different days, an experiment was designed to allow for both samples to be analyzed on the same day from the same donor. In this experiment, only the highest BSA-^{99m}Tc concentration (2,700 nM) sample was prepared with or without C-peptide. In addition, the AF-PSS and

PSS samples were made for both with and without C-peptide so that specific binding could be determined.

2.2.5.a C-peptide Purification

Reverse-phase high performance liquid chromatography (HPLC; Shimadzu, Kyoto, Japan) was utilized to purify crude C-peptide (85% purity; Peptide 2.0, Chantilly, VA). An Atlantis T3 OBD Prep Column (10 mm x 150 mm; Waters, Milford, MA) was utilized during the separation. HPLC gradient parameters are shown in Table 2.1. The purified C-peptide was lyophilized overnight (Labconco Corporation, Kansas City, MO) and characterized using mass spectrometry (Waters, MA). A C-peptide ELISA (ALPCO, Salem, NH) was conducted to prepare 8 μ M stock solutions in 18.2 M Ω water for monthly use.

Table 2.1. C-peptide Purification HPLC Gradient Method. Solvent A: 0.1% HPLC-grade trifluoroacetic acid (TFA; EMD Millipore, Burlington, MA) in HPLC-grade water (Sigma Aldrich). Solvent B: 0.089% TFA/60% HPLC-grade acetonitrile (Sigma Aldrich) in HPLC-grade water.

Time (min)	Flow Rate (mL/min)	% Solvent A	% Solvent B
5	5	100	0
40	5	40	60
50	5	0	100
60	5	stop	stop

2.2.6. BSA-^{99m}Tc Gamma Counter Troubleshooting

Initially, BSA-^{99m}Tc standard curves were constructed with larger volumes of the diluted stock solutions (0, 286, 571, and 1,000 μ L to a total volume of 1,000 μ L in PSS or AF-PSS (with the 1,000 μ L standard remaining undiluted)) to encompass supernatant gamma decay readouts. This resulted in a calibration curve of counts per minute (CPM) in relation to BSA-^{99m}Tc values ranging from 0-300 μ g. However, the isolated RBC samples usually ranged from 0-5 μ g BSA-^{99m}Tc, therefore, it was determined to make smaller standards to better encompass the RBC sample range. The updated standard curve included volumes of 0, 2, 5, 10 and 15 μ L of the BSA-^{99m}Tc/PSS (or AF-PSS) stock diluted to 1,000 μ L with the appropriate buffer. In addition, two 10 μ L standards were made so one could be diluted further to 1,000 μ L using 50, 100, and 250 μ L of the standard. Overall, this resulted in a standard curve with 8 points between 0-9 μ g BSA-^{99m}Tc. However, the overall results were similar whether the higher or lower standards were utilized. Previous data, with the higher standards, were kept due to similar results. To prevent wait time for higher standard decay into the instrument's linear range (10,000-1,400,000 CPM), the lower standards were utilized moving forward.

The sample order on the instrument was also tested utilizing a 73 μ Ci tricine/tin-^{99m}Tc stock. The stock was aliquoted into two empty vials, one containing 20.5 μ L and the other containing 2 μ L, to obtain values within the linear range. Of the six sample wells in the gamma counter tray, four were blanks and two were the samples. The samples were rotated into ten different orders and the CPM results were compared. This determined that the position of the samples did not change the CPM. However, just to maintain consistency, the samples were always run in the same order. Albumin free

samples were run first (the sample blank to increasing concentrations and then the standard zero to increasing concentrations) and then the albumin containing samples were run second (the sample blank to increasing concentrations and then the standard zero to increasing concentrations).

2.2.7 BSA-^{99m}Tc and C-peptide Binding

An ultrafiltration separation method was utilized to confirm C-peptide bound to BSA-^{99m}Tc in a similar manner as unlabeled BSA.³³ Ultrafiltration cups, shown in Figure 2.10, were 3D-printed using a Stratasys J750 3D-printer to fit inside of a 1.7 mL centrifuge tube, and 20 kDa MWCO membranes (Spectra/Por, New Brunswick, NJ) and polycarbonate membrane filters (0.1 μm, 76 mm; Sterlitech Corporations, Kent, WA) were cut to fit inside of the cups using a 5 mm diameter hole punch. Computer-aided design (CAD; Autodesk Inventor Professional, San Rafael, CA) software was utilized to design the device in three separate .STL files. A print-pause-print method enabled integration of the membrane. The first file contained a thick layer of VeroClear (clear rigid material) with four small holes in the middle that allow solution to pass once the device is created. The second file consisted of three Tango (rubber-like material) layers that allow for the membrane insertion. The last file was also made from VeroClear to create a cup-like structure for the sample solution. The ultrafiltration device was previously optimized by Jacobs et al.³³⁻³⁵

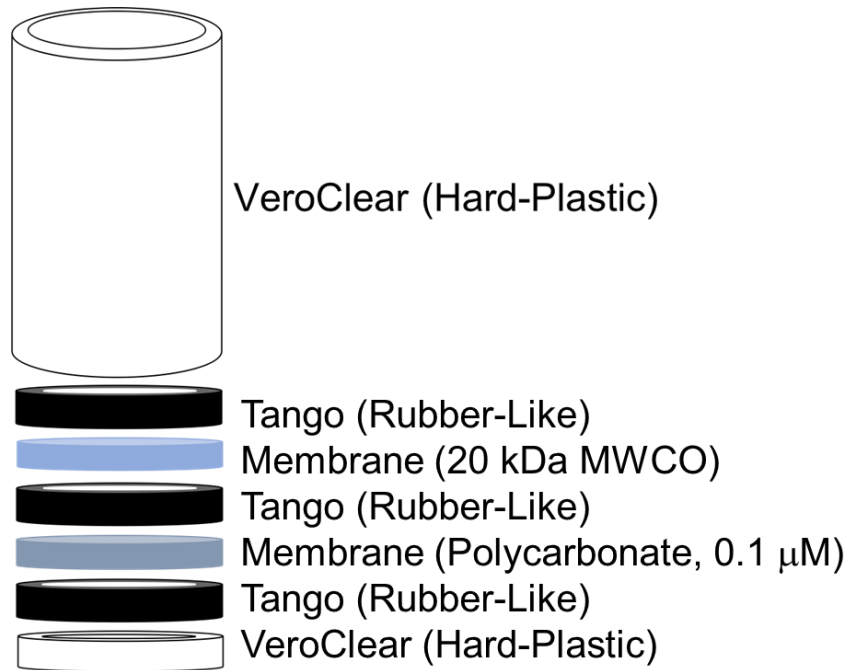


Figure 2.10: Ultrafiltration Device Manufacturing. A representation of the 3D-printed device used to separate the free C-peptide from C-peptide bound to BSA-^{99m}Tc. Figure adapted from Jacobs et al.

Samples contained either 2,700 nM BSA-^{99m}Tc and 20 nM C-peptide or 2,700 nM BSA and 20 nM C-peptide. In addition, 20 nM C-peptide controls were prepared without BSA. For each sample, 200 μ L of solution were added to separate filtration devices and centrifuged at 10,000 xg for 1 h. The filtered solution was diluted for C-peptide ELISA (ALPCO) to quantify the concentration of free C-peptide. The free C-peptide concentration was then subtracted from the total control to determine the concentration of bound C-peptide. The global affinity constant (nK_a'), used in cases with one point from a binding curve, could be calculated from the free fraction using the below equation.³⁶

$$\text{Equation 2.4: } nK_a' = \frac{1 - F}{F([P] - [A] + [A]F)}$$

where F is the measured free fraction, [P] is the total albumin concentration, and [A] is the total C-peptide concentration.³⁶

2.3 Results

2.3.1 PVDF Retention

The BSA-FITC stock that was filtered through the PVDF membrane had an average fluorescence of 3,957 (± 82) RFU, whereas the unfiltered stock had an average fluorescence of 4,156 (± 161) RFU (n=4, error=SEM). T-values were calculated using the Student's t-test equation,

$$\text{Equation 2.5: } t = \frac{y_1 - y_2}{\sqrt{\frac{s_1^2}{n_1} + \frac{s_2^2}{n_2}}}$$

where y_1 = average of value set one, y_2 = average of value set two, s_1 = standard deviation of value set one, s_2 = standard deviation of value set one, n_1 = number of values in value set one, and n_2 = number of values in value set two. The calculation resulted in $t=2.12$ and the t-table value was $t=3.182$ at 95% confidence interval and 3 degrees of freedom. Since the calculated t-value was less than the t-table value, the differences were not significant.

2.3.2 BSA-FITC Equilibrium Dialysis

The equilibrium dialysis experiment was successful in determining the concentration of free FITC in the BSA-FITC stock. The buffer compartment resulted in 0.9 (± 0.5) μM BSA-FITC, and the sample compartment resulted in 67.1 (± 1.7) μM BSA-FITC (n=3, error=SEM). Therefore, the total BSA-FITC was 68 μM , and the buffer compartment

was 1.5% of the total. In the scenario where 336 molecules of BSA bound per RBC, 1.5% of these, or about 5 molecules, are false due to the excess FITC. However, since the standard deviation in this example is 143 BSA molecules/RBC, 5 BSA molecules/RBC falls within the standard deviation. The free FITC does not significantly alter the results.

2.3.3 BSA-FITC/RBC Samples

The sample MESF values were calculated based off the validation bead calibration curves. The MESF value was converted to BSA molecules through the known FITC molecules/BSA, which was typically 14 moles FITC/mole albumin (as provided by the Sigma Aldrich Certificate of Analysis for BSA-FITC). In excess IgG, there were more BSA molecules per RBC than without IgG as shown in Figure 2.11. Since IgG should block nonspecific binding of BSA-FITC to the RBCs, it was expected that there would be less BSA molecules per RBC than without IgG. Therefore, the experimental results were opposite of the expected. Upon further literature review it was later discovered that IgG and albumin bind, which would account for more BSA-FITC binding in these experiments because IgG creates more binding sites.^{37,38} However, it was found that as more BSA-FITC was added, the fluorescence of the sample continued to increase as more BSA-FITC bound to cells.

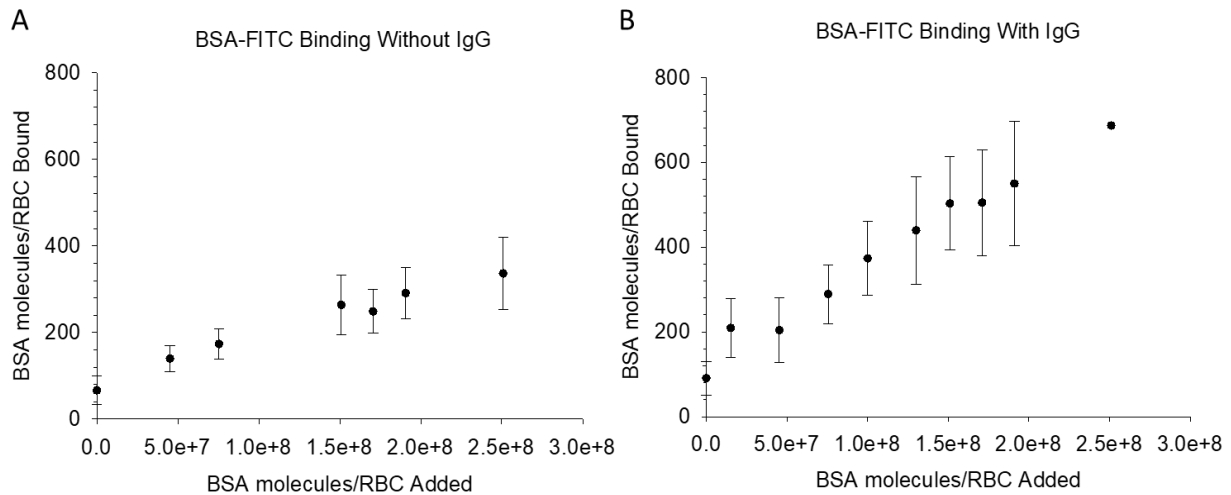


Figure 2.11: BSA molecules bound per RBC in response to BSA molecules added per RBC sample. A. The binding of BSA-FITC to RBC without IgG. B. The binding of BSA-FITC to RBC with IgG to act as a blocking agent. n=4, error=SEM.

As increasing concentrations of BSA-FITC were added to RBCs, there was a continued increase in fluorescence. This could signify that these concentrations are causing nonspecific binding and are past saturation. Data for BSA-FITC saturation was obtained prior to validation bead use, therefore, data is presented in terms of relative fluorescence as shown in Figure 2.12. Data is averaged after each day's blank was subtracted from their respective values. A linear trend was displayed with a coefficient of determination of 0.9986, signifying the linear trendline was accurately representing the data. As calculated, the correlation coefficient was 0.9993, indicating a strong positive correlation. As more BSA-FITC was added to the RBCs, fluorescence continued to increase. This could signify a nonspecific interaction or that saturation has long since been reached.

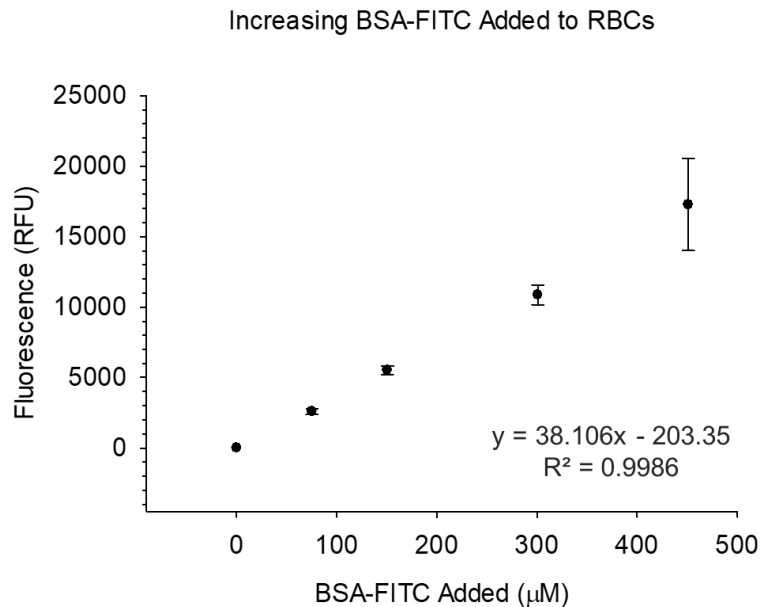


Figure 2.12: Increasing BSA-FITC Concentrations added to RBCs. Relative fluorescence units (RFU) as a function of increasing BSA-FITC concentrations (µM) added to RBC samples. An equation is displayed with a trendline fitted to the points. n=4, error=SEM.

2.3.4 BSA-^{99m}Tc Binding to RBCs

Determination of albumin binding to RBCs was performed by adding increasing concentrations (ranging from 0-2,700 nM) of BSA-^{99m}Tc to AF-PSS. A second sample was prepared by adding increasing BSA-^{99m}Tc concentrations (0-2,700 nM) to RBCs that were prepared in albumin-containing PSS. These blocking experiments, when subtracted from the AF-PSS binding, resulted in a specific binding curve that could be used to quantitatively determine the number of albumin molecules that were specifically bound to the RBC. The data in Figure 2.13 shows that BSA specifically binds to RBCs even in the absence of a binding ligand (such as C-peptide). The BSA specific binding saturated at an average of 14,021 (±1,489) BSA molecules/RBC. The resulting equilibrium

dissociation constant was $1.14 (\pm 0.07) \times 10^{-7}$ M, and the B_{\max} was $1.94 (\pm 0.02) \times 10^{-8}$ M or approximately 13,900 receptor molecules/RBC.

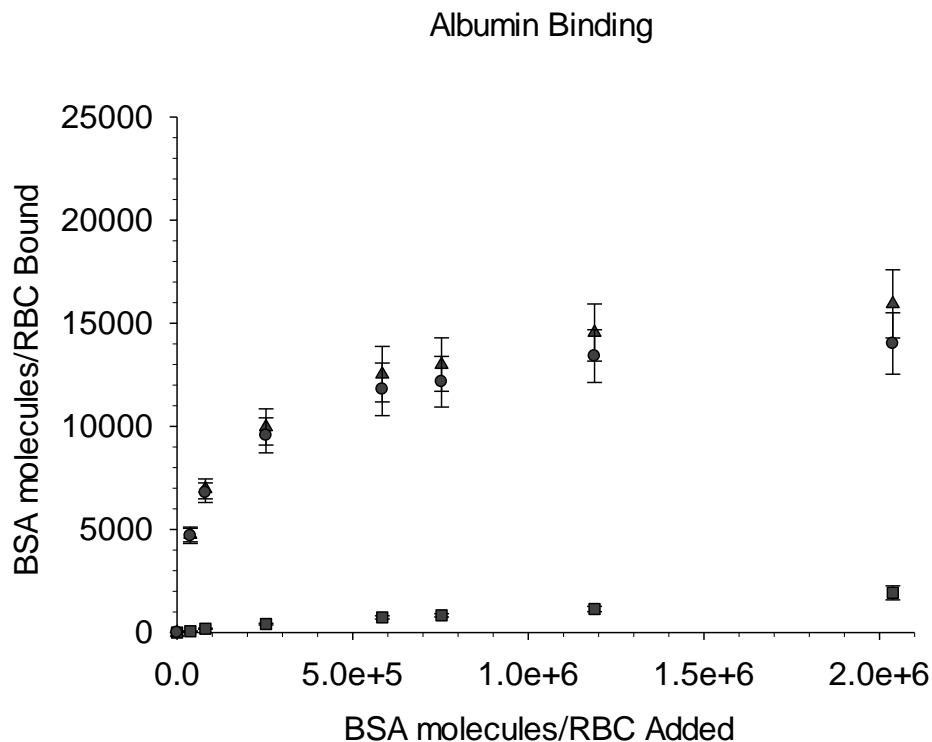


Figure 2.13: BSA-^{99m}Tc binding to RBCs. A saturation experiment conducted to determine the specific binding of BSA (circle) to RBCs. This was completed by preparing two sample types of BSA-^{99m}Tc with RBCs and subtracting the resulting data. One sample set was prepared in AF-PSS to represent total binding (triangle), and the other sample set was prepared in PSS so the excess unlabeled BSA could act as a blocking agent to demonstrate nonspecific binding (square). n=6, error=SEM.

2.3.5 BSA-^{99m}Tc and C-peptide Binding to RBCs

An experiment similar to that described above was performed, but in this case, both the albumin-containing and albumin-free samples contained C-peptide and Zn²⁺. The data in Figure 2.14 demonstrates specific binding of albumin to the RBCs in the presence of C-peptide and Zn²⁺, similar to the data in Figure 2.13. However, the BSA specific binding saturated at an average of 16,695 ($\pm 1,479$) BSA molecules/RBC. The

resulting equilibrium dissociation constant was $2.00 (\pm 0.05) \times 10^{-7}$ M, and the B_{\max} was $2.50 (\pm 0.01) \times 10^{-8}$ M or approximately 17,900 receptor molecules/RBC. The difference between BSA specific binding with or without C-peptide and Zn^{2+} was approximately 2,700 BSA molecules/RBCs when 2,700 nM BSA- ^{99m}Tc was added. The specific binding curves from both Figure 2.13 (without C-peptide or Zn^{2+}) and Figure 2.14 (with C-peptide and Zn^{2+}) were combined to demonstrate that more albumin specifically binds to RBCs in the presence of C-peptide and Zn^{2+} as shown in Figure 2.15.

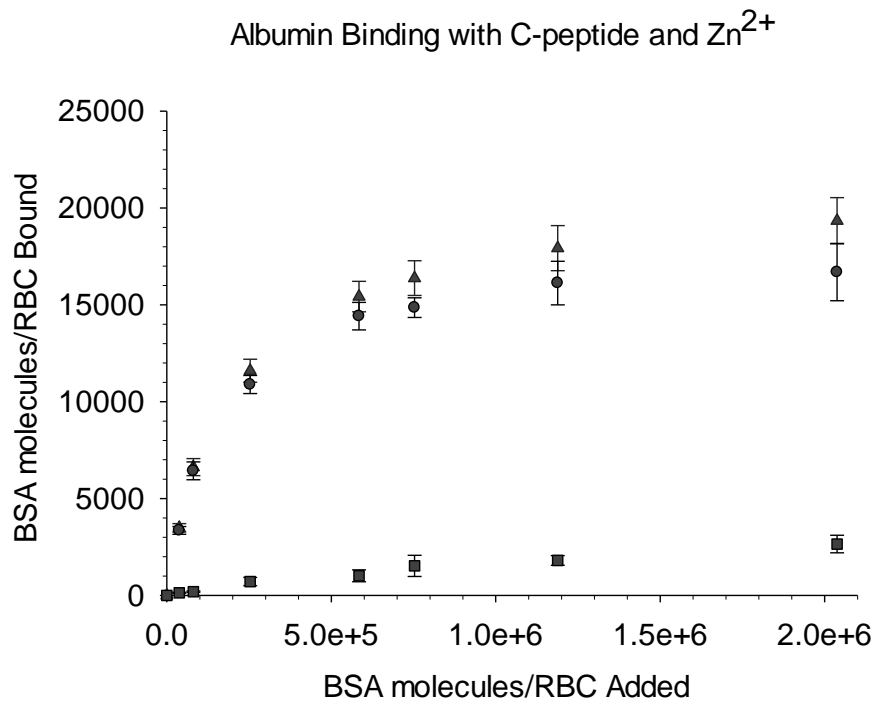


Figure 2.14: BSA- ^{99m}Tc binding to RBCs with C-peptide and Zn^{2+} . A saturation experiment conducted to determine the specific binding of BSA (circle) to RBC in the presence of C-peptide and Zn^{2+} . This was completed by preparing two sample types of BSA- ^{99m}Tc with RBCs and subtracting the resulting data. One sample set was prepared in AF-PSS to represent total binding (triangle), and the other sample set was prepared in PSS so the excess unlabeled BSA could act as a blocking agent to demonstrate nonspecific binding (square). $n \geq 4$, error=SEM.

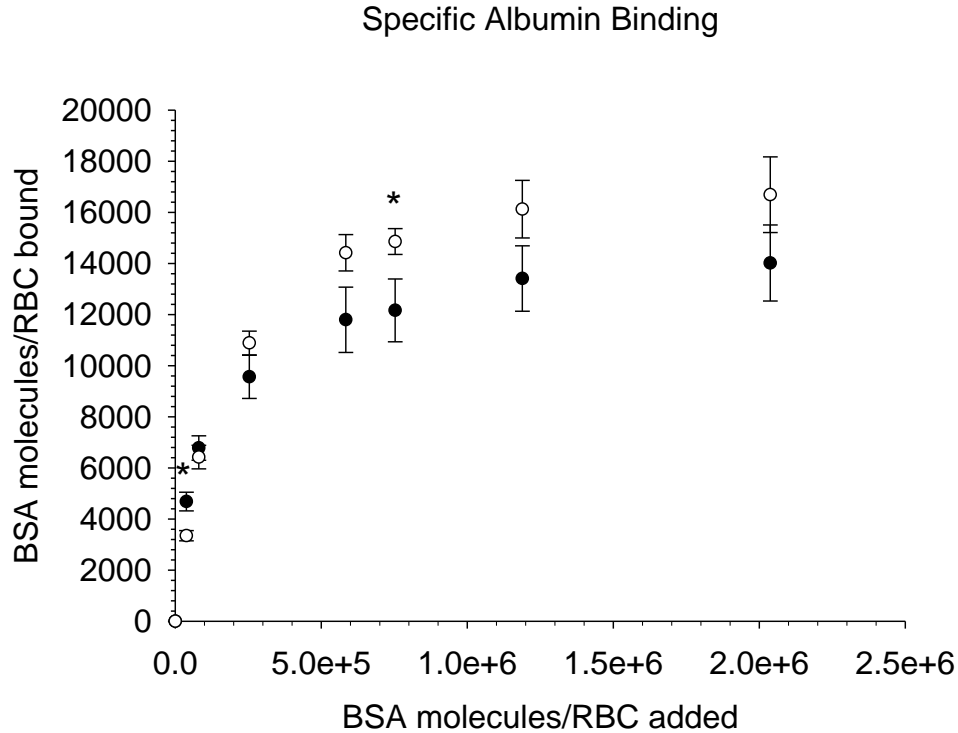


Figure 2.15: Specific Binding of BSA-^{99m}Tc to RBCs with and without C-peptide and Zn²⁺. The specific binding of BSA without C-peptide or Zn²⁺ (black) in comparison to the specific binding of BSA with C-peptide and Zn²⁺ (white) extracted from Figures 2.13 and 2.14. n≥4, error=SEM, *p<0.05.

The experiments shown in Figures 2.13 and 2.14 were conducted on different days from different blood donors; therefore, to improve experimental rigor, RBCs were prepared in 2,700 nM BSA-^{99m}Tc with and without C-peptide from RBCs drawn from a single donor and prepared on the same day. In addition, each sample was made in AF-PSS to show total binding and in albumin-containing PSS to show nonspecific binding as performed for the saturation experiments. In this way, it was possible to compare the difference in BSA specific binding with or without C-peptide on the same cells, and an average of 1,606 (±492) BSA molecules/RBC was determined as shown in Figure 2.16.

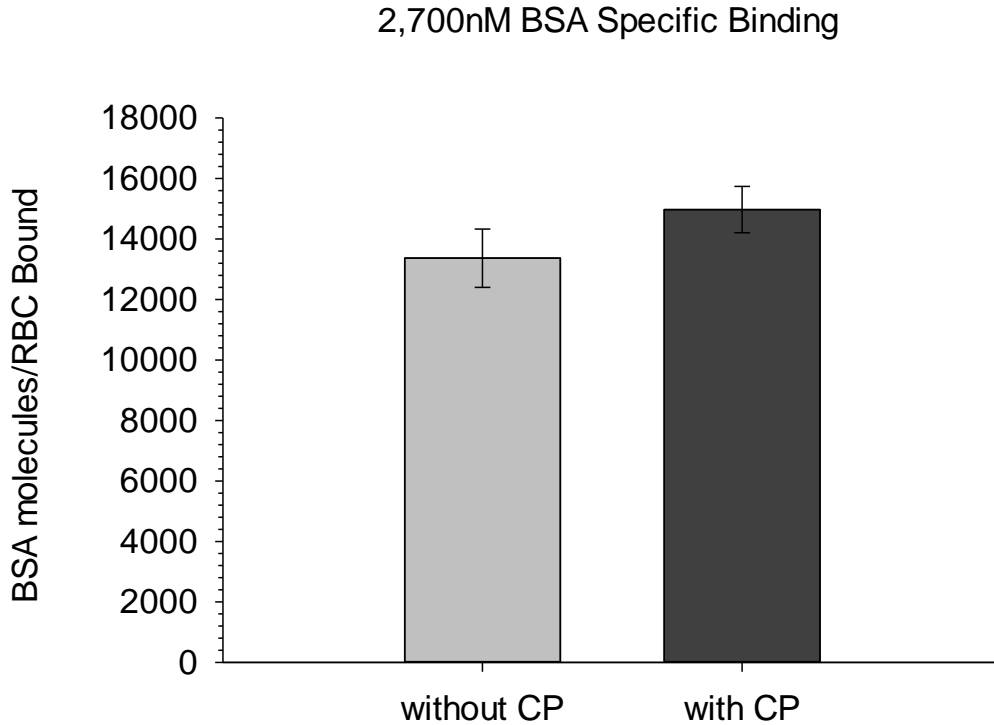


Figure 2.16: Specific Binding of BSA-^{99m}Tc to RBCs with or without C-peptide on the same donor RBCs. The specific binding of BSA without C-peptide (grey) in comparison to the specific binding of BSA with C-peptide (black). This experimental set up was conducted on the same day to compare the difference in BSA binding on the same donor cells. The albumin binding difference between with and without C-peptide is significantly different than zero ($p < 0.01$). $n = 5$, error = SEM.4

2.3.6 BSA-^{99m}Tc and C-peptide Binding

To demonstrate that BSA-^{99m}Tc was able to carry C-peptide in a similar manner as the unlabeled BSA, an ultrafiltration experiment was conducted to look at the binding of BSA to C-peptide. It was determined that BSA-^{99m}Tc was able to carry C-peptide in a similar manner as unlabeled BSA as shown in Figure 2.17. BSA-^{99m}Tc bound 18.8 (± 0.3) nM C-peptide with $nK_a' = 4.56 (\pm 1.04) \times 10^6 \text{ M}^{-1}$, whereas BSA bound 19.3 (± 0.2) nM with $nK_a' = 6.25 (\pm 1.08) \times 10^6 \text{ M}^{-1}$.

C-peptide Bound to BSA

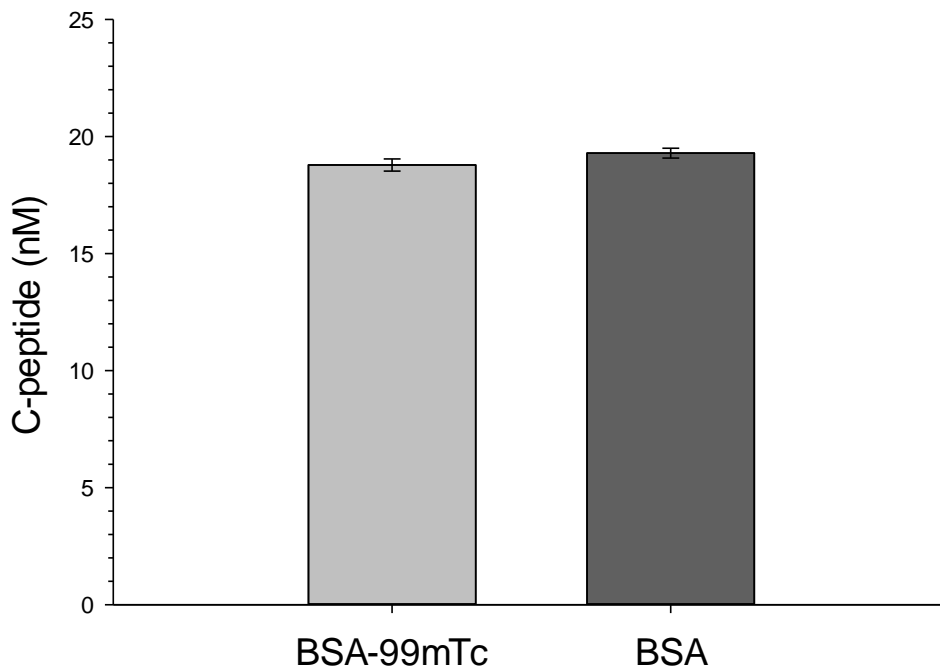


Figure 2.17: The binding of C-peptide to BSA-^{99m}Tc and BSA. A bar graph representing the binding of C-peptide to labeled (^{99m}Tc) and unlabeled BSA. BSA-^{99m}Tc bound 18.8 (±0.3) nM C-peptide with $nK_a = 4.56 (\pm 1.04) \times 10^6 \text{ M}^{-1}$, whereas BSA bound 19.3 (±0.2) nM with $nK_a = 6.25 (\pm 1.08) \times 10^6 \text{ M}^{-1}$. Values demonstrated no significant difference. $n=6$, error=SEM, $p>0.1$.

2.4 Discussion

Determining albumin binding to RBCs utilizing flow cytometry and BSA-FITC determined to be a problematic experiment. When increasing BSA-FITC concentrations, the fluorescence continued to increase. This could either signify that saturation had not been reached or that saturation had already been achieved, and the binding was nonspecific. In the flow cytometry samples, BSA-FITC was added to RBCs in ratios ranging from 0-3.0 x 10⁸ BSA molecule/RBC and still measuring a continued increase. In the gamma counter samples, BSA-^{99m}Tc was added to RBCs in ratios ranging from 0-2.0

$\times 10^6$ BSA molecules/RBC and seeing a saturation curve. This indicates that the BSA-FITC concentrations were too high to see the saturation curve. However, when BSA-FITC samples were prepared ranging from 0- 2.2×10^6 BSA molecules/RBC, the resulting fluorescence values were too low for differentiation from the blank on the flow cytometer. In addition, the standards prepared for the flow cytometer are commercially available MESF beads, rather than standards made from the stock (as in the case of the gamma counter method). This may skew the resulting BSA molecules/RBC bound values, which is why those figures show much lower values of albumin bound per RBC. Using beads has been criticized because they are synthetic rather than the biological samples they are supposed to represent.³⁹ This could affect the light scattering patterns, therefore, not being a sufficient standard representation. In conclusion, utilizing the gamma counter for albumin binding to RBCs is the best method of these two, since the instrument can detect the lower BSA molecules to RBC ratios.

The findings from this study correspond to the 1983 study at the University of California, San Francisco, which demonstrated that albumin-ligand complexes interact specifically with RBCs. It was estimated that the K_d value was on the order of 10^{-6} M, and the number of sites per cell was approximately 10^4 .¹⁰ However, the authors noted that the binding site nature is unknown.¹⁰ The K_d findings from this current study were on the order of 10^{-7} M, whereas results from the 1983 UCSF study were on the order of 10^{-6} M. However, the 1987 UCSF study indicated the apparent K_d was reported to be 208 (± 143) nM. When converted to similar terms, $2.08 (\pm 1.43) \times 10^{-7}$ M is comparable to the resulting K_d from this study of $1.14 (\pm 0.07) \times 10^{-7}$ M.¹¹ Since the K_d is smaller in this study, the albumin/RBC albumin receptor has a stronger affinity than previously believed. The B_{max}

data from this study were on the order of 10^{-8} M, which corresponds to 10^4 (approximately 13,900) number of sites per cell. This finding was on the same order of magnitude as the findings from the 1983 UCSF study of 10^4 binding sites per cell and the 1987 study with binding sites per cell being $2.1 (\pm 2.0) \times 10^4$.¹¹ The slight differences in values could possibly be due to variations in the albumin labeling techniques as this study utilized ^{99m}Tc , and the previous study utilized ^{125}I .¹¹ In addition, samples were incubated for 2 h at 37 °C in this experiment and 30 minutes at 4 °C in the previous experiment.¹¹ Typically rate constants are measured at 4 °C or room temperature, however for physiological relevant studies, it is more logical to utilize 37 °C for measurements.⁴⁰ Previous studies have suggested that the increased temperature may result in a decrease in the affinity; however, it was determined to not be as simplistic as previously believed, as not all antibodies are affected by temperature changes in the same manner.⁴⁰ The albumin receptor may not interact in this manner, as the increase in temperature in this experiment resulted in a higher affinity, than the previous study at a lower temperature. The increase in BSA binding to RBCs in the presence of C-peptide and Zn^{2+} compared to without C-peptide and Zn^{2+} was approximately 2,700 BSA molecules/RBC on separate cells and 1,600 BSA molecules/RBC on the same cells. These values are of particular interest in comparison to the 1,800 C-peptide molecules/RBC when analyzing C-peptide binding.⁵

The important takeaway of this research is that not only does an albumin receptor exist on RBCs, but also a separate albumin/C-peptide complex receptor. However, the nature of the receptor is still unknown currently. It is possible that the binding of albumin/C-peptide to the receptor could result in endocytosis of the entire complex and

then dissociation of the C-peptide prior to the return of albumin to the plasma.⁴¹ In another instance, the complex could result in a signaling function without endocytosis.⁴¹

Overall, chapter 2 describes that the specific binding of albumin to RBCs is higher in the presence of C-peptide, indicating two separate RBC receptors. Since groups have been searching for a receptor solely for C-peptide rather than an albumin/C-peptide complex, these findings could change how future researchers conduct their experiments. Further investigation into an albumin/C-peptide complex receptor will put us on the right track for implementing C-peptide as part of the T1D therapeutic regimen.

REFERENCES

REFERENCES

- (1) Yosten, G. L. C.; Kolar, G. R.; Redlinger, L. J.; Samson, W. K. Evidence for an Interaction between Proinsulin C-Peptide and GPR146. *J. Endocrinol.* **2013**, *218* (2), B1–B8.
- (2) Lindfors, L.; Sundström, L.; Fröderberg Roth, L.; Meuller, J.; Andersson, S.; Kihlberg, J. Is GPR146 Really the Receptor for Proinsulin C-Peptide? *Bioorganic Med. Chem. Lett.* **2020**, *30* (13).
- (3) Janabi, A. M. H. Proinsulin C-Peptide-Mediated Signalling and the Search for Its Receptor, University of Leicester, 2017.
- (4) Meyer, J. A.; Froelich, J. M.; Reid, G. E.; Karunaratne, W. K. A.; Spence, D. M. Metal-Activated C-Peptide Facilitates Glucose Clearance and the Release of a Nitric Oxide Stimulus via the GLUT1 Transporter. *Diabetologia* **2008**, *51* (1), 175–182.
- (5) Liu, Y.; Chen, C.; Summers, S.; Medawala, W.; Spence, D. M. C-Peptide and Zinc Delivery to Erythrocytes Requires the Presence of Albumin: Implications in Diabetes Explored with a 3D-Printed Fluidic Device. *Integr. Biol.* **2015**, *7*, 534–543.
- (6) Invitrogen Corporation. Theory of Binding Data Analysis. In *Fluorescence Polarization Technical Resource Guide*; 2006; pp 7-1-7–18.
- (7) Sanders, C. R. *Biomolecular Ligand-Receptor Binding Studies: Theory, Practice, and Analysis*; Vanderbilt University: Nashville, 2010.
- (8) Limbird, L. E.; Motulsky, H. Receptor Identification and Characterization. In *Handbook of Physiology- Cellular Endocrinology*; Wiley-Blackwell: Hoboken, 1998; pp 49–67.
- (9) Williams, M.; Jacobson, K. A. Radioligand Binding Assays for Adenosine Receptors. In *Adenosine and Adenosine Receptors*; Williams, M., Ed.; Springer Science & Business Media: Clifton, 1990; pp 17–56.
- (10) Ockner, R. K.; Weisiger, R. a; Gollan, J. L. Hepatic Uptake of Albumin-Bound Substances: Albumin Receptor Concept. *Am. J. Physiol.* **1983**, *245* (1), G13–G18.
- (11) Wright, T. L.; Lysenko, N.; Ockner, R. K.; Weisiger, R. A. Interaction of Natural and Synthetic Albumin Polymers with Hepatocytes. *Hepatology* **1987**, *7* (2), 294–301.
- (12) GraphPad. Equation: Two site binding <https://www.graphpad.com> (accessed Aug 5, 2020).

- (13) Steinhard, J.; Krijn, J.; Leidy, J. G. Differences between Bovine and Human Serum Albumins: Binding Isotherms, Optical Rotatory Dispersion, Viscosity, Hydrogen Ion Titration, and Fluorescence Effects. *Biochemistry* **1971**, *10* (22), 4005–4015.
- (14) Belatik, A.; Hotchandani, S.; Carpentier, R.; Tajmir-Riahi, H. A. Locating the Binding Sites of Pb(II) Ion with Human and Bovine Serum Albumins. *PLoS One* **2012**, *7* (5), 1–9.
- (15) BD Biosciences. Flow Cytometry Technical Bulletin <https://www.bdbiosciences.com> (accessed Mar 26, 2020).
- (16) BD. BD Accuri™ C6 Plus Flow Cytometry within Reach.™.
- (17) Hara, T.; Hirasawa, A.; Sun, Q.; Koshimizu, T.; Itsubo, C.; Sadakane, K.; Awaji, T.; Tsujimoto, G. Flow Cytometry-Based Binding Assay for GPR40 (FFAR1; Free Fatty Acid Receptor 1). *Mol. Pharmacol.* **2009**, *75* (1), 85–91.
- (18) Weizmann Institute of Science. Flow Cytometry: Sample Preparation https://www.weizmann.ac.il/LS_CoreFacilities (accessed Aug 5, 2020).
- (19) Pinger, C. W.; Heller, A. A.; Spence, D. M. A Printed Equilibrium Dialysis Device with Integrated Membranes for Improved Binding Affinity Measurements. *Anal. Chem.* **2017**, *89* (14), 7302–7306.
- (20) Benz, C.; Wiznitzer, S.; Lee, S. Flow Cytometric Analysis of Fluorescein-Conjugated Estradiol (E-BSA-FITC) Binding in Breast Cancer Suspensions. *Cytometry* **1985**, *6* (3), 260–267.
- (21) Kuo, C.-F.; Tsao, N.; Chou, H.-H.; Liu, Y.-L.; Hsieh, W.-C. Release of FITC-BSA from Poly (l-Lactic Acid) Microspheres Analysis Using Flow Cytometry. *Colloids Surf B Biointerfaces* **2012**, *89*, 271–276.
- (22) Breen, C. J.; Raverdeau, M.; Voorheis, H. P. Development of a Quantitative Fluorescence-Based Ligand-Binding Assay. *Sci. Rep.* **2016**, *6* (25769).
- (23) Guindani, C.; Frey, M.-L.; Simon, J.; Koynov, K.; Schultze, J.; Ferreira, S. R. S.; Araujo, P. H. H.; De Oliveira, D.; Wurm, F. R.; Mailander, V.; et al. Covalently Binding of Bovine Serum Albumin to Unsaturated Poly(Globalide-Co-E-Caprolactone) Nanoparticles by Thiol-Ene Reactions. *Macromol. Biosci.* **2019**, *19* (10).
- (24) Lewis, M. A guide to selecting control and blocking agents www.jacksonimmuno.com (accessed Jan 29, 2021).
- (25) Thompson, E. Gregory, Husney, Adam, Gabica, M. J. Immunoglobulins www.uofmhealth.org (accessed Jan 29, 2021).

- (26) Meszaros, L. K.; Dose, A.; Biagini, S. C. G.; Blower, P. J. Hydrazinonicotinic Acid (HYNIC) - Coordination Chemistry and Applications in Radiopharmaceutical Chemistry. *Inorganica Chim. Acta* **2010**, 363 (6), 1059–1069.
- (27) Surfraz, M. B. U.; King, R.; Mather, S. J.; Biagini, S.; Blower, P. J. Technetium-Binding in Labelled HYNIC-Peptide Conjugates: Role of Coordinating Amino Acids. *J. Inorg. Biochem.* **2009**, 103 (7), 971–977.
- (28) Peters, T. The Albumin Molecule: Its Structure and Chemical Properties. In *All About Albumin*; Academic Press: New York, 1995; pp 9–75.
- (29) Tait Research Laboratory. *Preparation of Lyophilized Tin Tricine Reagent*, 2000.
- (30) Zinn, K. R.; Chaudhuri, T. R.; Smyth, C. A.; Wu, Q.; Liu, H. G.; Fleck, M.; Mountz, J. D.; Mountz, J. M. Specific Targeting of Activated Endothelium in Rat Adjuvant Arthritis with a ^{99m}Tc-Radiolabeled e-Selectin-Binding Peptide. *Arthritis Rheum.* **1999**, 42 (4), 641–649.
- (31) Owunwanne, A.; Weber, D. A.; Mara, R. E. O. Factors Influencing Paper Chromatographic Analysis of Technetium-99m Phosphorus Compounds: Concise Communication. *J. Nucl. Med.* **1978**, 19, 534–538.
- (32) Solulink. *Protein-Protein Conjugation Kit Technical Manual*; 2011.
- (33) Jacobs, M. J.; Pinger, C. W.; Castiaux, A. D.; Maloney, K. J.; Spence, D. M. A Novel 3D-Printed Centrifugal Ultrafiltration Method Reveals in Vivo Glycation of Human Serum Albumin Decreases Its Binding Affinity for Zinc. *Metallomics* **2020**, No. 12, 1036–1043.
- (34) Pinger, C. Novel Analytical Tools for Studying a Potential Type-1 Diabetes Therapy, Michigan State University, 2018.
- (35) Castiaux II, A. 3D Printing in the Biosciences: Applications for Diabetic Complications, Michigan State University, 2018.
- (36) Zheng, X.; Li, Z.; Podariu, M. I.; Hage, D. S. Determination of Rate Constants and Equilibrium Constants for Solution-Phase Drug-Protein Interactions by Ultrafast Affinity Extraction. *Anal. Chem.* **2014**, 86 (13), 6454–6460.
- (37) Eilat, D.; Fischel, R.; Zlotnick, A. Albumin-Immunoglobulin Complexes in Human Serum: Classification and Immunochemical Analysis. *Scand. J. Clin. Lab. Invest.* **1981**, 14 (1), 77–88.
- (38) Hansen, O. P.; Hansen, T. M.; Jans, H.; Hippe, E. Red Blood Cell Membrane-Bound IgG: Demonstration of Antibodies in Patients with Autoimmune Haemolytic Anaemia and Immune Complexes in Patients with Rheumatic Diseases. *Clin. Lab. Haematol.* **1984**, 6 (4), 341–349.

- (39) Al-isawi, Z. J. Role of C-Peptide in the Vasculature, University of Leicester, 2019.
- (40) Johnstone, R. W.; Andrew, S. M.; Hogarth, M. P.; Pietersz, G. A.; McKenzie, I. F. C. The Effect of Temperature on the Binding Kinetics and Equilibrium Constants of Monoclonal Antibodies to Cell Surface Antigens. *Mol. Immunol.* **1990**, *27* (4), 327–333.
- (41) Weisiger, R. A. Functions of the Liver. In *Textbook of Hepatology: From Basic Science to Clinical Practice*; Rodes, J., Benhamou, J.-P., Blei, A., Reichen, J., Rizzetto, M., Eds.; Blackwell Publishing: Malden, 2007; pp 250–255.

Chapter 3- Binding of Albumin in Diseased States

3.1. Introduction

3.1.1 Glycated Albumin in T1D

Albumin is prone to glycation (a non-enzymatic mechanism where sugar molecules adhere to sites on other molecules) due to its high content of lysine and arginine residues.¹ In non-enzymatic glycation, or the Maillard reaction, sugar molecules, such as glucose or fructose, spontaneously interact with these amine containing amino acids on albumin.¹⁻³ This nucleophilic attack of the sugar on the amine groups results in a Schiff base, which undergoes a slow rearrangement to the more stable, irreversible Amadori product.^{1,3,4} Oxidation, dehydration, and crosslinking results in the irreversible production of advanced glycation end products (AGEs) as shown in Figure 3.1.^{1,3,4}

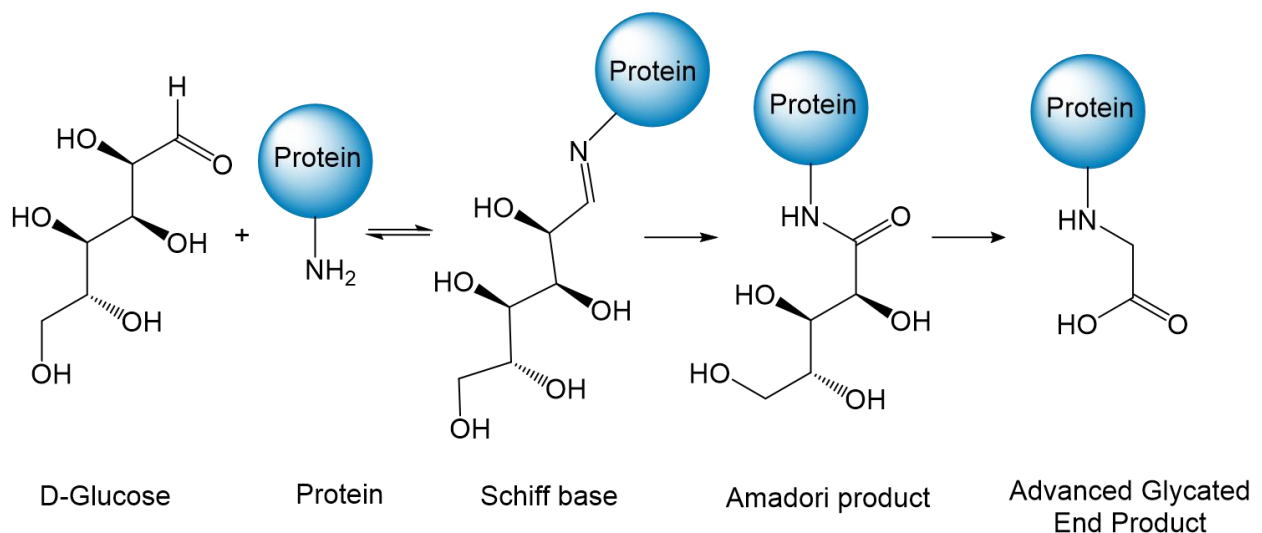


Figure 3.1: The Maillard Reaction. The mechanism of albumin glycation showing the Schiff base and Amadori product intermediates and the final advanced glycation end product (AGE).

The Maillard reaction, first discovered 100 years ago, is a physiological pathway to identify amino acids for turnover (the rate that amino acids are used and replaced).^{5,6} However, the persistent hyperglycemic conditions in T1D results in the acceleration of AGE formation.⁵ Glycation has been found to have effects on albumin's structure and function.^{4,7,8} Several studies have found that glycation impairs albumin's ability to bind ions and molecules.⁸⁻¹⁰ Since glycation has been shown to affect drug binding to Sudlow's Site II, but not Site I (the two main ligand binding sites on albumin), this indicates that some sites are not affected by glycation.^{11,12} More generally, AGEs have been found to cause damage to the blood vessel wall and limit extracellular matrix protein transport.¹³ A correlation had been reported between AGE levels and the development of diabetic neuropathy and retinopathy.^{14,15}

In healthy individuals, a normal range of glycated albumin is below 3%, as set by over half of scientific and clinical reports.^{4,16,17} However, normal glycation levels have been reported to be 17% in other studies.² It has been reported that the level of glycated albumin increases to 23% in T1D due to the higher blood glucose levels.¹⁸ Values differentiate depending on the method used to determine the glycation percentage. However, all groups agree that glycated albumin levels in patients with T1D is 2-5 times higher than healthy individuals.¹⁷ Measuring glycated albumin is a good reflection of the mean glycemic levels in the circulation over two to three weeks.^{1,2} Glycated albumin is measured by comparing the ratio of glycated albumin peak area to the total albumin peak area with common methods such as affinity chromatography, HPLC, and ion exchange chromatography.^{1,4} However, these methods are time consuming for clinical methods and therefore, an automated enzymatic assay (Lucica GA-L kit) has been developed.^{1,19}

3.1.1.a Glycated Albumin Binding to Zn²⁺ and C-peptide

Utilizing a syringe ultrafiltration method, our group previously analyzed the binding of glycated albumin to Zn²⁺ and C-peptide. The percentage of free Zn²⁺ was analyzed in normal HSA (nHSA), glucose-containing nHSA, and glycated HSA (gHSA) samples. The percent of free Zn²⁺ in nHSA (3.2 (±1.7)%) and glucose-containing nHSA (4.2 (±1.4)%) samples were not statistically different as shown in Figure 3.2.²⁰ There was a statistical difference (p<0.05) between the percentage of free Zn²⁺ in the gHSA (9.1 (±3.2)%) and nHSA samples.²⁰ These data indicate that nHSA and gHSA bind Zn²⁺ with different affinities.

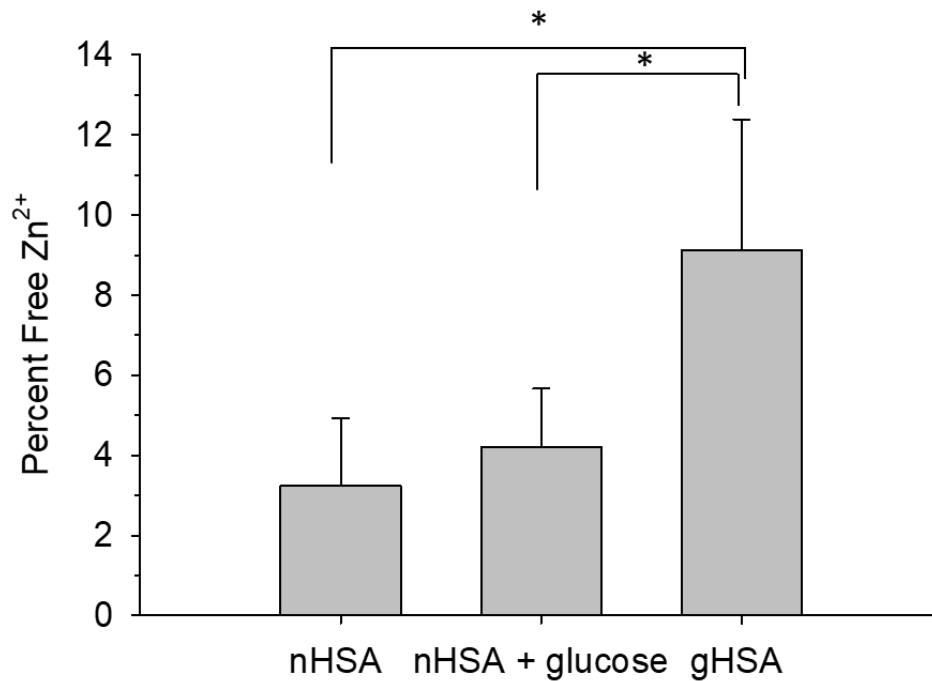


Figure 3.2: Normal or Glycated Albumin Binding to Zn²⁺. The percentage of free Zn²⁺ was analyzed for normal HSA (n=3), normal HSA in a glucose environment (n=5), and glycated HSA (n=5). The gHSA sample was statistically higher than nHSA. *p<0.05, error=standard deviation. Image borrowed from Pinger, C., 2018.

When analyzing C-peptide binding to nHSA and gHSA, there was no statistical difference between the percentage of free C-peptide (22.3 (±6.2)% and 21.2 (±7.4)%,

respectively) as shown in Figure 3.3.²⁰ This indicates that nHSA and gHSA bind C-peptide with equal affinities. When analyzing the RBC uptake of C-peptide in the presence of nHSA and gHSA, significantly less C-peptide bound to the RBCs with gHSA (0.8 (\pm 0.1) pmol) compared to nHSA (1.4 (\pm 0.1) pmol).²⁰ In addition, the RBC-derived ATP release was analyzed with C-peptide, Zn^{2+} , and either nHSA or gHSA. There was a 2.1 (\pm 0.2) fold increase in the nHSA sample's chemiluminescence intensity compared to the RBC control, which indicated significantly increased ATP release.²⁰ There was only a 1.4 (\pm 0.4) fold increase between the gHSA sample and the RBC control chemiluminescence intensity, which indicated no statistical difference in ATP release.²⁰ Overall, this indicates that even if gHSA binds C-peptide with a similar affinity as nHSA, the function of C-peptide when bound to the RBC is negatively affected when in the presence of gHSA.

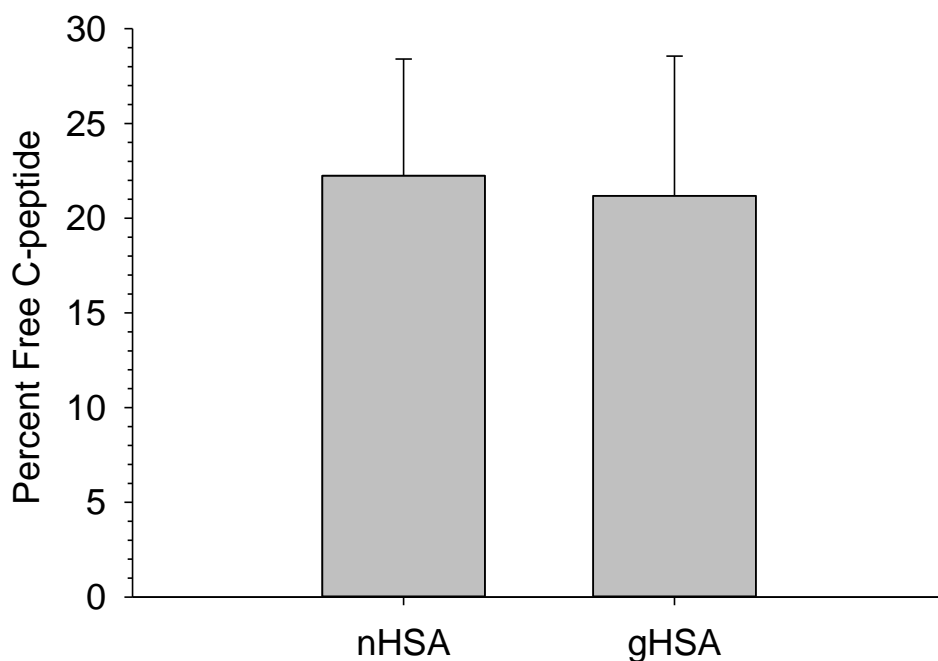


Figure 3.3: Normal or Glycated Albumin Binding to C-peptide. The percentage of free C-peptide was analyzed for normal HSA and glycated HSA. There was not a statistical difference. n=3, error=standard deviation. Image borrowed from Pinger, C., 2018.

3.1.2 Multiple Sclerosis

C-peptide and Zn^{2+} binding to RBCs were shown to be affected in the glycated conditions associated with T1D, therefore their delivery may be different in various disease states. Multiple Sclerosis (MS), a chronic inflammatory disease, entirely affects the central nervous system (CNS).²¹⁻²⁴ The CNS is comprised of the brain, spinal cord, and retina.²⁵ It is responsible for cognition, movement, senses, and emotions.²⁵ The brain is comprised of gray matter, which contains neuronal cells, and white matter, which contains myelinated axons.²⁵ Tight junctions in the cerebral endothelial cells (CEC) forms the blood-brain barrier (BBB) that limits diffusion of molecules and other foreign components into the CNS.^{25,26} Without the BBB, several molecules would flow into the

CNS that would disrupt function and lead to neural injury.²⁶ The functional unit of the CNS, known as a neuron, processes information through axons (electrical signals) and synapses (chemical signals).²⁵ The axons are covered in myelin produced by oligodendrocytes (a glial cell).²⁵ This myelin sheath is important for nerve signals.²⁵ However, in MS, inflammation occurs around the myelin sheath and it becomes damaged as shown in Figure 3.4, which results in lesion formation and slowing of conducted nerve signals.^{21,27} This damage to the brain and spinal cord may be facilitated by T-cells, both helper (CD4⁺) and cytotoxic (CD8⁺).^{23,28,29} MS received its name from the multiple scar lesions that result from this damage.²⁷ The resulting interference with signal conduction results in complications due to the inability to control vital functions.²⁵ People with MS often experience visual impairment, issues with walking or use of hands due to motor disturbances, incontinence, and sensory disruptions such as loss of touch, pain, and temperature.^{21,23} Macrophages and microglia mediate demyelination and phagocytosis of myelin debris, therefore, their presence could indicate continued myelin destruction.^{29,30}

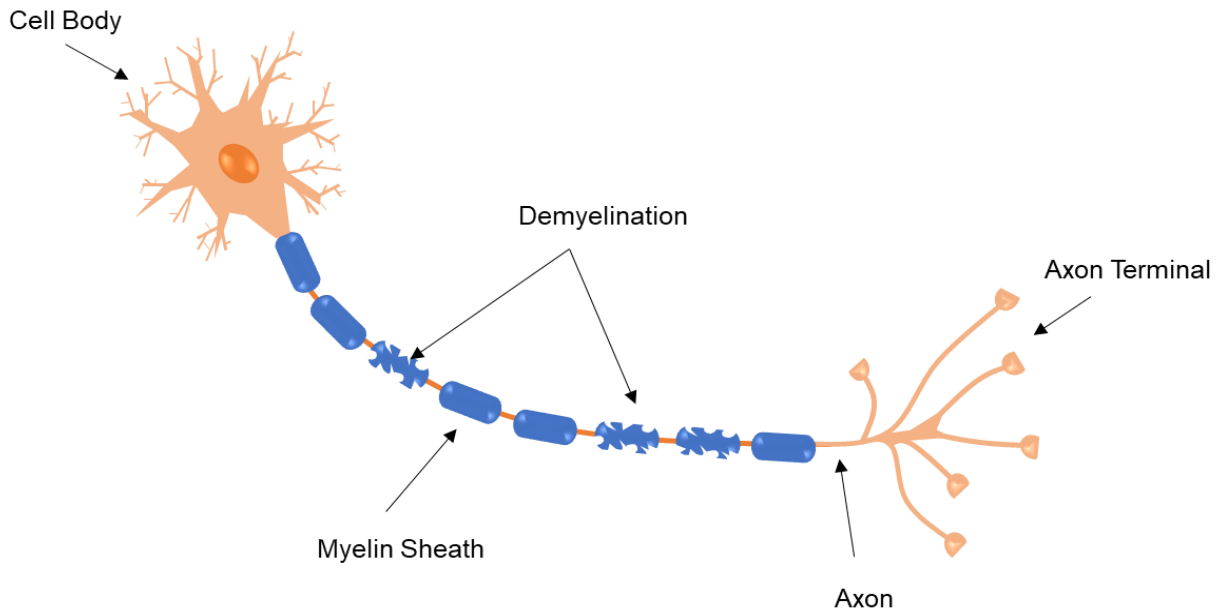


Figure 3.4: Depiction of a neuron. The neuron consists of the cell body, axon, myelin sheath, and axon terminal. In MS, demyelination (damage to the myelin sheath) occurs.

MS is the most widespread progressive neurological condition of young adults worldwide.³¹ Previously believed to be much lower, it is estimated that 730,000 adults are affected by MS in the United States and more than 2 million adults worldwide.^{21,23,31} More women are diagnosed with MS than men, with numbers ranging from 50-75% of diagnoses being for women.^{21,23} The reason for this increase is unknown, but studies point to the role of sex hormones (testosterone and estrogen) and body fat (usually women carry more body fat than men).³² Most MS diagnoses occur between the ages of 20 and 40 years old, however, up to 10% of patients develop symptoms prior to 18 years of age (pediatric-onset).^{33,34} In addition, MS cost the United States approximately 10 billion dollars a year.²³

MS is believed to have genetic and environmental factors.^{21,22} The risk of the general public to have MS is 0.1%, whereas, someone with a first-degree relative that

has MS has a risk of 2-4%.²³ More than 200 gene variants have been identified that raise the risk of developing MS.²³ Human leukocyte antigen (HLA) class II genes have a substantial influence, with the most significant being HLA DR2.^{21,23} However, the HLA region has been associated with several autoimmune diseases including Graves' disease, T1D, and rheumatoid arthritis.^{23,35} Environmental factors include geographic latitude/temperate climates, tobacco exposure, obesity, and mononucleosis.^{21,23}

There are four types of MS including relapsing remitting MS (RRMS), secondary progressive MS (SPMS), primary progressive MS (PPMS), and progressive relapsing MS (PRMS), as shown in Figure 3.5.^{36,37} RRMS consists of isolated attacks for days to weeks (relapse) followed by periods of no attacks for weeks to months (remission).³⁶ This accounts for 85% of MS cases and is the most common.³⁶ On average, patients experience ten years of RRMS followed by SPMS.³⁰ SPMS consists of gradual neurological deterioration, and after an initial period of attacks, isolated attacks do not occur.³⁶ PPMS consists of a steady decline from disease onset without remission.³⁶ PRMS is characterized by a steady decline from disease onset with isolated attacks.³⁶ It is estimated that 15% of patients with MS have a progressive type from onset.²³

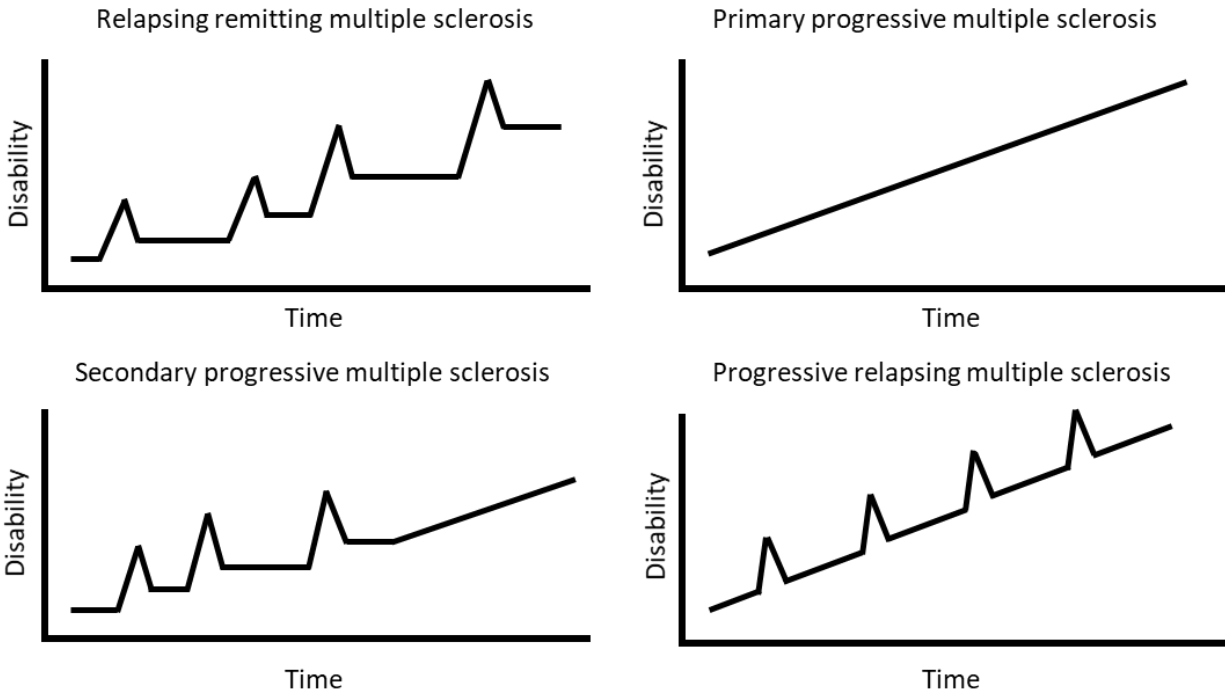


Figure 3.5: Four Types of Multiple Sclerosis. RRMS is characterized by attacks and periods of remission. SPMS is similar to RRMS but becomes a gradual deterioration without attacks. PPMS is characterized by steady deterioration without attacks. PRMS is characterized by steady deterioration with attacks.

3.1.2.a Multiple Sclerosis Diagnosis

Diagnosing MS is difficult since there is a combination of several neurological and physical examinations rather than one test.³⁸ Diagnosis is done by ruling out all other neurological disorders to conclude that it must be MS, therefore testing usually takes months, or years, prior to a final diagnosis.³⁹ Approximately 85-90% of people who develop MS experience a neurological disturbance prior to diagnosis, referred to as clinically isolated syndrome (CIS).^{39,40} Over time, several criteria have been proposed for MS diagnosis.⁴⁰ The McDonald criteria, published in 2001 then revised in 2005 and 2010, depends on a CIS development and lesion growth in space and time.^{38,40} The accuracy

of the original McDonald criteria to predict MS within 3 years was debated by two studies to be 80% and 83% accurate.^{39,41}

Currently, no MS biomarkers exist in the blood and magnetic resonance imaging (MRI) is needed to diagnosis MS.²³ MRI is based on atomic nuclei magnetization, where a strong magnetic field is applied to align the water protons in the tissue.⁴² The alignment is disturbed by a radio frequency (RF) energy, and the nuclei return to resting position, thus releasing RF energy.⁴² Fourier transformation converts the signal frequency information to corresponding intensity levels that are displayed as a matrix of pixels.⁴² Two different relaxation times are used to obtain images: T1 (longitudinal relaxation time; the rate that excited protons return to equilibrium) and T2 (transverse relaxation time; the rate that excited protons reach equilibrium).⁴² T1-weighted images use short repetition times (TR) and time to echo (TE), whereas T2-weighted images use longer TR and TE times.⁴² Fluid attenuated inversion recovery (FLAIR) is similar to T2-weighted images except it uses very long TR and TE to allow for better differentiation.⁴² Lesions and BBB changes are visible by MRI.²³ While MS lesions (or demyelination) can appear throughout the CNS, they are easier recognized in the white matter.^{23,29} However, inflammation, demyelination, and axonal loss are not easily distinguishable by T1 and T2-weighted images unless a gadolinium enhancement is utilized.^{26,29} Current research suggests this may be possible with dynamic contrast-enhanced (DCE)-MRI coupled with susceptibility-based MRI at seven-tesla (7T)^{23,24} The contrast enhancement of DCE-MRI may be useful for staging lesions and analyzing BBB opening.^{23,24} The changes in MS lesions can be viewed over time by overlapping the images, called the subtraction method, as shown in Figure 3.6.⁴³

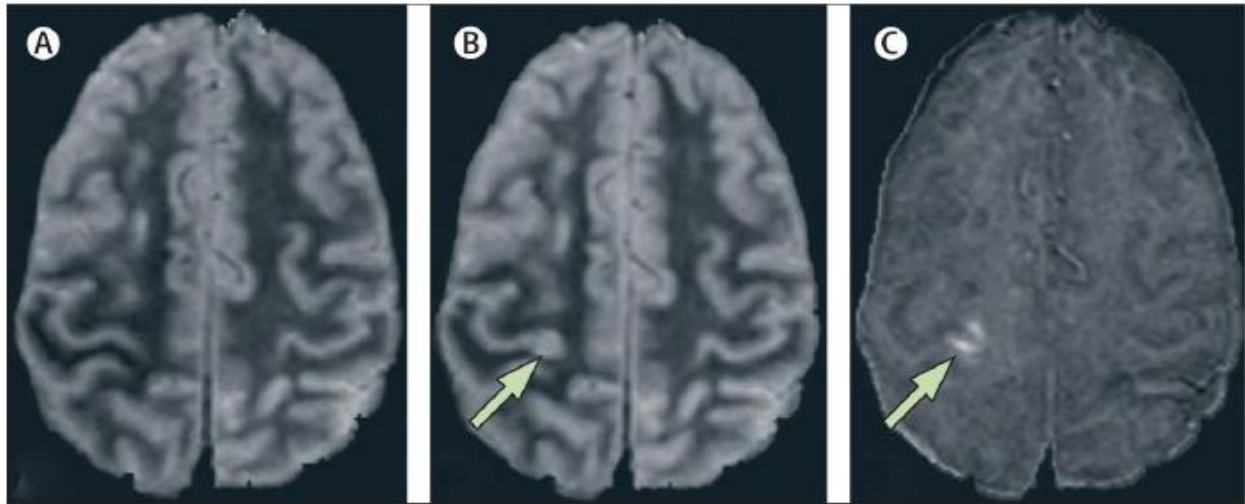


Figure 3.6: MS Lesion Change. The change in MS lesions over time can be viewed using the subtraction method. A. Baseline MRI scan. B. Follow-up MRI scan after 3 years with new lesion formation (arrow). C. Subtraction of image A from image B to demonstrate lesion formation (arrow). Image borrowed from Bakshi et al.

3.1.2.b Multiple Sclerosis Treatments

Currently, MS is incurable, but over a dozen treatments exist.²³ New MS lesion formation can be reduced by drugs that limit the T-cell access to the CNS.²³ These include glatiramer acetate, mitoxantrone, teriflunomide, and such monoclonal antibodies as natalizumab, alemtuzumab, and daclizumab.^{23,36} Some of these also deplete B-cells, which have been successful in reducing lesion formation.²³ Ocrelizumab was the first B-cell targeted therapy.²³ MS medications also include interferon- β , fingolimod, dimethyl fumarate, and dalfampridine.²³ These medications have been approved for RRMS to decrease the development of new lesions in the white matter and relapses.^{23,36} In addition, small studies are being conducted on transplantation and medication therapies that promote remyelination and myelin protection.²³

3.1.2.c Multiple Sclerosis and RBCs

Previously our lab reported that RBCs from patients with MS release higher concentrations of adenosine triphosphate (ATP) than RBCs from healthy donors.⁴⁴ As shown in Figure 3.7, RBCs from healthy controls released 138 (± 21) nM ATP, whereas RBCs from patients with MS released 375 (± 51) nM ATP.⁴⁴ Subsequently, nitric oxide (NO) production is increased in the blood of patients with MS.^{26,45} Evidence shows that NO is capable of disrupting the BBB and causing neuronal injury due to mitochondrial impairment.^{26,30,45} Oligodendrocytes, which form the myelin sheath, are more sensitive to NO toxicity.⁴⁵ MS lesions contain high concentrations of NO, which could be explained by the BBB disruption or the increase of NO production at sites of inflammation.⁴⁵ Usually the inducible isoform of nitric oxide synthase (iNOS; an enzyme that continuously produces NO since it is not calcium dependent), is not found in the CNS, but it becomes expressed within the lesions.^{26,45,46} Interestingly, NO may play a role in demyelination and axon injury, yet once the lesions form, more NO is produced due to iNOS.^{45,46} It is also important to note that RBCs from patients with MS bound significantly more C-peptide than RBCs from healthy controls (3.51 (± 0.59) pmol and 1.99 (± 0.32) pmol, respectively).⁴⁷ The increase in C-peptide uptake by MS RBCs would explain the increase in ATP release and subsequent NO production.

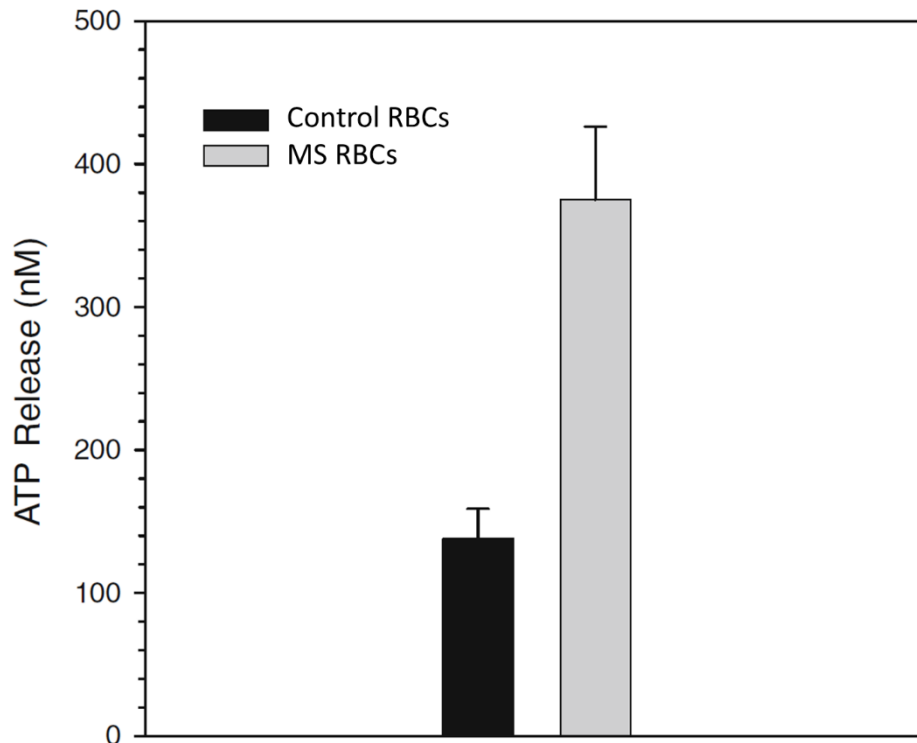


Figure 3.7: Control versus MS RBC ATP Release. ATP released from control RBCs (black bar) was 138 (± 21) nM ATP. ATP released from MS RBCs (grey bar) was 375 (± 51) nM ATP. $n \geq 11$, error=SEM. Figure borrowed from Letourneau et al.

3.2 Methods

3.2.1 BSA Enrichment

Boronate affinity columns (Talon 2 mL disposable gravity column with glycoprotein enrichment resin; Takara, Kusatsu, Shiga, Japan) were used to extract the enriched fraction of glycated albumin from control albumin (Sigma Aldrich, St. Louis, MO).⁴⁸ Each column contained 40 mg BSA per 2.5 mL wash buffer, which consisted of 50 mM HEPES (Thermo Fisher, Waltham, MA) and 0.5 M NaCl (Sigma Aldrich). After incubating the columns for 20 minutes on a shaker at 260 rpm, the column was washed 5 times with wash buffer to collect the nBSA. A sorbitol elution buffer, consisting of the wash buffer plus 100 mM sorbitol (Sigma Aldrich), was utilized to remove the gBSA by washing the

column 5 times. Using Amicon® Ultra-15 ultrafiltration centrifugal filter units (10 kDa; MilliporeSigma, Burlington, MA), the isolated nBSA and gBSA were purified through size exclusion separation and subsequent washing steps. The nBSA and gBSA were added to separate filter units, diluted up to 15 mL with 18.2 MΩ water, and centrifuged for 17 minutes at 3,260 xg. The bottom solution was discarded, and this step was repeated 6 additional times. After the last wash, the BSA solution above the membrane was transferred to a 50 mL CELLSTAR® polypropylene tube (Greiner Bio-One, Kremsmunster, Austria). The filter unit was washed with 2 mL 18.2 MΩ water, and the wash solution was added to the BSA solution. The resulting purified BSA solutions (nBSA and gBSA) were lyophilized (Labconco Corporation, Kansas City, MO) and stored at -20 °C.

3.2.2 Bicinchoninic Acid Assay on Isolated BSA

The concentration of isolated nBSA and gBSA were determined through a bicinchoninic acid (BCA) assay (Thermo Fisher). BSA standards (Thermo Fisher; A: 250 µg/mL, B: 125 µg/mL, C: 62.5 µg/mL, D: 31.25 µg/mL) were prepared using serial dilution of 2 mg/mL BSA in phosphate buffered saline (PBS) to a total volume of 800 µL. PBS contained 10.1 mM Na₂HPO₄ (Sigma Aldrich), 2.7 mM KCl (Thermo Fisher), 136.9 mM NaCl (Sigma Aldrich), and 1.8 mM KH₂PO₄ (Sigma Aldrich) at pH 7.40. 25 µL of the isolated nBSA and gBSA solutions and BSA standards A-D were added to a 96-well clear plate. Kit working solution was added to each well, and the plate was incubated for 30 minutes at 37 °C. After cooling the plate to room temperature, its absorbance was measured at 562 nm on a FlexStation-3 spectrophotometer (Molecular Devices, San Jose, CA).

3.2.3 Mass Spectrometry Identification of Isolated BSA

A Xevo G2-XS mass spectrometer (Waters, Milford, MA) was used to determine the glycation of isolated BSA. The electrospray ionization and time of flight mass analyzer were placed into positive-ion mode. The sample was separated using ultra-high pressure liquid chromatography (UPLC) with a desalting column (cyanopropyl guard column; Thermo Fisher). While in the column, 0.1% formic acid in water (solvent A) and increasing volumes of acetonitrile (solvent B) were added over 15 minutes. A chromatograph was obtained, and the peak (around 8 minutes of retention time) was analyzed in the 200-2,000 Da m/z range, to account for the protein charges. Using the MassLynx software (Waters), the spectrum was processed under the range of 66,000-69,000 Da because the software accounts for the protein charges. Glycation peaks were shifted +162 Da from the base peak. The ion counts of the peaks were divided by the total ion counts to obtain a percentage. In addition, other albumin isoforms, cysteinylated-BSA (+119 Da), Na-BSA (+23 Da), K-BSA (+39.1 Da), and SO₂H-BSA (+31 Da) were determined.

3.2.4 Isolation and Purification of RBCs for nBSA and gBSA Samples

Whole blood was collected from healthy donors into heparinized tubes (Thermo Fisher). The blood was centrifuged at 500 xg for 10 minutes at room temperature prior to the removal of the plasma and buffy coat by aspiration. RBCs were washed by resuspending in physiological salt solution (PSS) or albumin free (AF)-PSS (4.7 mM KCl (Thermo Fisher), 2.0 mM CaCl₂ (Thermo Fisher), 140.5 mM NaCl (Sigma Aldrich), 12.0 mM MgSO₄ (Thermo Fisher), 21.0 mM tris(hydroxymethyl) aminomethane (Invitrogen), 5.5 mM dextrose (Sigma Aldrich), and 0.5% bovine serum albumin for PSS, but not

AF-PSS (BSA, purity $\geq 98\%$; Sigma Aldrich) at pH 7.4). The RBCs were re-centrifuged, the buffer was aspirated off, and new buffer was added for a total of 3 washes. A StatSpin® CritSpin™ microhematocrit centrifuge (Beckman Coulter, Brea, CA) and digital hematocrit reader (StatSpin® CritSpin™; Beckman Coulter) were utilized to determine the RBC hematocrit for 7% RBC samples to be prepared.

3.2.5 nBSA and gBSA Sample Preparation

The isolated nBSA and gBSA were radiolabeled on the same day utilizing the technetium labeling procedure in section 2.2.4. Concentrations of nBSA and gBSA fractions were determined through a Lowry assay similar to section 2.2.4.e, but with a 0.5 mg/mL stock solution prepared using the isolated nBSA (standard volumes of 0, 20, 75, 150, 200, 300, and 400 μL). Stocks were created for both nHSA and gHSA to be approximately 3,200 nM in either AF-PSS or PSS (depending on the sample set). Samples were then prepared with the desired concentration of nBSA- $^{99\text{m}}\text{Tc}$ or gBSA- $^{99\text{m}}\text{Tc}$ (0, 50, 100, 340, 775, 1,000, 1,600, 2,700 nM), 7% RBC, and PSS (or AF-PSS). The purpose of using PSS or AF-PSS was to examine nonspecific or total binding, respectively, to calculate specific binding. 20 nM C-peptide (purified using section 2.2.5.a.) and Zn^{2+} were added to both nBSA and gBSA samples. nBSA- $^{99\text{m}}\text{Tc}$ and gBSA- $^{99\text{m}}\text{Tc}$ standards were made in PSS or AF-PSS with stock volumes of 0, 2, 5, 10, 15, 25, and 35 μL . Two 10 μL standards were made so that one could be diluted further to 1,000 μL using 50, 100, and 250 μL of the standard. Samples and standards were incubated for 2 h at 37 °C. The samples were centrifuged for 1 minute at 750 xg, and the supernatant was removed before adding AF-PSS. The RBCs were again centrifuged and washed 5 times with AF-PSS to remove loosely adsorbed proteins. RBC samples were

analyzed using a 2480 Wizard² automatic gamma counter (PerkinElmer, Waltham, MA) using the 20 second run time ^{99m}Tc method (140 KeV). Samples were then repeated for gBSA without C-peptide or Zn²⁺. In addition, gBSA samples with and without C-peptide or Zn²⁺ were prepared for ½ gBSA and ¼ gBSA samples. For ½ gBSA samples, equal volumes of gBSA and nBSA were combined prior to HYNIC conjugation. For ¼ samples, ¼ of the sample volume was gBSA and ¾ of the sample volume was nBSA. In this way, various glycation percentages of albumin binding to RBCs could be analyzed.

3.2.6 C-peptide Uptake on RBCs for nBSA and gBSA

On days when radiolabeling was occurring, samples were prepared using 2 µM nBSA or gBSA with 20 nM C-peptide and Zn²⁺. This experiment was previously conducted in the lab at 60 µM HSA, however, since these binding experiments were conducted with BSA at concentration of 2 µM or less, the experiment was repeated with BSA at a lower concentration. All reagents were the same between these samples and those created in section 3.2.5. In addition, 20 nM C-peptide controls and standards ranging from 0-25 nM were created. Samples and standards were incubated for 2 h at 37 °C before centrifuging at 500 xg for 5 minutes and removing the supernatant. Supernatant was stored at -20 °C until a C-peptide ELISA (ALPCO, Salem, New Hampshire) was conducted (diluted 1:50). The C-peptide supernatant values from the samples were then subtracted from the C-peptide supernatant values of the control to determine C-peptide binding to the RBC.

3.2.7 MS Sample Preparation

nBSA from section 3.2.1 was radiolabeled utilizing the technetium labeling procedure in section 2.2.4. nBSA concentration was determined through a Lowry assay

similar to section 2.2.4.e, but with a 0.5 mg/mL nBSA stock (volumes of 0, 20, 75, 150, 200, 300, and 400 μ L). RBCs were isolated from whole blood donated by patients with MS following section 3.2.4. nBSA- ^{99m}Tc samples (0, 50, 100, 340, 775, 1,000, 1,600, 2,700 nM) were prepared using MS RBCs (7%) with and without 20 nM C-peptide (purified in section 2.2.5.a) and Zn^{2+} . Two sets of samples were prepared, one in AF-PSS and one in PSS, to analyze total binding and nonspecific binding, respectively. The specific binding of nBSA to MS RBCs was determined by subtracting the nonspecific binding from the total binding. Standards were made from the 3,200 nM stock (0, 2, 5, 10, 15, 25, and 35 μ L) in either AF-PSS or PSS. Two 10 μ L standards were made to further dilute to 1,000 μ L using 50, 100, and 250 μ L volumes of the 10 μ L standard. Samples and standards were incubated for 2 h at 37 $^{\circ}\text{C}$. Samples were then centrifuged at 750 xg for 1 min, the supernatant was removed, and AF-PSS was added. Samples were washed in this way for a total of 5 times before being analyzed on a 2480 Wizard² automatic gamma counter (PerkinElmer) using the 20 second run time ^{99m}Tc method (140 KeV).

3.3. Results

3.3.1 Mass Spectrometry Spectra for Isolated BSA

Utilizing mass spectrometry, the percent glycation of each BSA sample could be determined. The nBSA was 11 (± 2)% glycated. The gBSA utilized for samples containing C-peptide and Zn^{2+} was 48 (± 2)% glycated. The gBSA utilized for samples without C-peptide or Zn^{2+} was 45.3 (± 0.6)% glycated. The $\frac{1}{2}$ gBSA with or without C-peptide and Zn^{2+} was 22.8 (± 0.7)% glycated. Lastly, the $\frac{1}{4}$ gBSA with or without C-peptide and Zn^{2+}

was 16.8 (± 0.5)% glycated. Example MS spectra are displayed in Figure 3.8 showing nBSA and gBSA from one single day.

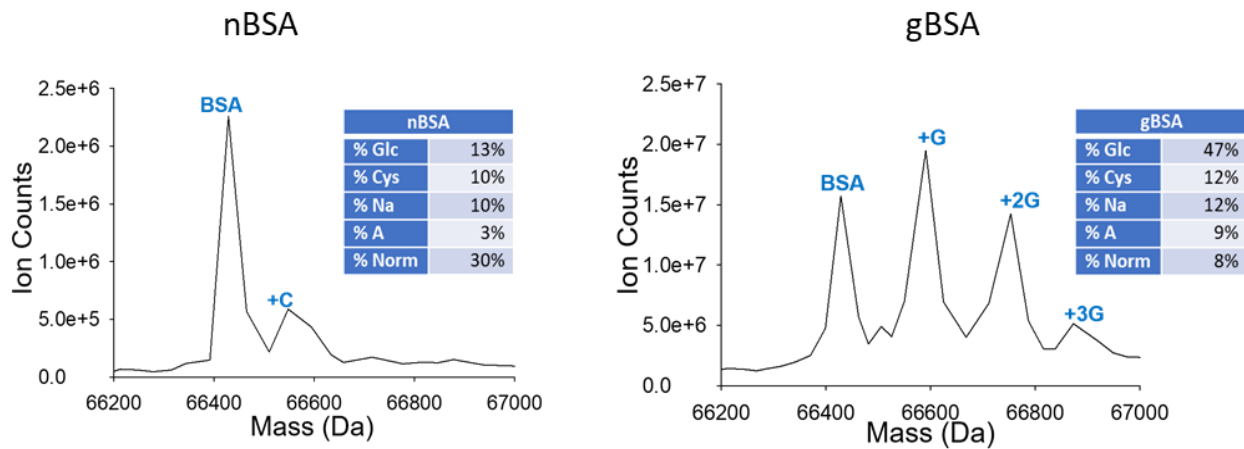


Figure 3.8: Mass Spectra of nBSA and gBSA. The spectra of isolated nBSA and gBSA with insets demonstrating percent glucose (Glc; +162 Da), cysteine (Cys; +119 Da), sodium (Na; +23 Da), acetonitrile (A; +41 Da), and normal (Norm). On this day, the nBSA was 13% glycated, and the gBSA was 47% glycated.

3.3.2 Binding of gBSA versus nBSA to RBCs

Determination of gBSA and nBSA binding to RBCs was performed by adding increasing concentrations of BSA-^{99m}Tc (ranging from 0-2,700 nM) to AF-PSS or PSS. AF-PSS samples provide the total BSA binding to RBC, whereas PSS samples provide the nonspecific binding of BSA to RBCs. By subtracting the PSS sample values from the AF-PSS sample values, the specific binding was calculated. The data in Figure 3.9 demonstrates the specific binding of nBSA (11% glycated; triangles) and gBSA (48% glycated; circles) to RBCs in the presence of C-peptide and Zn²⁺. The nBSA specific binding saturated at an average of 15,222 (± 627) BSA molecules/RBC. The resulting equilibrium dissociation constant was 6.3 (± 0.2) $\times 10^{-7}$ M, and the B_{max} was 2.60 (± 0.03) $\times 10^{-8}$ M or approximately 18,500 receptor molecules/RBC. The gBSA specific binding

saturated at an average of 17,011 (± 732) BSA molecules/RBC. The resulting equilibrium dissociation constant was $4.4 (\pm 0.2) \times 10^{-7}$ M, and the B_{\max} was $2.73 (\pm 0.04) \times 10^{-8}$ M or approximately 19,500 receptor molecules/RBC.

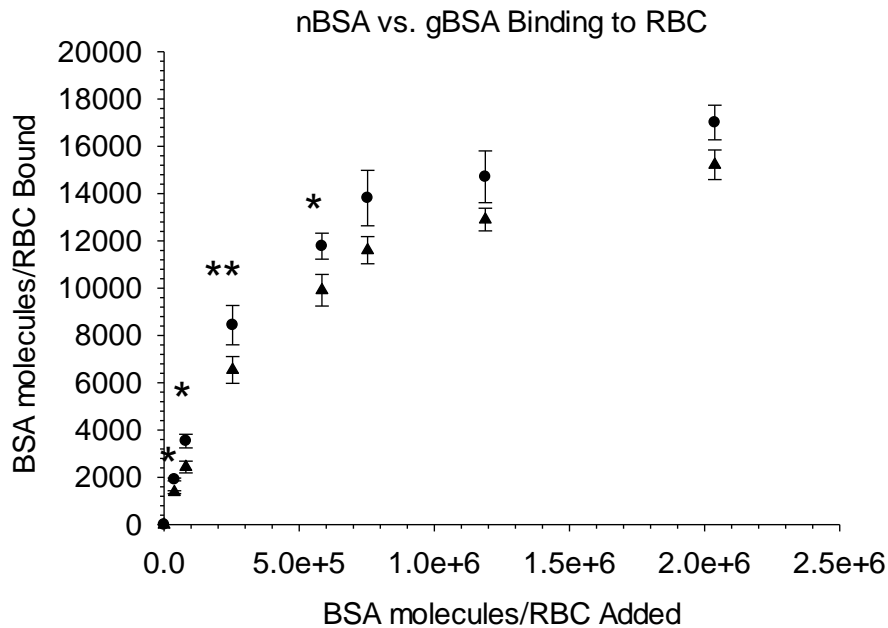


Figure 3.9: Binding of nBSA and gBSA to RBC. The binding of normal BSA (11%; triangles) and glycated BSA (48%; circles) to RBCs in the presence of C-peptide and Zn^{2+} . $n \geq 4$, error=SEM, * $p < 0.05$, ** $p = 0.05$.

3.3.2.a Binding of gBSA at Varying Glycation Percentages

The data in Figure 3.10 compares gBSA binding to RBC with and without C-peptide and Zn^{2+} at 48% and 45% glycation, respectively. The data for gBSA with C-peptide and Zn^{2+} is from the previous section. The gBSA specific binding without C-peptide or Zn^{2+} saturated at an average of 20,372 ($\pm 1,315$) BSA molecules/RBC. The resulting equilibrium dissociation constant was $4.2 (\pm 0.3) \times 10^{-7}$ M, and the B_{\max} was $3.21 (\pm 0.06) \times 10^{-8}$ M or approximately 23,000 receptor molecules/RBC. This trend is opposite of previous data (in Chapter 2) showing more BSA binding with C-peptide and Zn^{2+} compared to without. However, this was the first time the BSA binding was analyzed at a

high glycation percentage without C-peptide or Zn²⁺. Therefore, the trend between gBSA binding to RBCs with and without C-peptide and Zn²⁺ at another glycation percentage was analyzed.

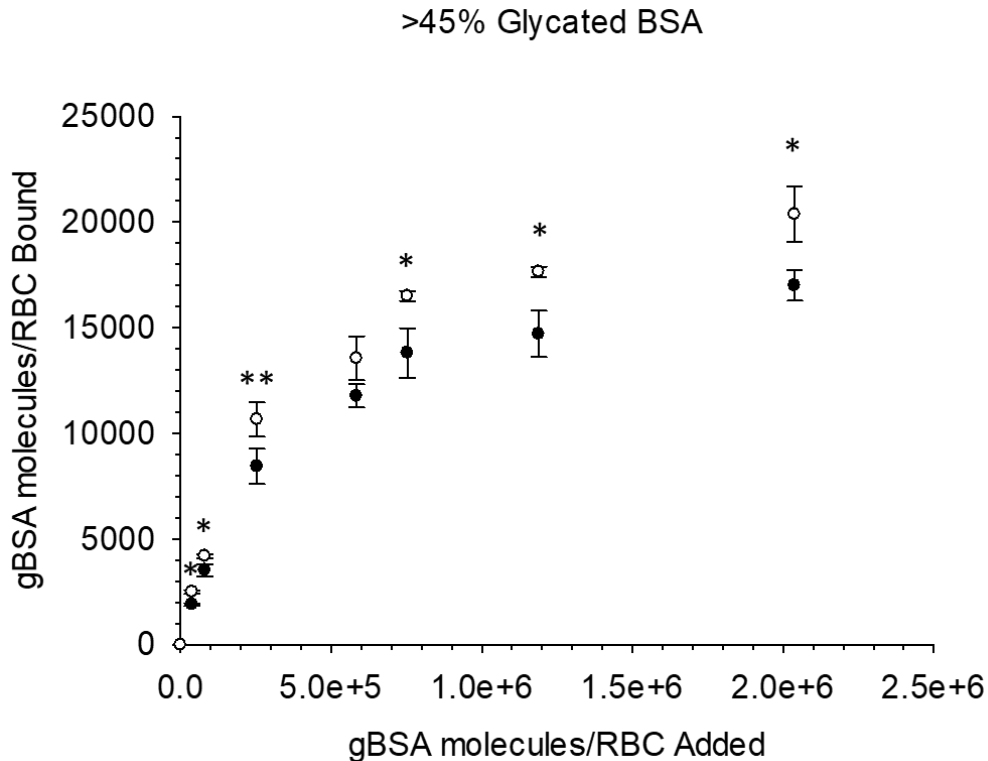


Figure 3.10: Binding of >45% Glycated BSA to RBC. The binding of gBSA to RBCs with (48%; closed circles) and without (45%; open circles) C-peptide and Zn²⁺. n=4, error=SEM, *p<0.05, **p=0.05.

The gBSA binding at 23% glycation with and without C-peptide and Zn²⁺ is shown in Figure 3.11. When C-peptide and Zn²⁺ were present, the gBSA specific binding saturated at an average of 16,249 (± 926) BSA molecules/RBC. The resulting equilibrium dissociation constant was $4.2 (\pm 0.2) \times 10^{-7}$ M, and the B_{max} was $2.57 (\pm 0.04) \times 10^{-8}$ M or approximately 18,300 receptor molecules/RBC. When C-peptide and Zn²⁺ were absent, the gBSA specific binding saturated at an average of 15,565 (± 591) BSA molecules/RBC. The resulting equilibrium dissociation constant was $4.1 (\pm 0.2) \times 10^{-7}$ M, and the B_{max} was

2.49 (± 0.03) $\times 10^{-8}$ M or approximately 17,800 receptor molecules/RBC. Upon calculating a p-value utilizing a t-test (two-sample assuming equal variance), the samples were not statistically different ($p > 0.25$) at 23% glycation with or without C-peptide and Zn^{2+} . Overall, the nBSA bound more BSA molecules/RBC with C-peptide and Zn^{2+} than without, while 23% glycation resulted in a statistically equal amount of BSA molecules binding per RBC with or without C-peptide and Zn^{2+} . When glycation was increased to 45%, more BSA molecules bound per RBC without C-peptide and Zn^{2+} than with. Therefore, a percent glycation value between nBSA and 23% gBSA was prepared to determine what was occurring between those points.

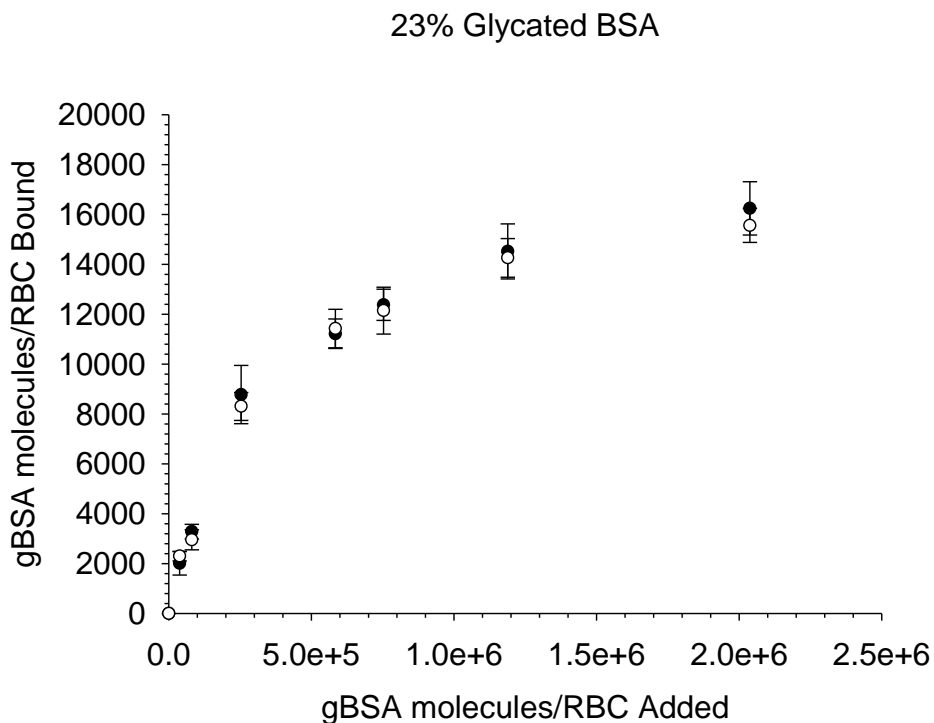


Figure 3.11: Binding of 23% Glycated BSA to RBC. The binding of gBSA to RBCs with (closed circles) and without (open circles) C-peptide and Zn^{2+} . There is no significant difference between the two curves ($p > 0.25$). $n=4$, error=SEM.

At 17% glycation, with C-peptide and Zn²⁺ samples demonstrated a saturation at 16,926 (±657) BSA molecules/RBC binding. The resulting equilibrium dissociation constant was 4.5 (±0.2) x 10⁻⁷ M, and the B_{max} was 2.78 (±0.04) x 10⁻⁸ M or approximately 19,800 receptor molecules/RBC. Without C-peptide or Zn²⁺, the specific binding saturated at 15,910 (±382) BSA molecules/RBC. The resulting equilibrium dissociation constant was 4.7 (±0.2) x 10⁻⁷ M, and the B_{max} was 2.57 (±0.03) x 10⁻⁸ M or approximately 18,300 receptor molecules/RBC. This data is demonstrated in Figure 3.12. The summary of data from all percentages of gBSA glycation is shown in Figure 3.13. This figure includes the 14% values from chapter 2 with the glycation percentage being based off the Sigma BSA average rather than the experimental data for each day.

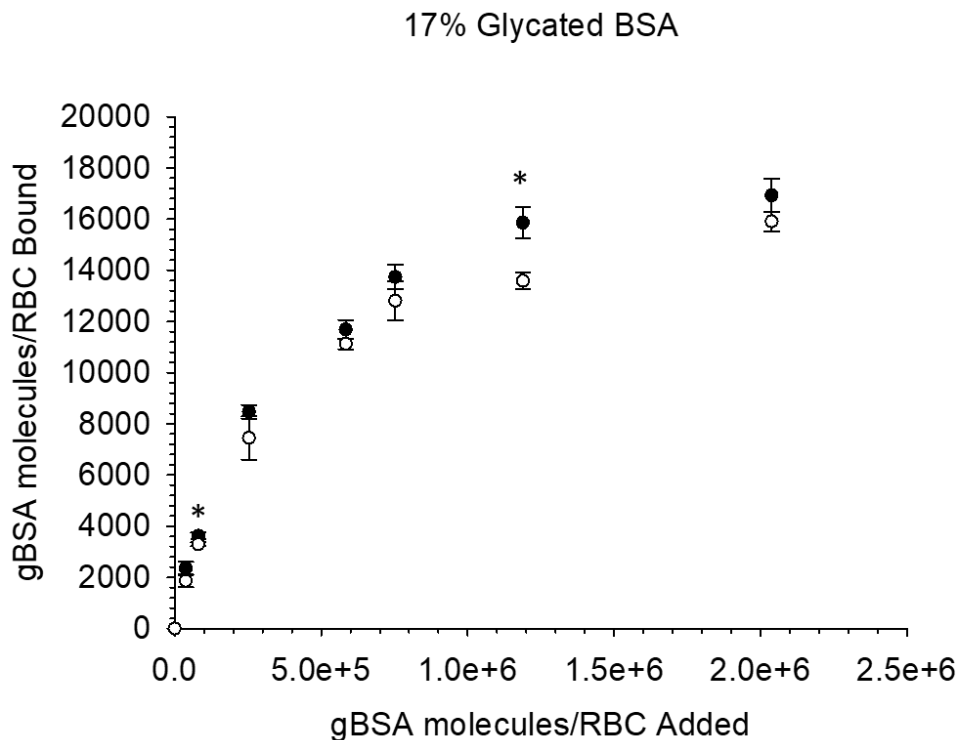


Figure 3.12: Binding of 17% Glycated BSA to RBC. The binding of gBSA to RBCs with (closed circles) and without (open circles) C-peptide and Zn²⁺. n=4, error=SEM, *p<0.05.

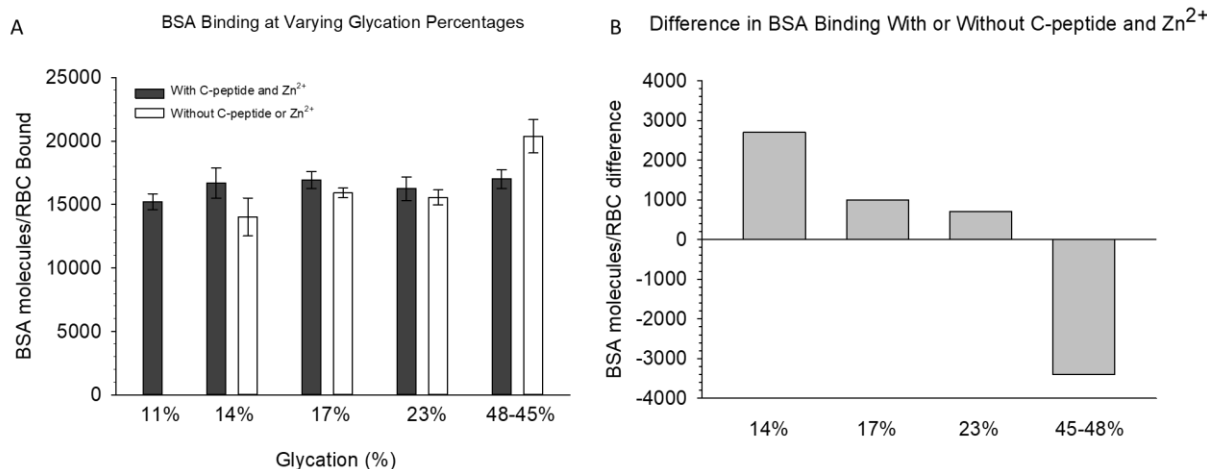


Figure 3.13: Binding of BSA to RBC at Varying Glycation Percentages. A) The specific binding of BSA to RBCs with (dark grey) and without (white) C-peptide and Zn²⁺ at saturation. Shown here are 11, 14, 17, 23, 45, and 48% glycation. n≥4, error=SEM. B) The difference in BSA binding to RBCs with or without C-peptide and Zn²⁺. BSA molecules/RBC bound values for data without C-peptide and Zn²⁺ was subtracted from BSA molecules/RBC bound values for data with C-peptide and Zn²⁺. Values are at saturation and represent approximate differences. n≥4.

3.3.3 C-peptide Uptake to RBCs

C-peptide uptake to RBCs with nBSA or gBSA was determined by analyzing the sample supernatant with a C-peptide ELISA. The nBSA at 12.0 (±0.7)% glycation resulted in RBC C-peptide uptake of 0.9 (±0.2) nM as shown in Figure 3.14. The gBSA at 46 (±2)% glycation resulted in RBC C-peptide uptake of 0.6 (±0.2) nM. The difference of 0.3 nM C-peptide uptake is statically different (p<0.05), indicating that the ability of gBSA to carry C-peptide to the cell is hindered.

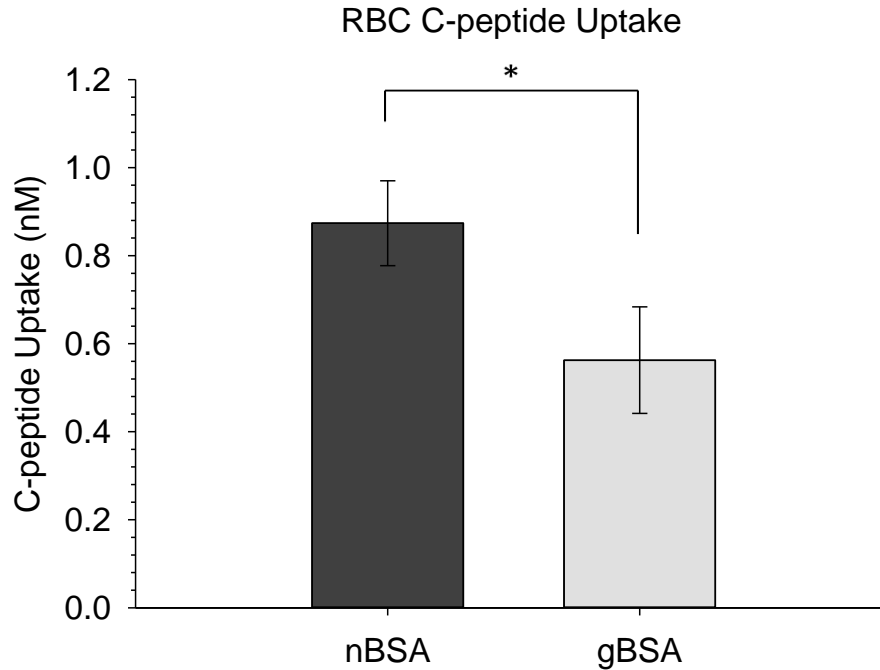


Figure 3.14: RBC C-peptide Uptake with nBSA or gBSA. The uptake of C-peptide (in nM) by RBC in the presence of Zn^{2+} and nBSA (12% glycation; dark grey bar) or gBSA (46% glycation; light grey bar). There is significantly less RBC C-peptide uptake when carried by gBSA compared to nBSA. $n=4$, error=SEM, $*p<0.05$.

3.3.4. Binding of BSA to MS RBCs

Determination of nBSA binding to RBCs from patients with MS was performed by adding increasing concentrations of nBSA- ^{99m}Tc (ranging from 0-2,700 nM) to AF-PSS (for total binding) or PSS (for nonspecific binding). The specific binding was calculated by subtracting the PSS sample values from the AF-PSS sample values. Experiments were conducted in the absence and presence of C-peptide and Zn^{2+} . The data in Figure 3.15 demonstrates the specific binding of nBSA (11% glycated) to MS RBCs in the presence (closed circles) and absence (open circles) of C-peptide and Zn^{2+} . The nBSA specific binding without C-peptide or Zn^{2+} saturated at an average of 16,894 (± 582) BSA molecules/RBC. The resulting equilibrium dissociation constant was $3.8 (\pm 0.5) \times 10^{-7}$ M,

and the B_{max} was $2.55 (\pm 0.09) \times 10^{-8}$ M or approximately 18,200 receptor molecules/RBC. The nBSA specific binding with C-peptide and Zn^{2+} saturated at an average of 17,855 (± 351) BSA molecules/RBC. The resulting equilibrium dissociation constant was $5.8 (\pm 0.05) \times 10^{-7}$ M, and the B_{max} was $2.93 (\pm 0.08) \times 10^{-8}$ M or approximately 20,900 receptor molecules/RBC. Figure 3.16 compares the BSA binding to RBCs with C-peptide and Zn^{2+} for both control RBCs (section 3.3.2) and MS RBCs.

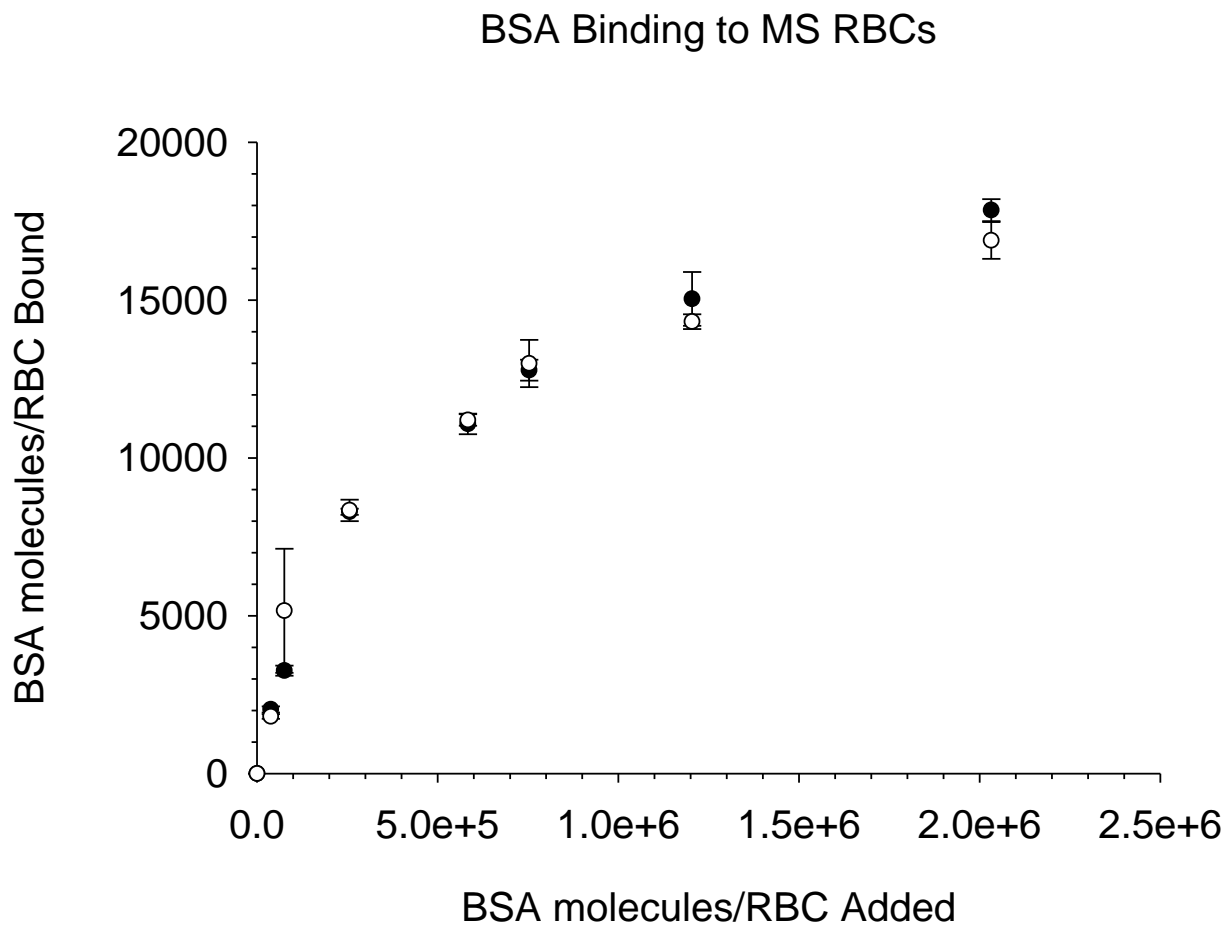


Figure 3.15: Binding of nBSA to MS RBCs. The binding of nBSA to RBCs from patients with MS with (closed circles) and without (open circles) C-peptide and Zn^{2+} . $n=3$ (except $n=2$ for the fourth point at 255,935 BSA molecules/RBC Added without C-peptide and Zn^{2+}), error=SEM.

BSA Binding to MS vs. Control RBCs

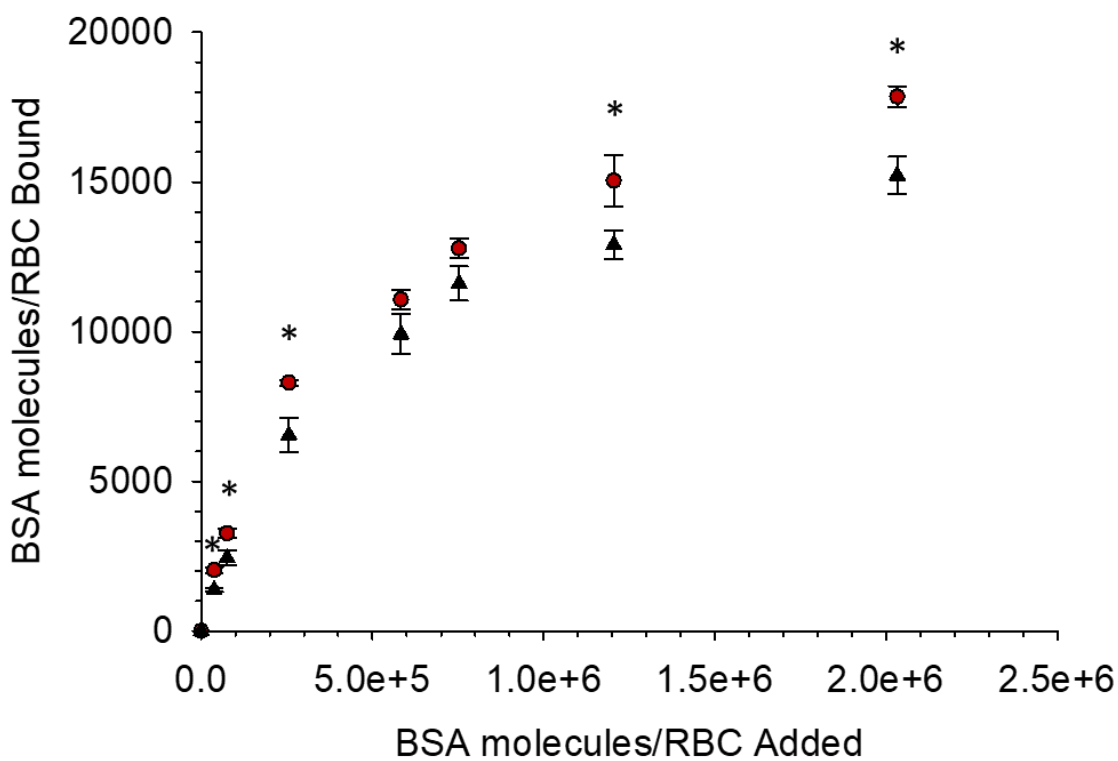


Figure 3.16: Binding of nBSA to MS and Control RBCs. The binding of nBSA to RBCs from patients with MS (red circles) compared to control RBCs (black triangles) when C-peptide and Zn^{2+} were present. $n \geq 3$, error=SEM, $*p < 0.05$.

3.4. Discussion

Previous data demonstrated that BSA binding to RBCs saturated at 16,695 ($\pm 1,479$) BSA molecules/RBC when C-peptide and Zn^{2+} were present.⁴⁹ However, in this chapter, nBSA binding to RBCs saturated at 15,222 (± 627) BSA molecules/RBC. The difference between this data could be due to BSA preparation. Previously, the BSA was used as is directly from the Sigma Aldrich bottle. In this experiment, the nBSA and gBSA were isolated through boronate affinity chromatography, and the percent glycation was determined through mass spectrometry. The hypothesis was that the BSA used previously had a higher percent glycation since the sample would contain nBSA and

gBSA, this would result in the higher number of BSA molecules binding per RBC. The glycation percentage was later confirmed to be 14% for these samples.

Previous data demonstrated that nBSA bound more BSA molecules/RBC with C-peptide and Zn^{2+} than without.⁴⁹ A 17% gBSA was created by combining nBSA and gBSA. This demonstrated more BSA molecules/RBC with C-peptide and Zn^{2+} than without, but not to the extent that is demonstrated in nBSA. nBSA demonstrated a difference of 2,700 BSA molecules/RBC binding with or without C-peptide and Zn^{2+} at saturation, whereas 17% gBSA demonstrated a difference of 1,000 BSA molecules/RBC binding with or without C-peptide and Zn^{2+} at saturation. When nBSA and gBSA were combined to create a 23% gBSA (a T1D range), there was a statistically equal amount of BSA molecules binding per RBC with or without C-peptide and Zn^{2+} . Finally, at glycation percentages higher than 45%, a reverse trend appeared with more BSA molecules/RBC without C-peptide and Zn^{2+} than with (3,400 BSA molecules/RBC difference). While more BSA is binding to the cell at higher glycation percentages, we are seeing less C-peptide binding to the cells. Previous data at 60 μ M HSA resulted in 1.4 (\pm 0.1) nM C-peptide uptake with nHSA and 0.8 (\pm 0.1) nM with gHSA. This experiment resulted in 0.9 (\pm 0.2) nM C-peptide uptake with 2 μ M nBSA and C-peptide uptake of 0.6 (\pm 0.2) nM with 2 μ M gBSA. Both experiments demonstrated statistical difference between RBC C-peptide uptake with normal or glycated albumins regardless of species (human or bovine) or albumin concentration (60 or 2 μ M). This indicates that while there is more gBSA binding to the cell than nBSA binding, the C-peptide is not binding in a manner similar to a healthy individual. This is of huge importance to understanding C-peptide binding to the RBCs of

patients with T1D. Not only is it important to include C-peptide in a new T1D therapy regime, but also healthy BSA.

The same radiolabeling technique was applied to analyze BSA-^{99m}Tc binding to RBCs from patients with MS. This was done to investigate the increase in NO release shown in patients. We have shown that C-peptide requires albumin to bind to the RBC, and binding results in an increase of RBC-derived ATP release and subsequent endothelial NO release. When nBSA binding to MS RBCs was analyzed in the presence of C-peptide and Zn²⁺, binding saturated at 17,855 (±351) BSA molecules/RBC. Whereas nBSA binding to MS RBCs without C-peptide and Zn²⁺ saturated at 16,894 (±627) BSA molecules/RBC. This is only a difference of 960 BSA molecules/RBC (opposed to 2,700 BSA molecules/RBC difference in control RBCs). When compared to the binding of BSA molecules/RBC with C-peptide and Zn²⁺ to healthy RBCs, the BSA binding in MS RBCs is higher than healthy RBCs (2,600 BSA molecules/RBC). This increase in BSA binding to the MS RBC compared to a control RBC justifies why we see an increase of ATP and NO release in patients with MS, as well as an increase in RBC C-peptide uptake. Future studies are needed to gather more data on BSA binding to MS RBCs with and without C-peptide and Zn²⁺. Current data indicates that MS RBCs have more BSA receptors than control RBCs (even without ligands present). However, this experiment was only conducted three times and more replicates are needed. Also, future studies should focus on comparing BSA binding to control RBCs to RBCs from patients with MS. This could be done as a comparison experiment with 2,700 nM BSA-^{99m}Tc (at saturation) with C-peptide and Zn²⁺ in control or MS RBCs. With the shortened experiment, more samples

could be analyzed on the same day as opposite to a full binding curve that can only analyze one MS patient per day.

REFERENCES

REFERENCES

- (1) Furusyo, N.; Hayashi, J. Glycated Albumin and Diabetes Mellitus. *Biochim. Biophys. Acta* **2013**, *1830* (12), 5509–5514.
- (2) Kim, K. J.; Lee, B. W. The Roles of Glycated Albumin as Intermediate Glycation Index and Pathogenic Protein. *Diabetes Metab. J.* **2012**, *36* (2), 98–107.
- (3) Nursten, H. E. *The Maillard Reaction: Chemistry, Biochemistry and Implications*; Royal Society of Chemistry, 2005.
- (4) Anguizola, J.; Matsuda, R.; Barnaby, O. S.; Hoy, K. S.; Wa, C.; DeBolt, E.; Koke, M.; Hage, D. S. Review: Glycation of Human Serum Albumin. *Clin. Chim. Acta* **2013**, *425* (21), 64–76.
- (5) Forbes, J. M.; Cooper, M. E. Mechanisms of Diabetic Complications. *Physiol. Rev.* **2013**, *93* (1), 137–188.
- (6) O'Brien, D. M.; Fogel, M. L.; Boggs, C. L. Renewable and Nonrenewable Resources: Amino Acid Turnover and Allocation to Reproduction in Lepidoptera. *Proc. Natl. Acad. Sci.* **2002**, *99* (7), 4413–4418.
- (7) Shaklai, N.; Garlick, R. L.; Bunn, H. F. Nonenzymatic Glycosylation of Human Serum Albumin Alters Its Conformation and Function. *J. Biol. Chem.* **1984**, *259* (6), 3812–3817.
- (8) Soudahome, A. G.; Catan, A.; Giraud, P.; Kouao, S. A.; Guerin-Dubourg, A.; Debussche, X.; Le Moullec, N.; Bourdon, E.; Bravo, S. B.; Paradela-Dobarro, B.; et al. Glycation of Human Serum Albumin Impairs Binding to the Glucagon-like Peptide-1 Analogue Liraglutide. *J. Biol. Chem.* **2018**, *293* (13), 4778–4791.
- (9) Blache, D.; Bourdon, E.; Salloignon, P.; Lucchi, G.; Ducoroy, P.; Petit, J. M.; Verges, B.; Lagrost, L. Glycated Albumin with Loss of Fatty Acid Binding Capacity Contributes to Enhanced Arachidonate Oxygenation and Platelet Hyperactivity: Relevance in Patients with Type 2 Diabetes. *Diabetes* **2015**, *64* (3), 960–972.
- (10) Ultrafiltration Binding Analyses of Glycated Albumin with a 3D-Printed Syringe Attachment [Unpublished]. *Anal. Bioanal. Chem.* **2018**.
- (11) Peters, T. Ligand Binding by Albumin. In *All About Albumin*; Academic Press: New Jersey, 1995; pp 76–132.
- (12) Merlot, A. M.; Kalinowski, D. S.; Richardson, D. R. Unraveling the Mysteries of Serum Albumin—More than Just a Serum Protein. *Front. Physiol.* **2014**, *5* (299), 1–7.

- (13) Al-isawi, Z. J. Role of C-Peptide in the Vasculature, University of Leicester, 2019.
- (14) Martin, A.; Komada, M. R.; Sane, D. C. Abnormal Angiogenesis in Diabetes Mellitus. *Med. Res. Rev.* **2003**, 23 (2), 117–145.
- (15) Wada, R.; Yagihashi, S. Role of Advanced Glycation End Products and Their Receptors in Development of Diabetic Neuropathy. *Ann. New York Acad. Sci.* **2005**, 1043, 598–604.
- (16) Peters, T. The Albumin Molecule: Its Structure and Chemical Properties. In *All About Albumin*; Academic Press: New York, 1995; pp 9–75.
- (17) Vernon Roohk, H.; Zaidi, A. R. A Review of Glycated Albumin as an Intermediate Glycation Index for Controlling Diabetes. *J. Diabetes Sci. Technol.* **2008**, 2 (6), 1114–1121.
- (18) Hirata, T.; Saisho, Y.; Morimoto, J.; Kasayama, S.; Koga, M.; Maruyama, T. The Ratio of Glycated Albumin to HbA1c Is Correlated with Diabetes Duration According to Decreases in Insulin Secretion in Patients with Autoimmune Type 1 Diabetes and Type 2 Diabetes. *J. Genet. Syndr. Gene Ther.* **2013**, 4 (7).
- (19) Kohzuma, T.; Koga, M. Lucica GA-L Glycated Albumin Assay Kit: A New Diagnostic Test for Diabetes Mellitus. *Mol. Diagnosis Ther.* **2010**, 14 (1), 49–51.
- (20) Pinger, C. Novel Analytical Tools for Studying a Potential Type-1 Diabetes Therapy, Michigan State University, 2018.
- (21) Steinman, L. Multiple Sclerosis: A Coordinated Immunological Attack against Myelin in the Central Nervous System. *Cell* **1996**, 85 (3), 299–302.
- (22) Evans, C.; Beland, S. G.; Kulaga, S.; Wolfson, C.; Kingwell, E.; Marriott, J.; Koch, M.; Makhani, N.; Morrow, S.; Fisk, J.; et al. Incidence and Prevalence of Multiple Sclerosis in the Americas: A Systematic Review. *Neuroepidemiology* **2013**, 40 (3), 195–210.
- (23) Reich, D. S.; Lucchinetti, C. F.; Calabresi, P. A. Multiple Sclerosis. *N. Engl. J. Med.* **2018**, 378 (2), 169–180.
- (24) Absinta, M.; Sati, P.; Gaitán, M. I.; Maggi, P.; Cortese, I. C. M.; Filippi, M.; Reich, D. S. Seven-Tesla Phase Imaging of Acute Multiple Sclerosis Lesions: A New Window into the Inflammatory Process. *Ann. Neurol.* **2013**, 74 (5), 669–678.
- (25) Tuladhar, A.; Mitrousis, N.; Führmann, T.; Shoichet, M. S. Central Nervous System. In *Translational Regenerative Medicine*; Atala, A., Allickson, J. G., Eds.; Elsevier Inc.: Waltham, 2015; pp 415–435.
- (26) Minagar, A.; Alexander, J. S. Blood-Brain Barrier Disruption in Multiple Sclerosis. **2003**, 9, 540–549.

- (27) Janes, T. M.; Spence, D. M. Steroid Inhibition of Erythrocyte-Derived ATP Reduces Endothelial Cell Production of Nitric Oxide in a 3D-Printed Fluidic Model. *Anal. Methods* **2018**, *10* (27), 3416–3422.
- (28) Marrack, P.; Kappler, J.; Kotzin, B. L. Autoimmune Disease: Why and Where It Occurs. *Nat. Med.* **2001**, *7* (8), 899–905.
- (29) Absinta, M.; Sati, P.; Reich, D. S. Advanced MRI and Staging of Multiple Sclerosis Lesions. *Nat. Rev. Neurol.* **2016**, *12* (6), 358–368.
- (30) Stadelmann, C.; Wegner, C.; Brück, W. Inflammation, Demyelination, and Degeneration - Recent Insights from MS Pathology. *Biochim. Biophys. Acta* **2011**, *1812*, 275–282.
- (31) Wallin, M. T.; Culpepper, W. J.; Campbell, J. D.; Nelson, L. M.; Langer-Gould, A.; Marrie, R. A.; Cutter, G. R.; Kaye, W. E.; Wagner, L.; Tremlett, H.; et al. The Prevalence of MS in the United States: A Population-Based Estimate Using Health Claims Data. *Neurology* **2019**, *92* (10), E1029–E1040.
- (32) Mowry, E.; Calabresi, P. A. Multiple Sclerosis: Why are women more at risk?
- (33) Gorman, M. P.; Healy, B. C.; Polgar-Turcsanyi, M.; Chitnis, T. Increased Relapse Rate in Pediatric-Onset Compared with Adult-Onset Multiple Sclerosis. *Arch. Neurol.* **2009**, *66* (1), 54–59.
- (34) Duquette, P.; Murray, T. J.; Pleines, J.; Ebers, G. C.; Sadovnick, D.; Weldon, P.; Warren, S.; Patty, D. W.; Upton, A.; Hader, W.; et al. Multiple Sclerosis in Childhood: Clinical Profile in 125 Patients. *J. Pediatr.* **1987**, *111* (3), 359–363.
- (35) Gough, S. C. L.; Simmonds, M. J. The HLA Region and Autoimmune Disease: Associations and Mechanisms of Action. *Curr. Genomics* **2007**, *8* (7), 453–465.
- (36) Loma, I.; Heyman, R. Multiple Sclerosis: Pathogenesis and Models. *Curr. Neuropharmacol.* **2011**, *9*, 409–416.
- (37) Krieger, S. C.; Sumowski, J. New Insights into Multiple Sclerosis Clinical Course from the Topographical Model and Functional Reserve. *Neurol. Clin.* **2018**, *36* (1), 13–25.
- (38) Polman, C. H.; Reingold, S. C.; Banwell, B.; Clanet, M.; Cohen, J. A.; Filippi, M.; Fujihara, K.; Havrdova, E.; Hutchinson, M.; Kappos, L.; et al. Diagnostic Criteria for Multiple Sclerosis: 2010 Revisions to the McDonald Criteria. *Ann. Neurol.* **2011**, *69* (2), 292–302.
- (39) Dalton, C. M.; Brex, P. A.; Miszkiel, K. A.; Hickman, S. J.; MacManus, D. G.; Plant, G. T.; Thompson, A. J.; Miller, D. H. Application of the New McDonald Criteria to Patients with Clinically Isolated Syndromes Suggestive of Multiple Sclerosis. *Ann. Neurol.* **2002**, *52* (1), 47–53.

- (40) Miller, D.; Barkhof, F.; Montalban, X.; Thompson, A.; Filippi, M. Clinically Isolated Syndromes Suggestive of Multiple Sclerosis, Part I: Natural History, Pathogenesis, Diagnosis, and Prognosis. *Lancet Neurol.* **2005**, *4* (5), 281–288.
- (41) Tintoré, M.; Rovira, A.; Río, J.; Nos, C.; Grivé, E.; Sastre-Garriga, J.; Pericot, I.; Sánchez, E.; Comabella, M.; Montalban, X. New Diagnostic Criteria for Multiple Sclerosis: Application in First Demyelinating Episode. *Neurology* **2003**, *60* (1), 27–30.
- (42) Mccarthy, M. J.; Cheung, M. K. Magnetic Resonance Imaging <https://casemed.case.edu> (accessed Apr 6, 2020).
- (43) Bakshi, R.; Thompson, A. J.; Rocca, M. A.; Pelletier, D.; Dousset, V.; Barkhof, F.; Inglese, M.; Guttmann, C. R.; Horsfield, M. A.; Filippi, M. MRI in Multiple Sclerosis: Current Status and Future Prospects. *Lancet Neurol.* **2008**, *7* (7), 615–625.
- (44) Letourneau, S.; Hernandez, L.; Faris, A. N.; Spence, D. M. Evaluating the Effects of Estradiol on Endothelial Nitric Oxide Stimulated by Erythrocyte-Derived ATP Using a Microfluidic Approach. *Anal. Bioanal. Chem.* **2010**, *397*, 3369–3375.
- (45) Smith, K. J.; Lassmann, H. The Role of Nitric Oxide in Multiple Sclerosis. *Neurology* **2002**, *1*, 232–241.
- (46) Kolb, H.; Kolb-Bachofen, V. Nitric Oxide in Autoimmune Disease: Cytotoxic or Regulatory Mediator? *Immunol. Today* **1998**, *19* (12), 556–561.
- (47) Lockwood, S. Y.; Summers, S.; Eggenberger, E.; Spence, D. M. An In Vitro Diagnostic for Multiple Sclerosis Based on C-Peptide Binding to Erythrocytes. *EBioMedicine* **2016**, *11*, 249–252.
- (48) Clontech. *Glycoprotein Enrichment Resin User Manual*; 2009.
- (49) Geiger, M.; Janes, T.; Keshavarz, H.; Summers, S.; Pinger, C.; Fletcher, D.; Zinn, K.; Tennakoon, M.; Karunarathne, A.; Spence, D. A C-Peptide Complex with Albumin and Zn²⁺ Increases Measurable GLUT1 Levels in Membranes of Human Red Blood Cells. *Sci. Rep.* **2020**, *10* (1), 1–9.

Chapter 4- Albumin/C-peptide Receptor Isolation

4.1 Introduction

4.1.1 Receptors

Even though Claude Bernard (1813-1878) didn't use the term "receptor," he initiated the search for how drugs interact with the body.¹ His work encouraged researchers to investigate how drugs work on whole organ systems rather than specific organs.¹ Paul Ehrlich (1854-1915), who was awarded a Nobel Prize in Physiology or Medicine in 1908 for his immunochemistry studies, and John Newport Langley (1852-1925) began using the phrase "receptive substance."^{1,2} By 1926, Alfred Joseph Clark (1885-1941) began studies to obtain a more quantitative description of a receptor through selectivity and saturability.^{1,3} Further attempts to understand receptors and the development of several theories continued for decades beyond this point.

Receptors can exist on the surface of a cell or on intracellular components of the cell.⁴ Receptors contain binding sites that are shaped to recognize the signaling molecule, or ligand, with high specificity.⁵ This specificity verifies that the receptor will only respond to the desired target rather than other molecules.⁵ Cell surface receptors transduce signaling cascades, activate second messenger pathways, regulate ion movement, or bring nutrients into the cell.⁴ The three main classes of cell-surface receptors are ion-channel-coupled receptors, enzyme-coupled receptors, and G-protein-coupled receptors. The latter will be discussed in further detail due to its importance in the history of the C-peptide receptor.⁵ Ion-channel-coupled receptors open or close the ion-channel based on the binding of proteins, which temporarily alters the plasma membrane permeability.⁵

Ligand activation of enzyme-coupled receptors, which have either intrinsic enzymes or direct association with an enzyme, commonly results in receptor dimerization and subsequent activation of the catalytic domain or associated enzyme.⁵ Dimerization refers to the formation of a dimer through the combination of two or more receptor chains.⁵

4.1.1.a G-Protein-Coupled Receptors

G-protein-coupled receptors (GPCRs) are one of the largest groups of related proteins in animals.⁶ There are over 800 GPCR genes in humans.⁶ GPCRs consist of seven transmembrane α -helices, and they transfer ligand signals into cellular responses.⁶ The interaction of the receptor and target molecule is mediated by the trimeric guanosine triphosphate (GTP)-binding protein (G-protein).⁵ In some scenarios, the G-protein interacts with the receptor prior to activation, whereas other times the interaction does not occur until after activation.⁵ There are three protein subunits of G-proteins (α , β , and γ) and four major families (I-IV).⁵ When a GPCR is activated, the $G\alpha$ subunit releases the bound guanosine diphosphate (GDP) and binds GTP instead, which results in a $G\alpha$ subunit conformation change and subsequent release of the $G\alpha$ subunit from the $G\beta\gamma$ subunit as shown in Figure 4.1.⁵ Once the target protein is activated, the plasma membrane ion permeability or the concentrations of the intracellular signaling molecules can be changed.⁵

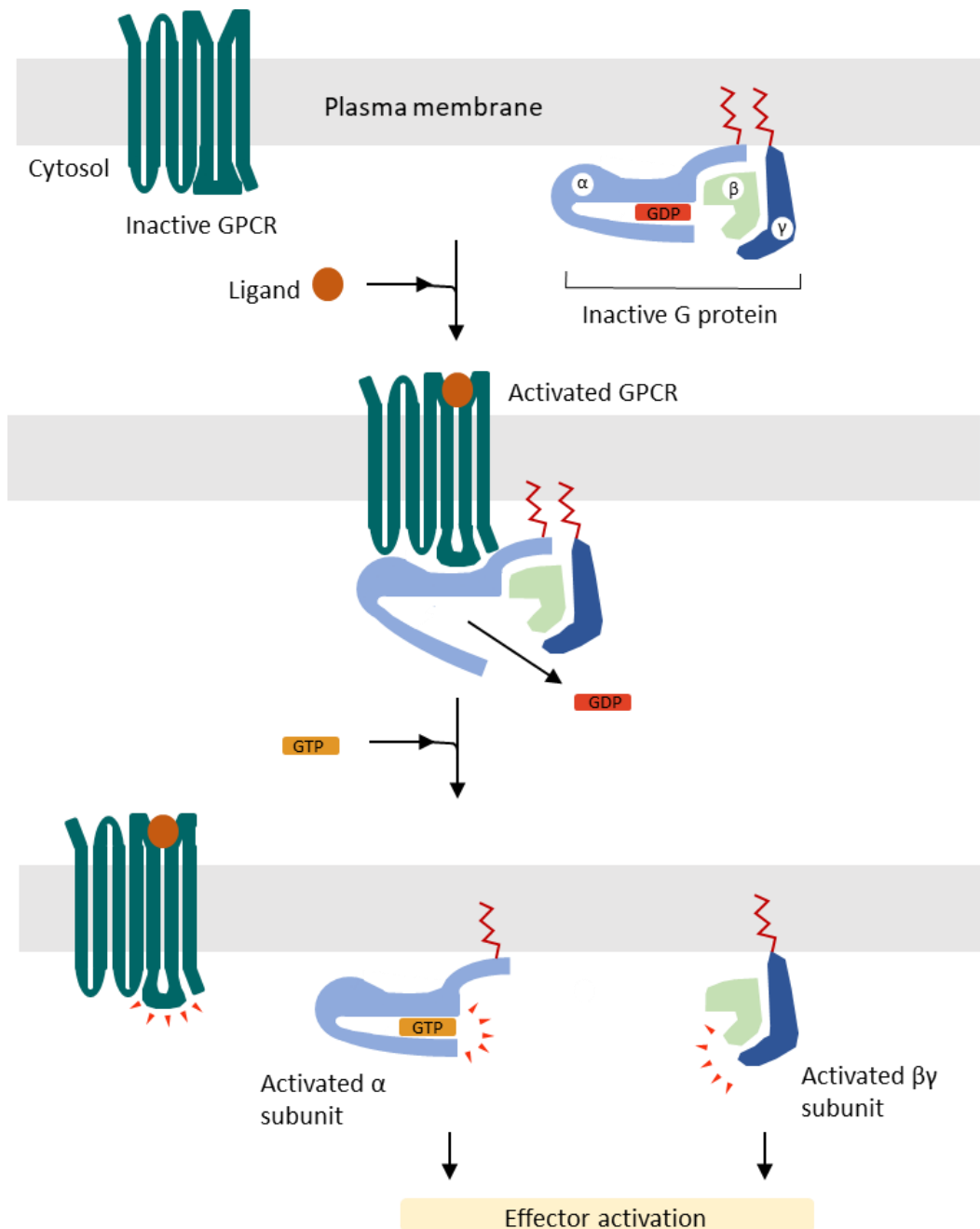


Figure 4.1: G-Protein Activation. Ligand binding to a GPCR results in a conformation change that allows it to bind to the GDP bound $G\alpha$ subunit. The $G\alpha$ subunit releases GDP and binds to GTP, resulting in separate activated $G\alpha$ and $G\beta\gamma$ subunits that cause subsequent signaling mechanisms. (Adapted from Alberts et al.)

GPCRs can activate phosphoinositide-specific phospholipase C (PLC β), that affects the second messengers inositol 1,4,5-triphosphate (IP $_3$) and diacylglycerol, or can activate/inactive adenylyl cyclase to alter intracellular cyclic adenosine monophosphate (cAMP) levels.⁵ There are several G α subunits such as q, s, or i. GPCRs that are coupled to G $_{q\alpha}$ (a stimulatory G α protein of family III) result in the activation of the inositol phospholipid signaling pathway to activate PLC β .⁵ GPCRs that are coupled to a stimulatory G protein (G $_{s\alpha}$ from family I), result in the activated G α subunit stimulating adenylyl cyclase. Whereas GPCRs that are coupled to an inhibitory G protein (G $_{i\alpha}$ from family II), result in the inhibition of adenylyl cyclase. In order to determine if a GPCR is coupled to G $_{s\alpha}$ or G $_{i\alpha}$, experiments are conducted using cholera toxin or pertussis toxin.⁵ Cholera toxin activates the G $_{s\alpha}$ subunit, leaving it to permanently stimulate adenylyl cyclase, whereas pertussis toxin prevents the G $_{i\alpha}$ subunit from releasing GDP, and it remains inactive.⁵

While numerous GPCRs are involved in diseases and therapy targets, approximately 150 of these receptors are orphans, as their physiological function and ligands remain unknown.⁵⁻⁷ GPCR known ligands include fatty acids, steroids, amino acids, peptides, and nucleotides.⁸ It has been difficult to identify many of these GPCRs due to their atypical features and the large variety within the superfamily.⁶ Additionally, GPCRs couple to G α subtypes either promiscuously or selectively making it difficult to classify.⁷

4.1.2 Receptor Identification Methods

There are several available methods for receptor discovery and identification. These include filter-based binding assays, gel chromatography-based methods, and affinity chromatography-based methods.⁹ Gel methods include blue native polyacrylamide gel electrophoresis (BN-PAGE) and free-flow electrophoresis.¹⁰ BN-PAGE is useful for separating intact protein complexes with masses ranging from 10 kDa to 10 MDa.^{10,11} BN-PAGE may be advantageous because a nonionic detergent is only added once, which reduces the risk of denaturation in detergent-sensitive proteins.¹¹ First, the protein complexes move toward the anode at pH 7.5 due to the charge shift caused by the bound Coomassie blue (anionic blue dye), which separates the proteins by size.¹¹ The complexes can undergo a second dimension separation (orthogonal modified BN-PAGE) that dissociates supramolecular assemblies to identify the interacted molecules and stoichiometric ratio.^{10,11} Sodium dodecyl sulfate-PAGE (SDS-PAGE) can be used to identify the denatured proteins in the complex.^{10,11} SDS-PAGE is a proven, reproducible method for a broad range of molecular masses that is commonly used in conjunction with liquid chromatography-mass spectrometry (LC-MS) for identification.¹⁰ After SDS-PAGE separates the proteins, the gel is sliced and digested using trypsin or other enzymes, and the proteins are identified through MS.¹⁰ A colorless native (CN)-PAGE can be used in cases where the Coomassie blue will interfere with measurements. CN-PAGE has a sensitivity that is at least 10-times higher than BN-PAGE, but the lower resolution (smeared protein bands) leads to increased difficulties obtaining molecular masses.^{11,12}

Another receptor isolation possibility is to pre-separate proteins at the peptide level using 2D chromatography; first, through charge and secondly, by hydrophobicity, known as multi-dimensional protein identification technology (MudPIT).^{10,13} MudPIT commonly uses strong cation exchange chromatography for the first dimension and reversed-phase chromatography for the second dimension, which is coupled to electrospray ionization (ESI)-MS.^{10,13}

Transmission electron microscopy (TEM) allows for the visualization of single molecules or complexes.¹⁴ To increase the contrast between receptor and ligand, colloidal gold particles are used as labels for TEM.^{14,15} Streptavidin-conjugated gold particles are commonly used alongside biotin-labeled receptors because of the high affinity of streptavidin for biotin.¹⁴ Gold particles do not result in the loss of enzymatic activity or ligand affinity for the bound protein, thus they are a useful tool for receptor ligand interactions.¹⁵

Another common method for determining binding properties of ligands is surface plasmon resonance (SPR) spectroscopy, which is popular due to its label-free detection and real-time capabilities.¹⁶ SPR is not capable of distinguishing specific and nonspecific binding, thus it is used in combination with surface enhanced Raman scattering (SERS).¹⁶ SPR alone cannot provide the molecule structural information of SERS.¹⁶ The SPR sensorgram and SERS spectrum are collected simultaneously.¹⁶ The Raman signal is enhanced using surface plasmon polaritons, and it provides chemical insight of the binding.¹⁶

Other methods include nuclear magnetic resonance (NMR) that is useful for measuring weak affinity binding, but is not effective for stronger affinities.⁹ Equilibrium dialysis, as discussed in chapter 2, is useful for the determination of binding constants because equilibrium is not affected when samples are removed for analysis.¹ Other common affinity-based methods include epitope-tagged proteins, tandem affinity purification, recombinant protein pull-downs, and co-immunoprecipitation.¹⁰ The latter will be discussed in further detail due to its importance to this project.

4.1.2.a Co-immunoprecipitation

Co-immunoprecipitation can be used to extract target proteins from a mixture due to their affinity to a solid support as shown in Figure 4.2.^{17,18} In this method, antibodies are coupled to a solid support, such as Sepharose or polystyrene, either covalently or noncovalently.¹⁹ Covalently bound antibody beads can be reused, however their activity will decrease over time. The number of re-uses, anywhere from 3 to 100, depends upon the bead and matrix.²⁰⁻²² Crosslinking is a useful tool that covalently binds interacting protein-protein complexes to isolate and characterize.¹⁷ The ends of crosslinking reagents are specific to functional groups on the molecules.¹⁷ Common crosslinkers include n-hydroxysuccinimide (NHS) esters and 1-ethyl-3-(3-dimethylaminopropyl) carbodiimide (EDC). NHS crosslinkers react with primary amines on the molecules, whereas EDC crosslinkers react with carboxylic acid groups.¹⁷ Using crosslinkers is the most straightforward technique if the protein antibodies are available.¹⁹ If antibodies are not available, the interaction can still be analyzed using antibodies specific to the tagged

proteins (possibly FLAG[®] or human influenza hemagglutinin (HA)).^{19,23,24} Isolated complexes are separated by SDS sample buffer and Western blotting.¹⁹

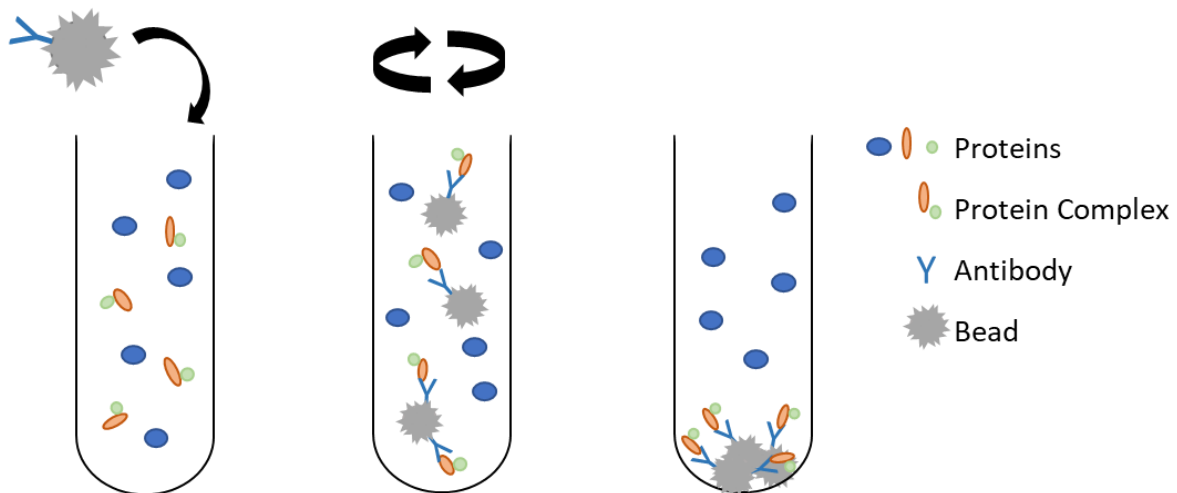


Figure 4.2: Co-immunoprecipitation Procedure. Antibody bound beads are added to a protein solution, and after an incubation period, the beads are pulled down (through centrifugation or magnetic interactions) to remove the proteins that are specific to the antibodies on the beads.

However, if the ligand has a low affinity for the receptor, immune affinity-based methods may fail if the proteins are hydrophobic and have a low abundance.²⁵ Ligand-based receptor capture trifunctional chemoproteomic reagent (LRC-TriCEPs) involves several interactions: NHS ester allows for binding the ligand, a trifluoroacetyl-protected hydrazine captures oxidized glycoprotein receptors, and a biotin group purifies the captured glycopeptides.²⁵ The NHS ester readily reacts with primary amines at pH 7-9 to form stable amide bonds with the ligand.²⁵ However, this method may also fail if several unique glycopeptides match the same protein or if the ligand has affinity for other structures on the cell surface.²⁵ Each LRC-TriCEPs experiment is a 4-day process broken down into ligand coupling/receptor capture, glycopeptide affinity purification, preparation

for mass spectrometry and spectra acquisition, and mass spectrometry data analysis and visualization.²⁵

4.1.3 C-peptide Receptor

C-peptide is capable of acting via specific binding on cellular surfaces and on internal proteins via internalization.²⁶ However, due to the complexity and high abundance of proteins within red blood cells (RBCs), the identification of low abundance proteins by LC-MS/MS, with tryptic digestion, is limited.²⁷ The first evidence that C-peptide may have a specific binding site, found by Flatt et al. in the 1980s, was reported using tumor pancreatic β -cells.²⁸ Since then, C-peptide has been shown to bind to such cell types as skin fibroblasts, renal tubular cells, and endothelial cells.^{29,30} However, research employing human lung fibroblasts, and many other cell types, were unsuccessful in isolating the C-peptide receptor.³¹ It was shown that insulin does not displace C-peptide from binding, suggesting that C-peptide does not interact with the insulin receptor.^{32,33} It was also determined that the C-terminal pentapeptide (EGSLQ) is important for binding since EGSLQ is capable of displacing C-peptide from a cell.²⁹ When the sequence of C-peptide is scrambled, it cannot displace C-peptide from a cell, thus indicating that C-peptide interacts specifically through a membrane-bound receptor, rather than a weaker nonspecific interaction with the cell membrane.^{29,34}

The signaling cascade resulting from C-peptide interaction with cells, discussed in chapter 1, may indicate that C-peptide is interacting with a GPCR on RBCs.³⁵ This is supported by C-peptide being sensitive to pertussis toxin (remembering that pertussis toxin prevents the $G_i\alpha$ subunit from releasing GDP, thus the receptor remains

inactive).^{29,36} Yosten et al. screened 136 orphan GPCRs as possible C-peptide receptors in human gastric tumor KATOIII cells and narrowed the list down to 24 possibilities.³⁷ Given C-peptide's signaling cascade, the list was again narrowed, with GPR160 and GPR146 as the top possibilities.³⁷ By knocking down the receptors individually, it was shown that GPR160 did not block C-peptide expression, whereas GPR146 did.³⁷ However, the Yosten group has yet to show a direct physical interaction between GPR146 and C-peptide.³⁷ Furthermore, there were no follow-up papers from the Yosten group on this subject. In continuance, another research group pointed out that the GPR146 antibody that was used in this research was actually polyclonal, which may result in nonspecific binding of other proteins besides GPR146, thus skewing the data.⁷ Therefore, it is possible that GPR146 is not the C-peptide receptor, but perhaps rather a co-receptor, part of the signaling mechanism, or is promiscuous.³⁷

While researchers at the University of Leicester believe that the C-peptide receptor may be $G_i\alpha$ -linked or even non-GPCR because of the pertussis toxin inhibition, they have provided evidence that it is not GPR146.⁷ The Willars research group indicated that not all receptors that result in $G\beta\gamma$ release are the traditional seven transmembrane receptor.⁷ Natriuretic peptide receptor-C (NPR-C) is one example of a receptor that is sensitive to pertussis toxin and links to $G_i\alpha$, but is not a seven transmembrane GPCR.⁷ If GPR146 was the C-peptide receptor, then GPR146 overexpression would increase C-peptide signalling.⁷ To investigate this theory about C-peptide binding, GPR146 was overexpressed in human embryonic kidney (HEK293) cells, and examined by researchers for alterations in C-peptide phosphorylation effects. These effects were not measured.⁷ Furthermore, internalization and knockdown studies of GPR146 were unsuccessful in

showing a physical interaction with C-peptide in HEK293 cells.⁷ Overall, none of the data that was collected indicated that GPR146 is the C-peptide receptor. Findings from Lindfors et al. also supports that GPR146 is not the receptor for C-peptide as shown through dynamic mass redistribution and arrestin binding assays.³⁸ While research did not show that GPR146 is C-peptide's receptor, GPR146 is still of interest as an orphan receptor due to its possible role as an interferon-stimulated gene and in other areas such as adipose tissues or retinal pigment epithelium.⁷

Previous reports contained data showing that rhodamine-labeled C-peptide is internalized and found within the cytosol and nucleolus of the studied cells (Swiss 3T3 fibroblast and HEK293).^{26,39} C-peptide was also shown inside the nucleus of high-glucose-stimulated mesangial cells and localized with early endosomes in human aortic endothelial cells (HAEC) and umbilical artery smooth muscle cells (UASMC).^{40,41} It was reported that C-peptide also bound to the intracellular protein tyrosine phosphatase 1B.⁴² C-peptide internalization was energy-dependent, due to the decrease in internalization at a lower temperature.^{26,41} It is unlikely that this is a direct translocation, but rather a classic endocytic pathway.^{26,41} These data show that C-peptide is found within the cell.

4.1.4 Insulin Secreting Cells

Working directly with primary β -cells to investigate insulin secretion has been difficult for researchers; the cells do not proliferate easily while in culture, and cadaver organ donors are not readily available.^{43,44} Mice pancreases were considered for replacements because the islets are similar in size to human islets; however, only 200-250 islets can be collected from a mouse pancreas, compared to 250,000-500,000 islets

from a human pancreas.^{44,45} In addition, isolation and purification of islets is time consuming.⁴⁴ A replacement insulin secreting cell line is necessary for conducting studies, and since the 1970s, much effort has been made to find an adequate alternative.^{43,44}

Key features of β -cell replacements include the ability to synthesize insulin and respond to glucose to secrete insulin in response.⁴⁴ Initially, attempts were made to isolate β -cells from human insulinoma, or pancreatic tumors, however, the cells did not release insulin in response to glucose.⁴⁴ This resulted in an effort to isolate rat insulinoma (RIN) cell lines from X-ray induced tumors, however, these cells were also not able to secrete insulin in response to physiologically relevant levels of glucose.⁴⁴ A more successful rat insulinoma cell line is the INS-1 cell line that responds to a range of glucose concentrations.^{43,44,46} While INS-1 cells have a higher insulin content than RIN cells, the insulin content is still only 20% of β -cells.^{43,44} Clones, such as INS-1D, INS-1E, and INS-1 832/13 are commonly used because they have higher insulin content and better glucose response.⁴⁴ One disadvantage of using INS-1 cells is that they require mercaptoethanol in the culture media.⁴³ Mercaptoethanol is toxic and denatures proteins within the media.⁴³ The work in this chapter focuses on developing beads for co-immunoprecipitation isolation of the C-peptide receptor. Anti-C-peptide bead studies focused on binding C-peptide from INS-1 cell secretions with 3D-printed devices, while albumin bead studies focused on developing an albumin bead to bind to C-peptide and the receptor for isolation.

4.2 Methods

4.2.1 C-peptide Bead Preparation

INS-1 cell secretions include C-peptide, therefore, to conduct experiments with and without C-peptide in the presence of INS-1 cell secretions, C-peptide antibody beads were prepared to selectively bind and remove C-peptide from secretions. If successful, these beads could also be useful in binding to and pulling down the elusive C-peptide receptor. The Dynabeads® MyOne™ Carboxylic Acid magnetic beads (Thermo Fisher, Waltham, MA) were rotated (Invitrogen HulaMixer, Carlsbad, CA) to mix for at least 30 minutes prior to transferring 1 mL of beads (10 mg/mL) to a new vial. The vial was placed on a DynaMag™-2 magnet (Thermo Fisher) for 2 minutes and the supernatant was removed. After removing the vial from the magnet, 1 mL of 15 mM 2-(N-morpholino)ethane sulfonic acid (MES; Sigma Aldrich, St. Louis, MO) buffer (0.2928 g MES were dissolved in 100 mL of 18.2 MΩ water at pH 6.0) was added and vortexed for 10 seconds. The vial was placed on the magnet for 2 minutes, and the supernatant was removed. Next, 1 mL of 15 mM MES buffer was again added, the tube was placed on the magnet for 2 minutes, and the supernatant was removed. The beads were resuspended in 100 μL of 15 mM MES buffer and 100 μL of N-ethyl-N'-(3-dimethylaminopropyl) carbodiimide hydrochloride (EDC; Thermo Fisher; 10 mg EDC were dissolved in 1 mL of cold 18.2 MΩ water immediately before use). The bead mixture was rotated for 30 minutes at room temperature, placed on the magnet for 2 minutes, and the supernatant was removed. 400 μg of rat and mouse C-peptide antibody (CC34; Novus, St. Louis, MO) were added to the isolated beads and 300 μL of 15 mM MES buffer was added to give an approximate total volume of 500 μL. The bead mixture was rotated

overnight at room temperature. The following day, the vial was placed on the magnet for 2 minutes, and the supernatant was removed. After removing the tube from the magnet, 1 mL of phosphate buffered saline (PBS) with 0.1% Tween[®]-20 was added to the beads and rotated for 10 minutes. PBS (10.1 mM Na₂HPO₄ (Sigma Aldrich), 2.7 mM KCl (Thermo Fisher), 136.9 mM NaCl (Sigma Aldrich), 1.8 mM KH₂PO₄ (Sigma Aldrich) at pH 7.40) and 0.1% Tween[®]-20 (Sigma Aldrich; diluted 1 mL of Tween[®]-20 to mark with 18.2 MΩ water in a 10 mL volumetric flask to make 10% Tween[®]-20, then added 1 mL of 10% Tween[®]-20 to 100 mL PBS) were previously prepared. After placing the vial on the magnet for 2 minutes and removing the supernatant, this wash step was repeated. The beads were then stored in 500 μL of PBS with 0.1% Tween[®]-20 and 0.1% bovine serum albumin (BSA; Sigma Aldrich; add 0.002 g BSA to 2 mL of PBS/0.1% Tween[®]-20 day of) at 4 °C until needed. This was repeated with 50 μL of 18.2 MΩ water instead of CC34 to prepare control beads.

4.2.2 ELISA on Prepared CC34 Beads

To determine if the CC34 was successfully bound to the Dynabeads[®], samples containing the prepared beads and rat C-peptide were prepared, and the free C-peptide was measured after the magnetic removal of the beads. 50 μL of CC34 beads and 50 μL of 1,600 pM rat C-peptide stock were combined. For a control, 50 μL of PBS/Tween[®]-20 were added to 50 μL of 1,600 pM rat C-peptide stock. The vials were placed on the magnet for 2 minutes, and the supernatant was removed for rat C-peptide enzyme-linked immunosorbent assay (ELISA; EMD Millipore, Burlington, MA) analysis.

4.2.3 Dynamic Cell 3D-Printed Device

A multi-well INS-1 cell flow device, shown in Figure 4.3, was printed on a Stratasys J750 PolyJet printer (Eden Prairie, MN) by customizing the selective cell-to-cell communication flow device.⁴⁷ A print-pause-print method was utilized to allow for the integration of the membrane.⁴⁸ A layer of VeroClear was printed to provide the device with rigidity, followed by a layer of TangoClear to allow for membrane adhesion, and then the printing was paused. The 0.1 μM polycarbonate membrane filter (76 mm; Sterlitech Corporation, Kent, WA) was placed to cover the two wells. After the membrane was added, printing was resumed to add another layer of TangoClear to secure the membrane, and a layer of VeroClear, to complete the device. The support material was carefully removed from the wells with water so that the membranes were not punctured. Grooves were drilled into the device to allow for commercial polyetheretherketone (PEEK) HPLC fittings (Sigma Aldrich) to be twisted into the device for the pump tubing to be connected. The wells were then cleaned thoroughly with water to ensure debris removal prior to the tubing connector insertion.

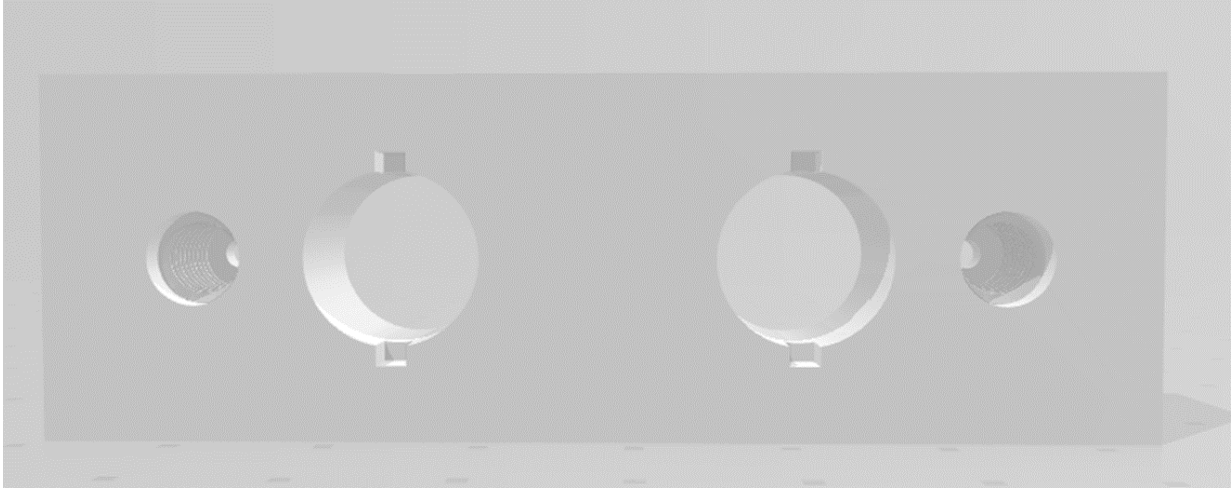


Figure 4.3: 3D-Printed Dynamic Cell Device. An image of the 3D-printed dynamic cell device from the .stl file. Outer circles are for peristaltic pump tubing connection. Inner circles were covered with membranes, and membrane inserts were placed in the wells.

4.2.4 Troubleshooting of Beads on 3D-Printed Device

Two of the 3D-printed devices prepared in section 4.2.3 were connected to a peristaltic pump (IDEX Corporation, Lake Forest, IL) using flared polyvinyl chloride (PVC) tubing (0.89 mm inner diameter; Pulse Instrumentation, Mequon, WI). The device was primed by continuously flowing PBS in a closed system. In device one, 70 μL of the control beads were added to the right well, and a 0.4 μm polyester membrane insert (Corning, Corning, NY) was placed in the well above the beads. The end-goal was to have INS-1 cells growing in the membrane insert, so their secretions (including C-peptide) could subsequently interact with the beads. In development stages, C-peptide stock was placed into the membrane insert. In device two, 70 μL of the CC34 beads were placed in the right well with the membrane insert. 70 μL of PBS were added to the left wells of both devices. This first attempt resulted in several issues with the device. While the first device held the beads, the beads visibly moved down the channel in the second device. Also, the beads moved up the sides of the wells when the membrane insert was placed inside.

Additional devices were attempted, and the same issues persisted. It was determined that the device needed to be reprinted to contain a membrane that covered the entire width of the device rather than only the wells to prevent leakage of the beads.

After reprinting the device, the new device was tested by adding 200 μL of water to each well and starting the flow. However, the water was completely removed from the right well and accumulated in the left well. Flow rates of 180 and 160 $\mu\text{L}/\text{min}$ were tested, but the issue persisted. Upon further investigation, bubbles were found to be moving through the tubing and remaining under the membrane. A clog was found in the tubing, and it was replaced. In addition, two devices were tested with 70 μL of CC34 beads or unlabeled beads in the right well, which were covered with the membrane insert containing 70 μL of 1,600 pM rat C-peptide, and 70 μL of PBS in the left wells. Issues with clogging and well sample volume persisted; therefore, a new set-up design was needed to prevent air from entering the system in the future. The PBS was collected from the device by disconnecting the first tubing and reversing flow into 15 mL tubes, which were stored at $-20\text{ }^{\circ}\text{C}$ until ELISA analysis.

The tubing connector points were removed to help reduce the possibility of air introduction in the system. The device was set up using two pumps for priming as shown in Figure 4.4, rather than one pump. The system began with PBS flowing through the tubing to one pump, which then connected to the device right well. The device left well was connected to a second pump, which then traveled to waste. This system was not continuous, therefore, it allowed for the removal of air bubbles prior to continuous set up on one pump. The devices were set-up on continuous flow, with control and CC34 in separate devices, and allowed to flow after this new priming method. The PBS was

collected from the channels after 2 h by allowing the solution to flow into 15 mL tubes. In addition, the solution from the membrane insert was collected. These were stored at -20 °C until ELISA analysis. However, it was still possible to visualize beads moving up the side of the device well after the membrane insert was placed.

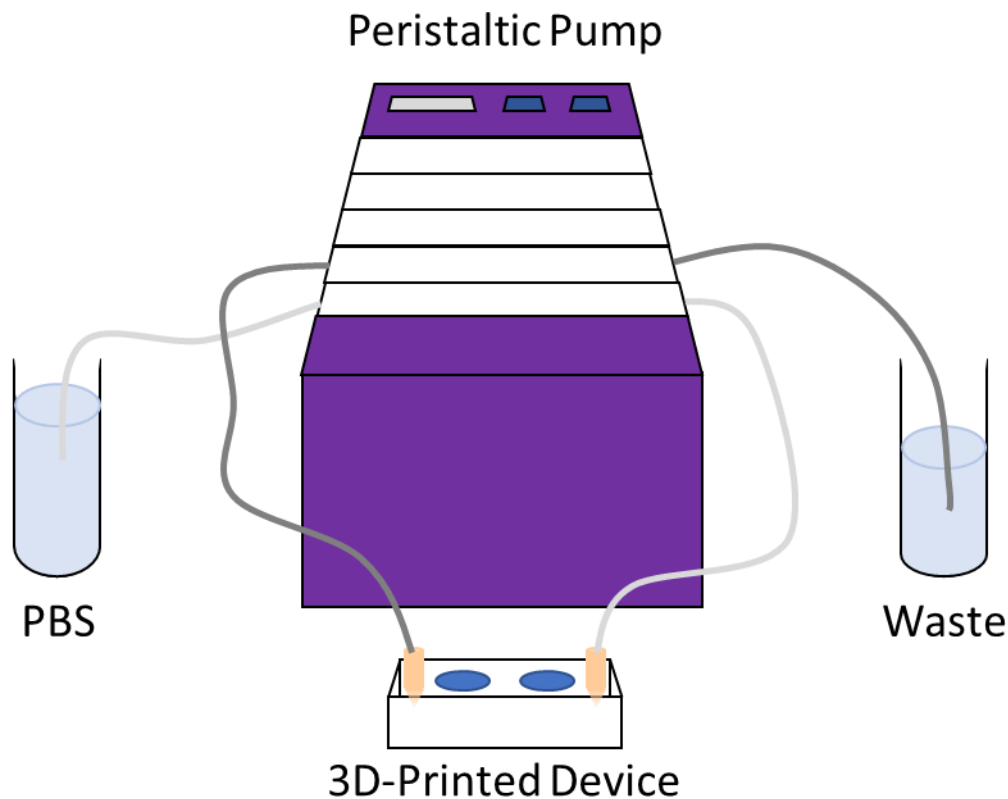


Figure 4.4: Priming Set-Up for the Dynamic Cell 3D-Printed Device. The tubing connected to the first pump (light grey) introduced PBS into the device. The tubing connected to the second pump (dark grey) removed the PBS from the device and out to waste. This set-up was maintained until the system was purged, and the device could be set up in a continuous flow without the PBS or waste tubes.

The device was updated to contain larger wells (from 1.0 cm to 1.2 cm) to prevent the beads from interacting with the sides of the well. Three of these devices were then tested in static conditions. Device one contained 70 μ L of control beads in the right well topped with the membrane insert containing 70 μ L of 1,600 pM rat C-peptide, and the left

well contained 70 μ L of PBS. Device two contained 70 μ L of CC34 beads in the right well topped with the membrane insert containing 70 μ L of 1,600 pM rat C-peptide, and the left well contained 70 μ L of PBS. Device three contained 70 μ L of PBS in both the right and left device wells, and the right well was topped with the membrane insert containing 70 μ L of 1,600 pM rat C-peptide. Each device was covered with a damp Kimwipe (Kimberly-Clark, Irving, TX), to limit device water loss and maintain total volume, and incubated for 2 h at room temperature. Every 20 minutes, the devices were shaken and the Kimwipe was dampened. The Kimwipes were completely replaced after 1 h with a fresh damp Kimwipe. The solutions from the bead well, buffer well, and membrane inserts were removed and pipetted into individual corresponding storage vials. These were stored at -20 $^{\circ}$ C for ELISA analysis. Upon trying to remove 70 μ L of solution, it was evident that the device wells still lost volume even with the Kimwipes in place to prevent evaporative water loss. A potential future experiment is to prime the devices, add the solutions, incubate for 2 h statically, and then dynamically for 2 h prior to removing the solutions from the wells, as well as the channels.

4.2.5 INS-1 Cell Growth

Parental INS-1 cells were obtained from Dr. Karl Olson at Michigan State University. The INS-1 cells were cultured in TPP[®] T-75 flasks (Sigma Aldrich) at 5% CO₂ (to maintain physiological pH with the sodium bicarbonate buffer system) and 37 $^{\circ}$ C in modified RPMI 1640 growth medium (-) glutamine (1 mM sodium pyruvate for mitochondrial fuel, 100 U/mL penicillin and 100 μ g/mL streptomycin to prevent bacterial contamination, 55 μ M β -mercaptoethanol for glutamine stabilization, 10% fetal bovine serum for protein supplementation, 2 mM L-glutamine, and 10 mM HEPES for

supplemental buffering in RPMI 1640).⁴⁹⁻⁵¹ Glutamine is used for many reasons in cell cultures: energy source, nitrogen reservoir for protein and nitrogenous compound synthesis, glutamate precursor for amino acid synthesis, and a growth limiter.⁵² The cells were grown to confluence, usually 10-14 days, while changing the media every 48 h. After confluence was reached, the cells were split for stimulation or for continued growth. A 0.25% trypsin-ethylenediaminetetraacetic acid (EDTA; J.T. Baker, Phillipsburg, NJ) solution was added to the cells and incubated for 5 minutes to remove the cells from the flask bottom. Trypsinization was stopped by adding growth media, and the cells were centrifuged at 1,500 xg for 5 minutes. The supernatant was removed, and the cells were resuspended in fresh growth media and counted by a hemocytometer (Reichert, Buffalo, NY). The cell density was then diluted, as necessary.

4.2.6 INS-1 Cell Secretion Collection

The INS-1 cells were washed three times with 4.0 mM glucose growth media and incubated for approximately 20 h. The growth media was prepared as in section 4.2.5, except for the RPMI1640, which was purchased without glucose or glutamine. The media was made without glucose or BSA, warmed to 37 °C, and then the glucose and BSA were added to the prewarmed solution prior to being dissolved in a CO₂ incubator at 37 °C. The INS-1 cells were then incubated with zero-glucose media for 1 h. This was followed by an incubation with 9 mL high-glucose stimulation buffer for 3 h. The high-glucose stimulation buffer contained 120 mM NaCl (Sigma Aldrich), 2.4 mM KCl (Sigma Aldrich), 1.1 mM MgSO₄ 7H₂O (Fisher Scientific), 1.2 mM KH₂PO₄ (Fisher Scientific), 16.7 mM glucose (Cambridge Isotope Lab, Tewksbury, MA), 10 mM HEPES (Tocris Bioscience, Bristol, UK), 2.5 mM CaCl₂ (Fisher Scientific), 25 mM NaHCO₃ (CCI, Vernon, CA), and

0.1% BSA (Sigma Aldrich) at pH 7.4. The stimulation buffer was removed from the T-75 flask and placed into a 15 mL collection tube. To remove any dislodged cells, the tube was centrifuged at 1,500 xg for 1 minute. The supernatant was aliquoted into 300 μ L fractions and stored at -20 °C.

4.2.7 INS-1 Cell Secretions and CC34 Beads

Increasing volumes of CC34 beads (50, 100, and 200 μ L) and control beads (50 and 200 μ L) were added to 300 μ L of INS-1 cell secretions, and a control was prepared using only cell secretions and no beads. Samples were incubated for 2 h at room temperature and inverted after 1 h. After incubation, the samples were placed onto the magnet for 2 minutes, and the supernatant was removed and collected. The collected supernatant was stored at -20 °C until ELISA analysis. Differences in sample volume were accounted for in the final calculations.

In addition, a sample was made to consist of excess bead volume (140 μ L) to cell secretion volume (100 μ L) to determine if the beads would be useful at larger volumes. A control was prepared with 140 μ L of PBS/Tween[®]-20 and 100 μ L of cell secretions. Rather than only waiting 2 h, these samples were incubated overnight at room temperature to analyze whether more incubation time was required. The samples were placed on the magnet for 2 minutes, and the supernatant was collected and stored at -20 °C until ELISA analysis (1:10 sample dilution in assay buffer).

The bead storage buffer was tested by making identical samples in either storage buffer (PBS/Tween[®]-20/BSA) or PBS. The beads, which remained in the storage buffer, were placed on the magnet for 2 minutes, and the supernatants were removed. For

sample one, 100 μL of storage buffer was added. The beads in sample two were washed three times with PBS by placing them on the magnet for 2 minutes and removing the supernatant. After washing, 100 μL of PBS was added to the second sample beads. 100 μL of cell secretions were added to each bead set, and the samples were incubated for 2 h, with inversion at 1 h, at room temperature. The supernatant was removed after 2 minutes on the magnet and stored at $-20\text{ }^{\circ}\text{C}$ for ELISA analysis (1:10 sample dilution in assay buffer).

One last attempt was made to determine the ability of the prepared CC34 beads to bind C-peptide from the INS-1 cell secretions. The beads were prepared as in section 4.2.1, but rather than being stored in 500 μL of PBS/Tween[®]-20/BSA, only 350 μL was added to increase bead density. Samples were prepared in a similar manner as before, but with a standard addition method in one of the samples to ensure that rat C-peptide was in the sample. Sample one, as shown in Table 4.1, consisted of the CC34 beads (100 μL) and the 1,600 pM C-peptide standard (10 μL plus 90 μL assay buffer). Sample two consisted of the CC34 beads (100 μL) and the cell secretions (100 μL). Sample three consisted of the CC34 beads (100 μL), the 1,600 pM C-peptide standard (10 μL), and cell secretions (100 μL). This sample needed to be volume adjusted in the final calculations to account for the additional 10 μL of total volume. Sample four acted as a control with 100 μL cell secretions and 100 μL PBS/Tween[®]-20/BSA. The samples were incubated for 2 h, inverted at 1 h, at room temperature. After incubation, the samples were placed on the magnet for 2 minutes, and the supernatant was collected to be stored at $-20\text{ }^{\circ}\text{C}$ until ELISA analysis.

Table 4.1: Sample Preparation of CC34 Beads and INS-1 Cell Secretions. The volumes of CC34 beads, 1,600 pM rat C-peptide stock, INS-1 cell secretions, and buffer added for the four samples used in this experiment. *Sample was volume adjusted in final calculation.

Sample	CC34 beads	1,600 pM C-peptide Stock	INS-1 Cell Secretions	PBS/Tween-20®/BSA
1	100 µL	10 µL plus 90 µL assay buffer	X	X
2	100 µL	X	100 µL	X
3*	100 µL	10 µL	100 µL	X
4	X	X	100 µL	100 µL

4.2.8 Preparation of Carboxylic Acid Albumin Dynabeads®

Due to the binding of an albumin/C-peptide complex to the RBC receptor (as discussed in chapter 2), BSA beads were tested as a possible method to pull-down the receptor. Prior to receptor identification, the best coupling method for BSA and magnetic beads had to be determined. Dynabeads® M-270 Carboxylic Acid (Invitrogen) were purchased, and the standard two-step coating procedure without N-hydroxyl succinimide (NHS) ester was utilized.

Overall, the carboxylic acid groups on the Dynabeads® interact with the EDC crosslinker to form an o-acylisourea active ester shown in Figure 4.5.⁵³ The ester then interacts with the primary amine groups on the BSA to form the crosslinked BSA and an isourea by-product.⁵³ BSA and the magnetic beads are bound through an amide bond. Once the BSA is bound to the magnetic bead, its ability to bind C-peptide was tested to determine if this could be used to pull-down the albumin/C-peptide receptor complex.

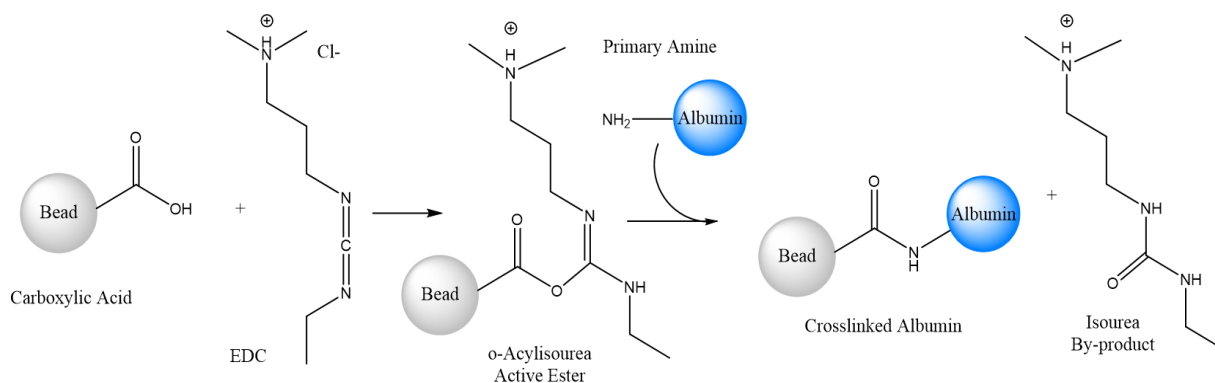


Figure 4.5: Carboxylic Acid Bead Interaction with Albumin. The carboxylic acid bead is linked to the primary amine of albumin (BSA) through an EDC crosslinker.

The Dynabeads[®] (30 mg/mL) were thoroughly inverted by a sample mixer (Invitrogen HulaMixer) for 30 minutes prior to removing 100 μ L and adding to a new vial. The beads were washed in 100 μ L of 0.01 M NaOH (Macron Fine Chemicals; Avantor, Center Valley, PA) to deprotonate the carboxylic acid bead and incubated for 10 minutes, while inverting. The vial was placed in the DynaMag[™]-2 magnet (Thermo Fisher) for 2 minutes, and the supernatant was removed. This wash step was repeated once with 0.01 M NaOH and three times with 18.2 M Ω water. EDC (Thermo Fisher) was prepared by dissolving 0.048 g EDC in 1000 μ L of cold 18.2 M Ω water. 100 μ L of this 250 mM EDC solution were added to the beads and vortexed for 10 seconds. The beads were incubated for 30 minutes at room temperature with rotation. The tube was placed on the magnet for 2 minutes, and the supernatant was removed. The beads were then washed with 100 μ L of cold 18.2 M Ω water once and then again with 100 μ L of 50 mM MES (0.976 g MES in 100 mL of 18.2 M Ω , pH 5.0; Sigma Aldrich) to avoid hydrolysis of the activated carboxylic acid groups.⁵⁴ The beads were now activated, and the process was immediately continued.

After removing the supernatant by magnet, BSA (60 μg of BSA in 60 μL of 50 mM MES buffer, pH 5.0) was added to the activated beads. 40 μL of 50 mM MES buffer (pH 5.0) was added to the beads and vortexed for 10 seconds. The beads were then incubated for 1 h at room temperature while rotating. After incubation, the beads were placed on the magnet for 2 minutes, and the supernatant was removed and stored for bicinchoninic acid (BCA) assay analysis.

The beads were then washed four times with PBS/0.1% Tween-20[®] buffer to prevent nonspecific binding. The beads were incubated for 10 minutes at room temperature while inverting. After incubation, the beads were placed on the magnet for 2 minutes, and the supernatant was removed. The beads were resuspended in 100 μL of PBS and stored at 4 °C for experimentation.

4.2.9 Bicinchoninic Acid Assay: Measuring Albumin Total Concentration

A BCA assay (Thermo Fisher) was utilized to determine the concentration of BSA in the saved supernatant from section 4.2.8 to determine if BSA successfully bound to the beads during preparation. BSA standards (Thermo Fisher; A: 250 $\mu\text{g}/\text{mL}$, B: 125 $\mu\text{g}/\text{mL}$, C: 62.5 $\mu\text{g}/\text{mL}$, D: 31.25 $\mu\text{g}/\text{mL}$) were prepared using serial dilution of 2 mg/mL BSA in 50 mM MES buffer to a total of 800 μL . 25 μL of BSA standards A-D and samples were added to separate wells in a 96-well clear plate. Kit working solution was added to each well, and the plate was incubated at 37 °C for 30 minutes. After the plate was cooled to room temperature, sample absorbance was measured on a FlexStation-3 spectrophotometer (Molecular Devices, San Jose, CA) at 562 nm. The resulting

supernatant BSA concentration was subtracted from the added 931 $\mu\text{g/mL}$ BSA concentration (13.4 μM) to determine the BSA concentration bound to the beads.

4.2.10 BSA Bead Samples

Samples were prepared with the BSA magnetic beads (50 μL) and 15 μM C-peptide stock solution (50 μL). Controls were prepared with 50 μL of PBS and 50 μL of C-peptide stock solution (15 μM). The vials were incubated for 2 h at 37 $^{\circ}\text{C}$ while shaking (Troemner, Thorofare, NJ). After incubation, the vials were placed on the magnet for 2 minutes, and the supernatant was removed and stored at -20 $^{\circ}\text{C}$ for ELISA analysis. The beads were stored at 4 $^{\circ}\text{C}$ in 50 μL of PBS. This experiment was repeated with a 1:10 diluted C-peptide stock solution (in water).

4.2.11 Rat/Mouse C-peptide ELISA

Samples from section 4.2.10 were diluted 1:5 in assay buffer for ELISA analysis. The standard rat/mouse C-peptide 2 ELISA assay procedure was followed.⁵⁵ Horseradish peroxidase (HRP) wash buffer was prepared by diluting the 10X HRP wash buffer 10-fold with 18.2 M Ω water. Well strips were prewashed with wash buffer (300 μL) three times before adding 20 μL of matrix solution to the blank, standards, and kit quality control samples. The blank and sample wells received 30 μL of assay buffer, while only 10 μL of assay buffer was added to the standards and quality control samples. 20 μL of the blank, standards, and samples were added to the appropriate wells before adding 50 μL of antibody solution (1:1 of capture and detection antibodies). The plate was incubated, while sealed, at room temperature for 2 h before washing the wells 3 times with 300 μL of wash buffer. 100 μL of enzyme solution was added to each well prior to a 30-minute

incubation at room temperature while sealed. After decanting the solution, the wells were washed 6 times with 300 μL of wash buffer. 100 μL of substrate solution were added to each well, and the plate was shaken for approximately 20 minutes prior to the addition of 100 μL of stop solution. The absorbances were read on a FlexStation-3 spectrophotometer at 450 nm and 590 nm within 5 minutes of the stop solution addition.

4.3 Results

4.3.1 C-peptide binding to CC34 Beads

When the initial CC34 beads were compared to a bead-less control, there was a decrease in free C-peptide concentration when the beads were present. The supernatant from the CC34 beads was 602 (± 10) pM, whereas the control was 1,352 (± 139) pM; indicating the beads bound approximately 750 pM C-peptide as shown in Figure 4.6. Therefore, the bead preparation method was successful in binding CC34 to the Dynabeads[®]. It is important to note that for the CC34 bead results in this section and sections 4.3.2 and 4.3.3, each experiment was only conducted once, and the statistics are based on duplicates within the ELISA wells (with error represented in standard deviation).

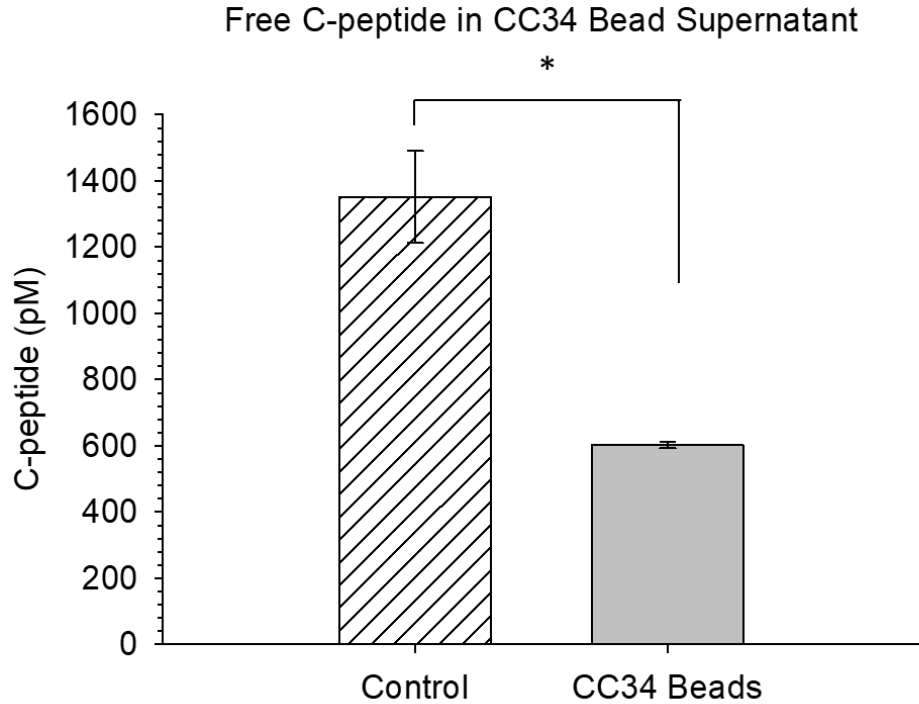


Figure 4.6: Free C-peptide in CC34 Bead Supernatant. The striped bar represents C-peptide stock without beads, while the grey bar represents C-peptide stock with CC34 beads. This indicates that the CC34 beads were successful in binding to the rat C-peptide stock. (n≥2 (ELISA duplicate), error=standard deviation, *p<0.05).

4.3.2 ELISA Analysis of the C-peptide in 3D-Printed Device/Beads

The first set of C-peptide stock and CC34 bead samples (conducted in the same volume) had a free C-peptide concentration of 45.3 (±1.7) pM in the control bead solution, and the CC34 bead solution contained 42.8 (±6.3) pM free C-peptide. Therefore, there was an uptake of approximately 2.5 pM C-peptide by the CC34 beads in comparison to the control beads. However, the second set of samples (from the new priming method) resulted in the control beads containing 71.8 (±6.5) pM C-peptide, while the CC34 bead solution contained 75.3 (±7.3) pM C-peptide. In the second experiment, the control beads bound to approximately 3.6 pM more C-peptide than the CC34 beads. This result could

indicate that the control beads bound more C-peptide than the CC34 beads, however, it is inconclusive since the first experiment demonstrated the opposite results. Further repetition would be necessary to make a final determination on the efficiency of the control beads as a true control.

The data from the static device experiment with damp Kimwipes is shown in Table 4.2. At the experiment conclusion, device one (containing control beads) did not contain volume in the buffer well, therefore, complete analysis was not possible. The membrane insert contained 1,201 (± 5) pM C-peptide, and the control bead solution contained 350 (± 28) pM free C-peptide. This resulted in a total C-peptide concentration between the membrane insert and control bead solution of 1,551 (± 33) pM (not being able to account for the buffer well). The membrane insert in device two (containing CC34 beads) contained 935 (± 92) pM C-peptide, the CC34 bead solution contained 110 (± 2) pM free C-peptide, and the buffer well contained 91.3 (± 0.1) pM C-peptide. The total C-peptide concentration in device two was 1,136 (± 94) pM. Device three (containing no beads) membrane insert contained 1,072 (± 29) pM C-peptide, the right buffer well contained 191 (± 10) pM C-peptide, and the left buffer well contained 92.1 (± 0.6) pM C-peptide. The total C-peptide concentration in device three was 1,355 (± 40) pM. C-peptide was detectable in the device left well, and the device total C-peptide concentrations do not equate to the total C-peptide added (1,600 pM), therefore, the beads are not binding all the C-peptide, and the beads move through the channel. To determine how the beads interacted with

C-peptide, the C-peptide bound to the CC34 beads would need to be analyzed by washing the beads.

Table 4.2: Results for Static 3D-Printed Device Experiment. The concentrations of C-peptide (pM) in each of the three devices used: control beads, CC34 beads, and no beads. The C-peptide concentrations were reported for the membrane insert, the bead solution, and the buffer well. The total C-peptide concentration for the device was then calculated and compared to the added 1,600 pM C-peptide concentration. *The total C-peptide concentration was not able to be comparably calculated for device one since there was not any solution in the buffer well (n=1, error=standard deviation for ELISA well duplicates).

Device	Membrane Insert C-peptide (pM)	Bead Solution free C-peptide (pM)	Buffer Well C-peptide (pM)	Total C-peptide Concentration (pM)
1 (Control Beads)	1,201 (±5)	350 (±28)	X	1,551 (±33)*
2 (CC34 Beads)	935 (±92)	110 (±2)	91.3 (±0.1)	1,136 (±94)
3 (No Beads)	1,072 (±29)	191 (±10)	92.1 (±0.6)	1,355 (±40)

4.3.3 ELISA Analysis of INS-1 Cell Secretions and Beads

Initially, all the CC34 bead sample C-peptide concentrations were higher than the controls, therefore, the accuracy of these data was hindered by being outside of the standard curve. It was necessary to conduct an ELISA on cell secretion dilutions to determine which dilution was required to be within the standard curve. The dilution factor was determined to be around 1:5 (as low as 1:10) in assay buffer from the ELISA kit, since this is how the standards were prepared. When comparing the increasing volumes of CC34 beads to control beads, results indicated that the control beads could bind more C-peptide than the CC34 beads. This indicates that the control bead was still actively binding matrix molecules, therefore, the control beads would need to be bound by an antibody other than CC34, such as IgG, so that it does not bind to C-peptide. At 50 µL

bead volume, the free C-peptide in the CC34 bead sample was 4,636 (± 72) pM, whereas the free C-peptide in the control bead sample was 1,146 (± 44) pM. At 200 μ L bead volume, the free C-peptide in the CC34 bead was 2,843 (± 66) pM compared to the 197 (± 7) pM free C-peptide concentration in the control bead samples. Keeping in mind that the CC34 data falls outside of the calibration curve, CC34 bead samples were prepared again and analyzed.

When analyzing the CC34 beads initially, the results were promising as the free C-peptide concentration decreased with an increase in CC34 bead volume. No (0 μ L) CC34 beads resulted in 3,769 (± 100) pM free C-peptide, 50 μ L CC34 beads resulted in 2,980 (± 98) pM free C-peptide, 100 μ L CC34 beads resulted in 2,734 (± 28) pM free C-peptide, and 200 μ L CC34 beads resulted in 2,074 (± 130) pM free C-peptide. Once the difference in total volume was considered, this trend was no longer evident as shown in Figure 4.7. No (0 μ L) CC34 beads resulted in 3,769 (± 100) pM free C-peptide, 50 μ L CC34 beads resulted in 3,477 (± 114) pM free C-peptide, 100 μ L CC34 beads resulted in 3,645 (± 330) pM free C-peptide, and 200 μ L CC34 beads resulted in 3,456 (± 217) pM free C-peptide. This indicates that the initial trend was not real, but instead was due to the differences in total volume. Even though adding increasing volumes of C-peptide beads did not result in total C-peptide binding for the volumes selected, some binding may have occurred, although not statistically different. When analyzing a surplus volume of beads to cell secretions, there was a further decrease in free C-peptide. The sample without beads resulted in a total C-peptide concentration of 1,760 (± 360) pM, whereas the CC34 bead free C-peptide concentration was 1,378 (± 141) pM. These beads may not be adequate in removing all the C-peptide from larger volumes of cell secretions since a

much larger volume of beads would be required. Due to the cost of the beads and CC34, it would be better to find an alternative route.

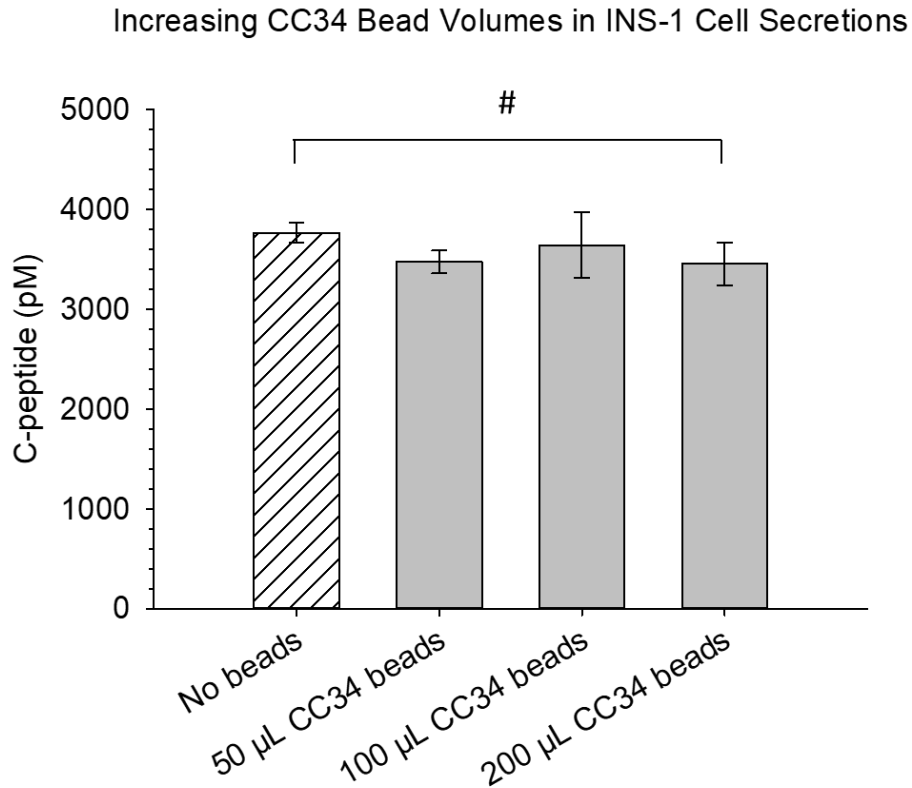


Figure 4.7: Increasing CC34 Bead Volumes in INS-1 Cell Secretions. The striped bar represents the C-peptide concentration in the diluted cell secretions without beads, while the grey bars represent the free C-peptide concentrations from cell secretions with CC34 beads ($n \geq 2$ (ELISA duplicate), error=standard deviation, # $p > 0.05$).

There was not a significant difference ($p=0.29$) between using the storage buffer (sample one) or plain PBS (sample two) in the cell secretion experiments as shown in Figure 4.8. The control, sample one (storage solution), and sample two (PBS) free C-peptide concentrations were 1,264 (± 49) pM, 1,093 (± 11) pM, and 1,065 (± 78) pM, respectively. There was no statistical difference between the free C-peptide

concentrations in varying buffers, thus the original storage buffer was not altered for future experiments.

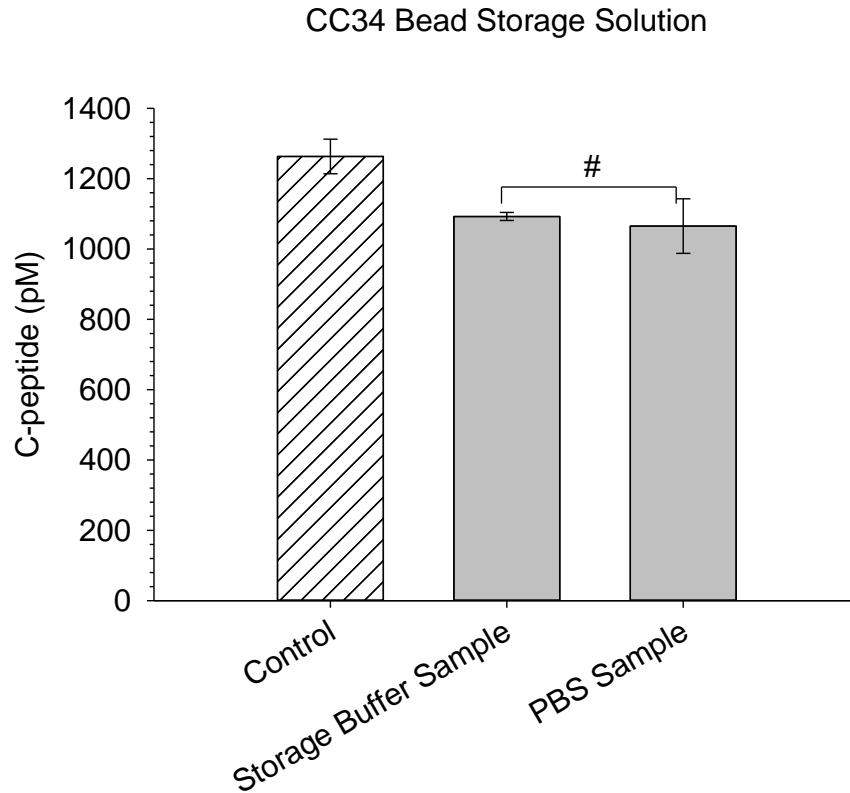


Figure 4.8: The Comparison of CC34 Beads in Storage Buffer or PBS with Cell Secretions. The C-peptide concentration of the control sample (striped), which consisted of INS-1 cell secretions and PBS without beads. The grey bars represent the free C-peptide concentration from the CC34 beads, in either PBS/Tween®-20/PBS or PBS, with INS-1 cell secretions ($n \geq 2$ (ELISA duplicate), error=standard deviation, # $p=0.29$).

Upon completing the standard addition cell secretion/bead experiment, free C-peptide was determined through the C-peptide calibration curve, and sample three (containing the additional standard) was volume corrected through calculation. The bead and C-peptide standard in sample one resulted in a free C-peptide concentration of 93 (± 6) pM. The cell secretion control (sample four) resulted in a C-peptide concentration of 2,968 (± 25) pM. Sample four was cell secretions diluted in half, therefore, the total

C-peptide concentration in the stock was 5,936 (± 50) pM. From these two totals, it was determined that sample two (containing cell secretions and beads) and sample three (containing beads and cell secretions plus standard) should have had C-peptide concentrations of 2,968 (± 50) pM and 2,915 (± 56) pM, respectively. Sample two resulted in a free C-peptide concentration of 2,427 (± 1), therefore, the CC34 beads bound 541 (± 1) pM C-peptide. Sample three resulted in a free C-peptide concentration of 2,361 (± 120) pM, and the CC34 beads bound 581 (± 157) pM. Due to the large error in sample three results, the two samples are not significantly different indicating that the beads did not bind additional C-peptide in the presence of the standard.

It is important to keep in mind that these studies were only completed once to develop a method. While the prepared CC34 beads were successful in binding C-peptide, there was still an excess of C-peptide in the cell secretions. As a result, these beads could not be used to remove the C-peptide from cell secretion experiments to determine the effects of C-peptide-free cell secretions. Due to the lack of successful results, experiments were not repeated for accurate averages and error. Overall, this specific bead may not be a cost-effective method for this purpose, and other beads or coupling methods need to be tested. Even though this bead is not adequate for cell secretion experiments, the fact that it does bind C-peptide makes it a possible candidate to pull-down the C-peptide receptor on RBCs.

4.3.4 Carboxylic Acid Albumin Beads

A BCA assay was utilized to determine the concentration of BSA bound to the activated beads. Figure 4.9 compares the BSA concentration in the stock solution (consisting of BSA and MES Buffer) and the bead supernatant (containing the BSA supernatant) after magnetic bead coupling. BSA concentrations were 13.4 μM in the stock and 2.2 (± 0.1) μM in the supernatant. The difference between the BSA stock and supernatant (11.2 μM) indicates that BSA successfully bound to the magnetic bead.

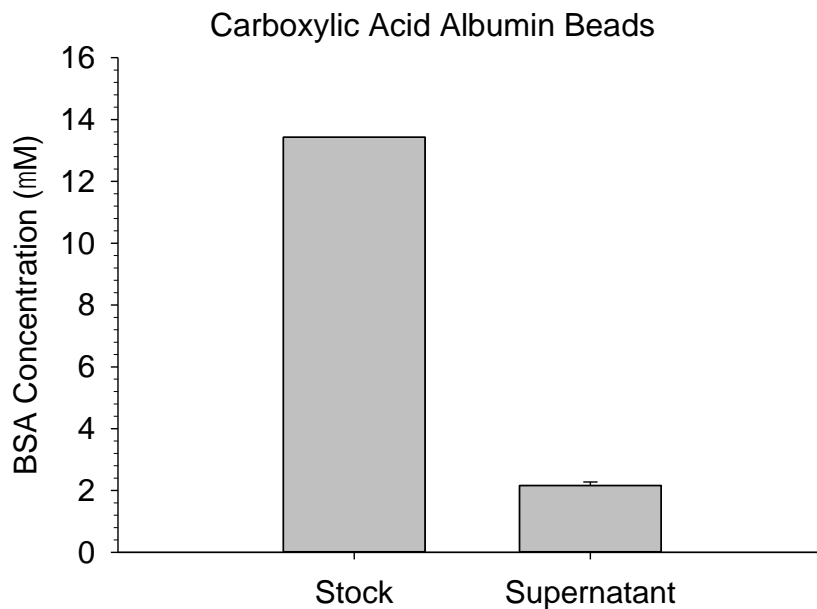


Figure 4.9: BSA Concentration during Bead Preparation. The difference between the concentration of BSA added to the beads and the concentration of BSA found in the supernatant after bead coupling (n=1 stock, n=2 supernatant, error=standard deviation).

The amount of C-peptide that bound to the BSA bound beads was determined by an ELISA of the supernatant C-peptide, which was collected after magnetic separation. The control contained C-peptide and PBS. In Figure 4.10A, the initial concentration of C-peptide control solution was 11.5 (± 3.1) μM , which showed no significant difference in concentration compared to the collected supernatant (11.6 (± 2.0) μM). This would

indicate that C-peptide did not bind to the BSA coated magnetic beads. However, it was considered that there may be a difference, but it was not visible at such a high C-peptide concentration. Therefore, the C-peptide concentration was diluted 1:10 as shown in Figure 4.10B. The results show a slight elevation of 0.1 μM in the C-peptide sample (0.49 μM) compared to the control (0.39 μM), which could be within error if repeated. However, the results indicated that C-peptide did not bind to the BSA magnetic bead.

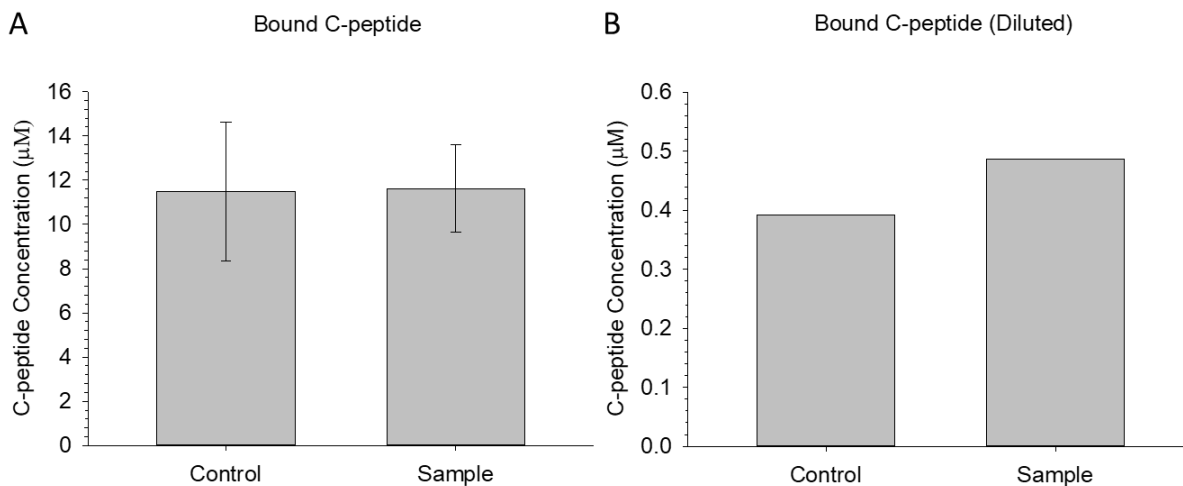


Figure 4.10: C-peptide Concentrations after BSA Bead Interaction. A) The comparison of the control (without BSA beads) and the sample (with BSA beads) at higher C-peptide stock concentrations ($n=2$, error=standard deviation, $p>0.05$). B) The repetition of the experiment in figure A, but with a diluted C-peptide stock ($n=1$).

4.4 Discussion

The dynamic cell 3D-printed device was not successful in maintaining the CC34 beads in the wells to allow for the interaction with integrated INS-1 cell secretions. However, there was some promise in the ability of the CC34 bead to bind to C-peptide in the initial experiment with stock rat C-peptide. Issues occurred when the beads were introduced to the INS-1 cell secretions, and there was not a statistical difference between

the free C-peptide concentration in the control solution compared to the solution from the beads. Further experiments need to be conducted to determine the matrix effects in the INS-1 cell secretions and identify the potential issues that are disrupting C-peptide interaction with the beads. The INS-1 cell secretions are within the high-glucose stimulation buffer, which contains salts, glucose, and BSA. The C-peptide may be binding to BSA and not further interacting with the anti-C-peptide bead. If this were the case, this bead would not be useful as a pull-down method for the albumin/C-peptide complex receptor. One possible issue could be the ratio of anti-C-peptide beads to C-peptide in the INS-1 cell secretions. There may be binding occurring, but the amount of free C-peptide may not be statistically different than the original C-peptide concentration in the INS-1 cell secretions. Even though equal and excess volume ratios of anti-C-peptide beads to INS-1 cell secretions were tested, the beads were suspended in PBS while the INS-1 cell secretions were in stimulation buffer. The INS-1 cell secretion C-peptide concentration was validated through a C-peptide ELISA, whereas the bead density was not confirmed, therefore, this may not be a true equal volume ratio. A higher density of beads would need to be investigated to determine if a higher ratio of anti-C-peptide beads to C-peptide is needed.

Once the beads are optimized, they will be useful for another device that was designed in the Spence lab. A y-shaped microfluidic mixing device (Figure 4.11) was fabricated to measure the adenosine triphosphate (ATP) release (through chemiluminescence at the outlet) resulting from the interactions between human RBCs (introduced in the bottom inlet) and INS-1 cell secretions (introduced in the top inlet).⁵⁶ The novelty of this device is its ability to be printed without the use of a photocurable

support material despite its characteristic complex microfluidic mixing channel. This device has already been used to detect an increase in RBC-derived ATP release when INS-1 cell secretions are present compared to when the secretions are not added (unpublished data).⁵⁶ Once the CC34 beads are optimized, they will be useful when accompanied with the y-shaped device to determine if the RBC-derived ATP release still occurs without the C-peptide secretions from INS-1 cells.

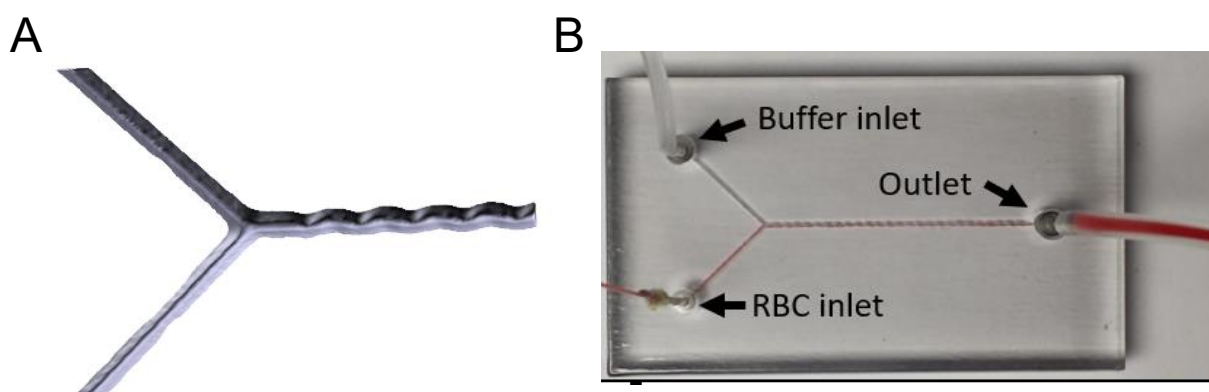


Figure 4.11: 3D-Printed y-shaped Microfluidic Device. A) Micro-CT (X-ray imaging technique) image of the y-shaped device to visualize the device channel (PerkinElmer QuantumGX micro-CT, Waltham, MA). B) An image of the device showing the buffer inlet, RBC inlet that contains a 75 μm inner diameter silica capillary to mimic RBC shear stress in microvascular blood vessels, and the outlet. The flowing of 7% RBC in buffer mixing with a flowing reagent solution (luciferin/luciferase). The luciferin/luciferase reacts with RBC-derived ATP to produce a chemiluminescent signal that is detected through a PMT in a black-box.

The carboxylic acid beads bind to the amine groups on BSA limiting the available amine groups that C-peptide may bind to (noting the importance of C-peptide E27 for BSA binding as discussed in chapter 1). This could explain why there was not a difference in the free C-peptide concentrations after the interaction with the BSA beads, even though it was determined that BSA was successfully bound to the beads. Amine BSA Dynabeads[®] will be tested in the future. The amine groups on the magnetic beads will bind to the carboxylic acid groups of the BSA, leaving the amine groups of BSA available

for C-peptide interaction. If this bead is determined to be successful, then the experiment can proceed to separation of the albumin/C-peptide complex receptor. The BSA magnetic beads and C-peptide would be added to a solution of lysed RBCs. After a 2 h incubation, the beads would be pulled down with a magnet. The goal would be to pull-down the receptor with the magnet, and the proteins could then be separated prior to mass spectrometry analysis. If there are issues with interactions of the lysed RBCs then the complex could be added to whole RBCs with a crosslinker, and the RBCs would be lysed after the interaction.

In conclusion, both the anti-C-peptide and BSA beads demonstrated advantages and disadvantages. The magnetic feature of the beads allows both to be used to pull-down the C-peptide receptor easily. However, both beads demonstrate difficulties in binding to their desired targets. The anti-C-peptide beads successfully bound to a C-peptide standard, but no binding was present in the complex matrix of INS-1 cell secretions. In addition, it may be difficult for this bead to bind to both C-peptide and BSA to separate the albumin/C-peptide complex receptor. The BSA was successfully bound to the carboxylic acid bead, but the BSA was then not able to bind to C-peptide in solution. The amino acid groups on the beads may determine whether the BSA binds C-peptide, therefore, different beads will be tested in the future. If these beads are successful, the larger size of the attached BSA, in comparison to C-peptide, will be better in the analysis of binding to C-peptide and the receptor.

REFERENCES

REFERENCES

- (1) Limbird, L. E. *Cell Surface Receptors: A Short Course on Theory and Methods*, Second.; Kluwer Academic Publishers: Norwell, 1996.
- (2) Maehle, A.-H. "Receptive Substances": John Newport Langley (1852-1925) and His Path to a Receptor Theory of Drug Action. *Med. History* **2004**, 48 (2), 153–174.
- (3) Parascandola, J. A.J. Clark: Quantitative Pharmacology and the Receptor Theory. *Trends Pharmacol. Sci.* **1982**, 3, 421–423.
- (4) Limbird, L. E.; Motulsky, H. Receptor Identification and Characterization. In *Handbook of Physiology- Cellular Endocrinology*; Wiley-Blackwell: Hoboken, 1998; pp 49–67.
- (5) Alberts, B.; Johnson, A.; Lewis, J.; Morgan, D.; Raff, M.; Roberts, K.; Walter, P. Cell Signaling. In *Molecular Biology of the Cell*; Garland Science: New York, 2008; pp 813–887.
- (6) Gloriam, D. E. I.; Schiöth, H. B.; Fredriksson, R. Nine New Human Rhodopsin Family G-Protein Coupled Receptors: Identification, Sequence Characterisation and Evolutionary Relationship. *Biochim. Biophys. Acta* **2005**, 1722 (3), 235–246.
- (7) Janabi, A. M. H. Proinsulin C-Peptide-Mediated Signalling and the Search for Its Receptor, University of Leicester, 2017.
- (8) Kolar, G. R.; Grote, S. M.; Yosten, G. L. C. Targeting Orphan G Protein-Coupled Receptors for the Treatment of Diabetes and Its Complications: C-Peptide and GPR146. *J. Intern. Med.* **2017**, 281 (1), 25–40.
- (9) Sanders, C. R. *Biomolecular Ligand-Receptor Binding Studies: Theory, Practice, and Analysis*; Vanderbilt University: Nashville, 2010.
- (10) Stasyk, T.; Huber, L. A. Zooming in: Fractionation Strategies in Proteomics. *Proteomics* **2004**, 4 (12), 3704–3716.
- (11) Wittig, I.; Braun, H. P.; Schägger, H. Blue Native PAGE. *Nat. Protoc.* **2006**, 1 (1), 418–428.
- (12) Wittig, I.; Schagger, H. Advantages and Limitations of Clear-Native PAGE. *Proteomics* **2005**, 5, 4338–4346.
- (13) De Palma, A.; Roveri, A.; Zaccarin, M.; Benazzi, L.; Daminelli, S.; Pantano, G.; Buttarello, M.; Ursini, F.; Gion, M.; Mauri, P. L. Extraction Methods of Red Blood Cell Membrane Proteins for Multidimensional Protein Identification Technology

- (MudPIT) Analysis. *J. Chromatogr. A* **2010**, 1217 (33), 5328–5336.
- (14) Gestwicki, J. E.; Strong, L. E.; Kiessling, L. L. Visualization of Single Multivalent Receptor-Ligand Complexes by Transmission Electron Microscopy. *Angew. Chemie Int. Ed.* **2000**, 39 (24), 4567–4570.
- (15) Silver, P. N.; Intensifi, G.; Yamamoto, A.; Masaki, R. *High-Resolution Imaging of Cellular Proteins*; Schwartzbach, S. D., Skalli, O., Schikorski, T., Eds.; Human Press: New York, 2016.
- (16) Kim, J. Y.; Zeng, Z. C.; Xiao, L.; Schultz, Z. D. Elucidating Protein/Ligand Recognition with Combined Surface Plasmon Resonance and Surface Enhanced Raman Spectroscopy. *Anal. Chem.* **2017**, 89 (24), 13074–13081.
- (17) ThermoFisher Scientific. Crosslinking Protein Interaction Analysis <https://www.thermofisher.com> (accessed Mar 29, 2018).
- (18) Stewart, A.; Fisher, R. A. Co-Immunoprecipitation: Isolation of Protein Signaling Complexes from Native Tissues. In *Laboratory Methods in Cell Biology: Biochemistry and Cell Culture*; Conn, M. P., Ed.; Elsevier: Boston, 2012; Vol. 112, pp 33–54.
- (19) Lee, C. Coimmunoprecipitation Assay. In *Circadian Rhythms: Methods and Protocols*; Rosato, E., Ed.; Humana Press: New Jersey, 2007; pp 401–406.
- (20) GenScript. AmMag™ Ni magnetic beads.
- (21) ThermoFisher Scientific. Protocols: Immunoprecipitation with Dynabeads Protein G.
- (22) Zhao, L.; Whiteaker, J. R.; Voytovich, U. J.; Ivey, R. G.; Paulovich, A. G. Antibody-Coupled Magnetic Beads Can Be Reused in Immuno-MRM Assays to Reduce Cost and Extend Antibody Supply. *J. Proteome Res.* **2015**, 14 (10), 4425–4431.
- (23) Wang, X.; Goshe, M. B.; Soderblom, E. J.; Phinney, B. S.; Kuchar, J. A.; Li, J.; Clouse, S. D. Identification and Functional Analysis of in Vivo Phosphorylation Sites of the Arabidopsis Receptor Kinase. *Plant Cell* **2005**, 17, 1685–1703.
- (24) Dong, C.; Jang, M.; Malach, A.; Liesch, J.; Groth, G.; Chang, C. Molecular Association of the Arabidopsis ETR1 Ethylene Receptor and a Regulator of Ethylene Signaling. *J. Biol. Chem.* **2010**, 285, 40706–40713.
- (25) Frei, A. P.; Moest, H.; Novy, K.; Wollscheid, B. Ligand-Based Receptor Identification on Living Cells and Tissues Using TRICEPS. *Nat. Protoc.* **2013**, 8 (7), 1321–1336.
- (26) Lindahl, E.; Nyman, U.; Melles, E.; Sigmundsson, K.; Ståhlberg, M.; Wahren, J.;

- Öbrink, B.; Shafqat, J.; Joseph, B.; Jörnvall, H. Cellular Internalization of Proinsulin C-Peptide. *Cell. Mol. Life Sci.* **2007**, *64* (4), 479–486.
- (27) Kakhniashvili, D. G.; Bulla, L. A.; Goodman, S. R. The Human Erythrocyte Proteome. *Mol. Cell. Proteomics* **2004**, *3* (5), 501–509.
- (28) Flatt, P. R.; Swanston-Flatt, S. K.; Hampton, S. M.; Bailey, C. J.; Marks, V. Specific Binding of the C-Peptide of Proinsulin to Cultured B-Cells from a Transplantable Rat Islet Cell Tumor. *Biosci. Rep.* **1986**, *6* (2), 193–199.
- (29) Rigler, R.; Pramanik, A.; Jonasson, P.; Kratz, G.; Jansson, O. T.; Nygren, P.-A.; Stahl, S.; Ekberg, K.; Johansson, B.-L.; Uhlen, S.; et al. Specific Binding of Proinsulin C-Peptide to Human Cell Membranes. *Proc. Natl. Acad. Sci.* **1999**, *96* (23), 13318–13323.
- (30) Henriksson, M.; Pramanik, A.; Shafqat, J.; Zhong, Z.; Tally, M.; Ekberg, K.; Wahren, J.; Rigler, R.; Johansson, J.; Jörnvall, H. Specific Binding of Proinsulin C-Peptide to Intact and to Detergent-Solubilized Human Skin Fibroblasts. *Biochem. Biophys. Res. Commun.* **2001**, *280* (2), 423–427.
- (31) Luzi, L.; Zerbini, G.; Caumo, A. C-Peptide: A Redundant Relative of Insulin? *Diabetologia* **2007**, *50* (3), 500–502.
- (32) Yosten, G. L. C.; Kolar, G. R. The Physiology of Proinsulin C-Peptide: Unanswered Questions and a Proposed Model. *Physiology* **2015**, *30* (4), 327–332.
- (33) Zierath, J.; Handberg, A.; Tally, M.; Wallberg-Henriksson, H. C-Peptide Stimulates Glucose Transport in Isolated Human Skeletal Muscle Independent of Insulin Receptor and Tyrosine Kinase Activation. *Diabetologia* **1996**, *39* (3), 306–313.
- (34) Henriksson, M.; Shafqat, J.; Liepinsh, E.; Tally, M.; Wahren, J.; Jörnvall, H.; Johansson, J. Unordered Structure of Proinsulin C-Peptide in Aqueous Solution and in the Presence of Lipid Vesicles. *Cell. Mol. Life Sci.* **2000**, *57* (2), 337–342.
- (35) Wahren, J.; Kallas, Å.; Sima, A. A. F. The Clinical Potential of C-Peptide Replacement in Type 1 Diabetes. *Diabetes* **2012**, *61* (4), 761–772.
- (36) Walcher, D.; Aleksic, M.; Jerg, V.; Hombach, V.; Zieske, A.; Homma, S.; Strong, J.; Marx, N. C-Peptide Induces Chemotaxis of Human CD4-Positive Cells: Involvement of Pertussis Toxin-Sensitive G-Proteins and Phosphoinositide 3-Kinase. *Diabetes* **2004**, *53* (7), 1664–1670.
- (37) Yosten, G. L. C.; Kolar, G. R.; Redlinger, L. J.; Samson, W. K. Evidence for an Interaction between Proinsulin C-Peptide and GPR146. *J. Endocrinol.* **2013**, *218* (2), B1–B8.
- (38) Lindfors, L.; Sundström, L.; Fröderberg Roth, L.; Mueller, J.; Andersson, S.;

- Kihlberg, J. Is GPR146 Really the Receptor for Proinsulin C-Peptide? *Bioorganic Med. Chem. Lett.* **2020**, *30* (13).
- (39) Lindahl, E.; Nyman, U.; Zaman, F.; Palmberg, C.; Cascante, A.; Shafqat, J.; Takigawa, M.; Sävendahl, L.; Jörnvall, H.; Joseph, B. Proinsulin C-Peptide Regulates Ribosomal RNA Expression. *J. Biol. Chem.* **2010**, *285* (5), 3462–3469.
- (40) Li, Y.; Zhao, M.; Li, B.; Qi, J. Dynamic Localization and Functional Implications of C-Peptide Might for Suppression of INOS in High Glucose-Stimulated Rat Mesangial Cells. *Mol. Cell. Endocrinol.* **2013**, *381* (1–2), 255–260.
- (41) Luppi, P.; Geng, X.; Cifarelli, V.; Drain, P.; Trucco, M. C-Peptide Is Internalised in Human Endothelial and Vascular Smooth Muscle Cells via Early Endosomes. *Diabetologia* **2009**, *52* (10), 2218–2228.
- (42) Jägerbrink, T.; Lindahl, E.; Shafqat, J.; Jörnvall, H. Proinsulin C-Peptide Interaction with Protein Tyrosine Phosphatase 1B Demonstrated with a Labeling Reaction. *Biochem. Biophys. Res. Commun.* **2009**, *387* (1), 31–35.
- (43) Skelin, M.; Rupnik, M.; Cencic, A. Pancreatic Beta Cell Lines and Their Applications in Diabetes Mellitus Research. *ALTEX* **2010**, *27* (2), 105–113.
- (44) Persaud, S. J.; Hauge-Evans, A. C.; Jones, P. M. Insulin-Secreting Cell Lines. Potential for Research and Diabetes Therapy. In *Cellular Endocrinology in Health and Disease*; Ulloa-Aguirre, A., Conn, P. M., Eds.; Elsevier Inc.: Boston, 2014; pp 239–256.
- (45) Dolensek, J.; Rupnik, M. S.; Stozer, A. Structural Similarities and Differences between the Human and the Mouse Pancreas. *Islets* **2015**, *7* (1).
- (46) Millipore. *INS-1 832 / 13 Rat Insulinoma Cell Line*; 2018.
- (47) Castiaux II, A. 3D Printing in the Biosciences: Applications for Diabetic Complications, Michigan State University, 2018.
- (48) Pinger, C. W.; Heller, A. A.; Spence, D. M. A Printed Equilibrium Dialysis Device with Integrated Membranes for Improved Binding Affinity Measurements. *Anal. Chem.* **2017**, *89* (14), 7302–7306.
- (49) ThermoFisher Scientific. RPMI 1640 Medium.
- (50) Rumala, C. Z.; Liu, J.; Locassale, J. W.; Corkey, B. E.; Deeney, J. T.; Rameh, L. E. Exposure of Pancreatic B-Cells to Excess Glucose Results in Bimodal Activation of MTORC1 and MTOR-Dependent Metabolic Acceleration. *iScience* **2020**, *23*.
- (51) ThermoFisher Scientific. HEPES www.thermofisher.com (accessed Feb 9, 2021).

- (52) HiMedia. L-Glutamine [www.](#) (accessed Feb 9, 2021).
- (53) ThermoFisher Scientific. Carbodiimide Crosslinker Chemistry [www.thermofisher.com](#) (accessed Feb 4, 2021).
- (54) Invitrogen Corporation. Dynabeads M-270 Carboxylic Acid [www.thermofisher.com](#) (accessed Feb 9, 2021).
- (55) EMD Millipore. *Rat/Mouse C-Peptide 2 ELISA Kit*, 2013.
- (56) Pinger, C.; Geiger, M.; Bunn, M.; Castiaux, A.; Spence, D. A 3D-Printed Microfluidic Platform for Studying Cell-to-Cell Communication. In *Pittcon*; Philadelphia, PA, 2019.

Chapter 5- Conclusions and Future Directions

5.1 Conclusions

Prior to the discovery of insulin, nearly 100 years ago, the prognosis for patients with type 1 diabetes (T1D) was poor.¹ In some patients with T1D, the expected lifespan past diagnosis was only four years with a low quality of life.² Due to the exogenous administration of insulin, the life expectancy of patients with T1D has increased. In fact, the life expectancy of a person with T1D is now only 12 years less than a person without T1D.³ However, patients with T1D undergoing regular insulin therapy still develop complications such as neuropathy, nephropathy, retinopathy, and cardiovascular disease.⁴ The development of complications suggest that an additional component is required in T1D treatment.

C-peptide, a 31-amino acid pancreatic β -cell secretion, is not present in T1D nor reintroduced with insulin therapy.⁵ While C-peptide was originally believed to be biologically inactive, the peptide has been studied as a possible missing component to T1D treatment.^{5,6} Many C-peptide studies in diabetic animal models and small-scale human studies have described improvements; however, skepticism remains on C-peptide's activity due to the lack of an identified receptor and previous failure in human clinical trials.⁷⁻¹⁶

Previous studies have suggested that a G-protein-coupled receptor on varying cell types bind to C-peptide.^{17,18} However, in our lab, C-peptide binding to red blood cells (RBCs) only occurs in the presence of albumin, a blood carrier protein.¹⁹ Also, prior unpublished data from Ockner et al. has demonstrated that albumin specifically binds to

RBCs.²⁰ The purpose of this dissertation was to examine the possibility that C-peptide binds to RBCs through an albumin/C-peptide complex receptor rather than a receptor solely for C-peptide.

5.1.1 Albumin Binding to RBCs

Experiments in chapter 2 focused on quantitatively determining the binding of albumin to RBCs. Initial flow cytometry studies analyzed the binding of a fluorescently tagged bovine serum albumin (BSA-FITC) to RBCs. However, the fluorescence continued to increase, rather than saturate, as more BSA-FITC was added. Upon comparing the albumin molecules added to RBC ratio for both flow cytometry and gamma counter (BSA-^{99m}Tc) samples, it was determined that the flow cytometry sample albumin concentrations were too high to see a saturation curve (being at the linear part of the total binding curve). However, when lower albumin concentration samples were analyzed on the flow cytometer, the fluorescence values were too low to differentiate from the blank. In addition, it is thought that the MESF (molecules of equivalent soluble fluorochrome) beads used as a standard in the flow cytometry experiments were not a good representation of the sample, whereas the gamma counter experiments were able to use the same albumin for the standards and samples. Therefore, the gamma counter data was used to analyze albumin binding.

Binding data obtained using gamma radiation decay demonstrated that albumin binds to RBCs in a specific and saturable manner, which indicates an albumin receptor on the membrane. A 1983 study at the University of California San Francisco reported a K_d on the order of 10^{-6} M for albumin binding to RBCs, whereas this study was on the

order of 10^{-7} M.²⁰ However, a 1987 study from the same group reported a K_d on the order of 10^{-7} M, which is comparable to the current studies here.²¹ In addition, the number of binding sites per cell were the same order of magnitude (10^4) between the current study and previous studies.^{20,21}

When C-peptide was added to the sample, an increase in albumin binding was present. This indicates the presence of two separate albumin receptors on RBCs: one for albumin and one for albumin/C-peptide (especially when C-peptide binding is absent without albumin). The increase in albumin molecules bound to RBCs in the presence of C-peptide was statistically equal to the C-peptide molecules that bound to the RBC as previously determined by enzyme-linked immunosorbent assay (ELISA).¹⁹ This data indicates that the elusive C-peptide receptor is not solely for C-peptide, but rather a complex that consists of albumin and C-peptide.

5.1.2 Albumin Binding in Diseased States

Experiments in chapter 3 focused on glycated albumin binding to healthy RBCs as well as albumin binding to MS RBCs. Radiolabeled albumin (BSA-^{99m}Tc) was utilized to analyze albumin binding in chapter 3 as well. However, the BSA in chapter 2 was further isolated for use in chapter 3. BSA was separated into normal BSA (nBSA) and glycated BSA (gBSA) prior to mass spectrometry analysis to determine glycation percentages.

First, nBSA and gBSA binding to RBCs were compared in the presence of C-peptide and Zn^{2+} . It was later determined that the glycation percentages were 11% for nBSA and 48% for gBSA. Surprisingly, gBSA binding saturated at $\sim 3,300$ BSA molecules/RBC higher than nBSA. Therefore, gBSA had a higher binding affinity to the

RBC than nBSA. Previous results indicated that gBSA had the same affinity to C-peptide as nBSA, but C-peptide uptake was lower on RBCs when gBSA was present compared to nBSA. The gBSA experiments were repeated without C-peptide or Zn^{2+} when glycation was 45% to compare to gBSA binding to RBCs with C-peptide and Zn^{2+} . In this experiment, more gBSA binding was measured when C-peptide and Zn^{2+} were absent than in their presence. This is the opposite trend as shown in chapter 2 and the opposite trend as what was expected.

To analyze the gBSA binding trend with and without C-peptide or Zn^{2+} , additional percent glycation were prepared (17% and 23%). When gBSA was 23% glycated, the gBSA binding to RBC with C-peptide and Zn^{2+} was statistically equivalent to gBSA binding without C-peptide and Zn^{2+} . As glycation decreased to 17%, results showed more gBSA binding with C-peptide and Zn^{2+} compared to without. The difference in BSA molecules/RBC with or without C-peptide and Zn^{2+} was 2,700 BSA molecules/RBC for 14% glycation (from chapter 2), but only 1,000 BSA molecules/RBC for 17% glycation. C-peptide ELISA studies indicated there was less C-peptide uptake on the RBC when gBSA was the carrier protein compared to nBSA. This suggests that while gBSA may bind more readily to RBC, it is not interacting with cells in a similar manner to nBSA in the presence of C-peptide and Zn^{2+} , which may not effectively deliver C-peptide or Zn^{2+} to the cell. ATP studies at varying albumin glycation would be helpful to solidify this hypothesis.

RBCs from patients with MS have more C-peptide uptake than RBCs from healthy controls, therefore, we hypothesized there would be more albumin binding to MS RBCs (to carry the C-peptide).²² nBSA binding to MS RBCs with C-peptide and Zn^{2+} saturated at 960 BSA molecules/RBC higher than nBSA binding without C-peptide and Zn^{2+} . This

was the same trend we found in healthy RBCs, but with a lower difference (960 vs 2,700) between BSA binding curves with or without C-peptide and Zn^{2+} . However, the MS curve with C-peptide and Zn^{2+} saturated at 2,600 BSA molecules/RBC higher than for healthy RBCs with C-peptide and Zn^{2+} (also at 11% glycated). The binding of albumin/C-peptide/ Zn^{2+} results in an increase of RBC-derived ATP release, and previous data has shown an increase of ATP release from MS RBCs.²³ This albumin binding data provides insight into why patients with MS have more RBC C-peptide uptake as well as higher ATP and NO concentrations.^{24,25}

5.1.3 Receptor Isolation

The 3D-printed cell device was not successful in holding the anti-C-peptide CC34 beads for INS-1 cell secretion interaction, and further device designs would be required to pursue this. Initial data demonstrated that the CC34 beads were able to bind C-peptide from a rat C-peptide stock, however, binding issues occurred when the beads were added to the INS-1 cell secretions. Additional experiments are required to determine any matrix effects interfering with the bead interaction. After troubleshooting the bead design, they could be useful for other 3D-printed devices in our lab, such as the y-shaped microfluidic mixing device, to analyze the ATP release without C-peptide from the cell secretions.

Chapter 4 also analyzed albumin beads as a possible method to pull-down the albumin/C-peptide complex receptor from RBCs. The magnetic nature of the beads would allow for the C-peptide receptor to be readily pulled down by a magnet. The carboxylic acid beads were successful in binding BSA, which was proven through a BCA assay. However, there was not a difference in the C-peptide concentration after the BSA bound

beads were added to the solution. One possibility for this observation could be the limited availability of amine groups on the BSA molecule for C-peptide to bind to since the carboxylic acid group of the beads interact with the amine groups on the albumin. Ideas for future experiments will be discussed in the next section of this chapter.

5.2 Future Studies on Albumin Beads for Receptor Identification

Amine M-270 Dynabeads (ThermoFisher Scientific, Waltham, MA) will be purchased for future experiments. The magnetic bead amine groups will bind to the BSA carboxylic acid groups, which leaves the BSA amine groups available for C-peptide binding. The initial experimental design will follow the amine Dynabeads method “3.B.3 activation with cross-linkers with amine and carboxyl reactivity, for coating with carboxyl-containing ligand”.²⁶ This method utilizes the carboxyl-groups of albumin to bind to the amine groups on the bead surface using an 1-ethyl-3-(3-dimethylaminopropyl)carbodiimide (EDC) crosslinker. Prior to the washing of the coated beads, this method requires the use of hydroxylamine, therefore, extra safety precautions are required. A balance will be moved to the fume hood for use and N100 masks will need to be purchased for additional safety. Hydroxylamine hydrochloride (Sigma Aldrich, St. Louis, MO) is currently being stored in a desiccator within the corrosive cabinet to prevent any dangerous interactions. In addition, disposable polypropylene spatulas (Fisher Scientific) will be purchased to prevent interactions with the currently owned metal spatulas.

After the albumin beads are successful in binding C-peptide, the experiment will proceed with receptor isolation. The albumin magnetic beads would be added to a

solution of C-peptide and lysed RBCs for a 2 h incubation. The beads will then be pulled down with a magnet. Ideally, the beads will pull down the receptor from the RBC membrane. The albumin, C-peptide, and receptor would then be separated from the bead prior to analysis on a mass spectrometer. If the lysed RBCs present binding issues, the complex would be added to whole RBCs with a crosslinker. Then the RBCs would be lysed after the interaction with albumin and C-peptide, prior to separation.

5.3 Future Studies on C-peptide Binding to RBCs

To analyze C-peptide binding to RBCs directly (rather than through the supernatant) labeled C-peptide was either purchased or labeled. A fluorescently tagged C-peptide (C-peptide-FITC) was purchased (Peptide 2.0, Chantilly, VA) for flow cytometry analysis, and C-peptide was radiolabeled in the lab with ^{99m}Tc for gamma counter detection. Preliminary studies and data will be discussed in this section.

5.3.1 Fluorescent Tag

Through Peptide 2.0, I requested a FITC tag to be placed on the N terminus of C-peptide. This was done through an aminohexanoic acid (Ahx) crosslinker, and the resulting theoretical molecular weight was 3,522.88 g/mol. The lyophilized material required dilution in water, and the resulting solution vials were stored at $-20\text{ }^{\circ}\text{C}$ until desired.

C-peptide-FITC RBC samples with or without albumin were prepared and incubated at $37\text{ }^{\circ}\text{C}$ for 2 h. After incubation, the samples were analyzed on the flow cytometer in the same manner as BSA-FITC samples. At 20 nM, the average number of

C-peptide molecules bound per RBC was only 389 (± 38), in comparison to the expected 1,800 C-peptide molecules/RBC.¹⁹ Even after increasing the C-peptide concentration to 40 nM, only 750 C-peptide molecules were detected per RBC. Saturation may have occurred around 20-30 nM, as shown in Figure 5.1, however, additional C-peptide-FITC concentrations between 25-40 nM would be needed. Even if saturation did occur, the values do not match up to previous literature values, as stated previously.

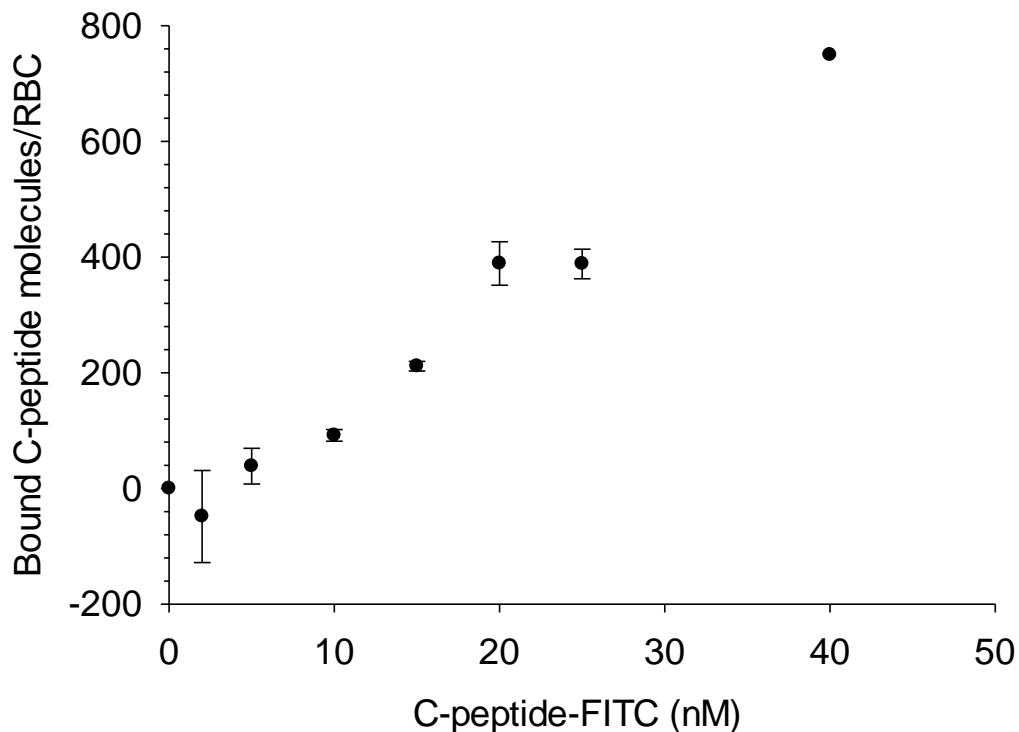


Figure 5.1: Total binding of C-peptide-FITC molecules bound per RBC. C-peptide-FITC was added to albumin containing RBC samples and analyzed using flow cytometry. The number of bound C-peptide molecules/RBC was then calculated.

Due to concerns that the molecule difference may be due to instrumentation (flow cytometer versus spectrophotometer), the supernatant of C-peptide-FITC samples were analyzed on a spectrophotometer. Even with the spectrophotometer, the expected results were not obtained. This could indicate that FITC is altering the biological activity of

C-peptide and a different label should be selected. One possibility would be to use rhodamine-labeled C-peptide as it has been used previously for experiments on other cell types such as endothelial cells, skin fibroblast, and renal tubular cells.^{27,28}

5.3.2 Radiolabeled C-peptide

It was decided to radiolabel C-peptide utilizing the same method as BSA rather than moving forward with another fluorescent label. Normally, the labeled protein concentration is determined through Lowry, however, the Lowry assay does not work for C-peptide since it lacks aromatic amino acids. Additionally, Bradford does not work for C-peptide because it lacks arginine and/or lysine amino acids. Therefore, it was required to run a C-peptide ELISA on the radiolabeled C-peptide. This required additional safety requirements as the whole ELISA would then be considered radioactive. Further ELISAs were conducted to determine that dilutions of the chosen fraction (1:100 and 1:10,000) were required to obtain absorbance values within the standard curve. Through TLC, the labeling efficiency of ^{99m}Tc to C-peptide was determined to be low ranging from 62-94%, whereas BSA is normally greater than 98%. Rerunning fraction 4 back through the column was attempted to remove excess free ^{99m}Tc. (As a reminder from chapter 2, fraction 4 was the first SEC fraction with the highest radioactivity, and it contained the labeled albumin.) Less free ^{99m}Tc was detected in the new fraction 4 as shown in Table 5.1B. However, when analyzed on the dose calorimeter, fraction 4 read as 0 µCi, therefore, the gamma counter would be needed to read the activity of each fraction to determine the desired fraction. There was a vast inconsistency in the amount of free ^{99m}Tc within the fractions between different days, as not every day required a second column. This would

need to be addressed before the labeling method was considered reproducible and used for binding studies.

Table 5.1: Free ^{99m}Tc of SEC C-peptide fractions. A) TLC was used to determine the free ^{99m}Tc for fraction 4 and 5 of C-peptide- ^{99m}Tc separated by SEC. B) Fraction 4 from A) was run back through the column to analyze whether additional free ^{99m}Tc could be removed. Fractions 4-6 from the second column were analyzed using TLC. All fractions were selected based on their activities determined by the dose calorimeter or gamma counter.

A	Fraction (of first column)	% Free ^{99m}Tc	B	Fraction (of second column-Fraction 4)	% Free ^{99m}Tc
	Fraction 4	37.99		Fraction 4	18.97
	Fraction 5	60.58		Fraction 5	71.05
				Fraction 6	95.66

HPLC was also used to separate free ^{99m}Tc from labeled C-peptide- ^{99m}Tc . The HPLC was successful in separating out the two fractions, however, the C-peptide- ^{99m}Tc was then diluted in the HPLC solutions. Evaporating off the excess solution (acetonitrile and trifluoroacetic acid) was a safety concern due to the radioactivity. Upon comparing the fractions from SEC and HPLC, the free ^{99m}Tc was approximately 15% and 17%, respectively, as shown in Table 5.2. Therefore, it was determined that the extra time and effort required for HPLC was not worthwhile for this experiment.

Table 5.2: Free ^{99m}Tc of SEC C-peptide fractions and HPLC collection. TLC was used to determine the free ^{99m}Tc for fractions 4-6 of C-peptide- ^{99m}Tc separated by SEC, as well as the collection from HPLC.

Fraction/Method	% Free ^{99m}Tc
Fraction 4	14.97
Fraction 5	68.31
Fraction 6	91.45
HPLC	17.36

If additional troubleshooting methods are unsuccessful in labeling C-peptide with ^{99m}Tc , then C-peptide- ^{125}I could be purchased (due to its use in prior studies).^{29,30} The binding of C-peptide to RBCs could be directly analyzed with or without albumin present. Since ^{125}I produces a structural substitution, the structure and biological activity of C-peptide could be affected.³¹ Prior to conducting RBC binding studies, the biological activity of C-peptide would need to be analyzed through developed methods such as C-peptide ELISA or ATP release. Another experimental difference would be the cold ligand, which is normally excess BSA. In experiments without albumin, the use of BSA as a cold ligand would skew data results. Therefore, excess C-peptide would need to be added to allow for nonspecific binding analysis.

5.4 GLUT1 Aggregation Studies

In collaboration with Dr. Ajith Karunaratne's group at the University of Toledo, the aggregation of GLUT1 was studied. Chinese hamster ovary (CHO) cells were grown and labeled by Mithila Tennakoon, a student in Dr. Karunaratne's group. The GLUT1

proteins of the CHO cells were fluorescently labeled with green fluorescent protein (eGFP), while the GLUT4 proteins were labeled with mCherry. Each cell contained both mCherry and eGFP labeled GLUT proteins. The cells were imaged in confocal mode with a Nikon Ti-R/B-inverted microscope (Melville, NY) equipped with Yokogawa CSU-X1 spinning disk unit (5000 rpm; Sugar Land, TX) and an iXon ULTRA 897BV back-illuminated deep-cooled EMCCD (electron multiplying charge-coupled device) camera (Cambridge Scientific, Watertown, MA) as shown in Figure 5.2.³²

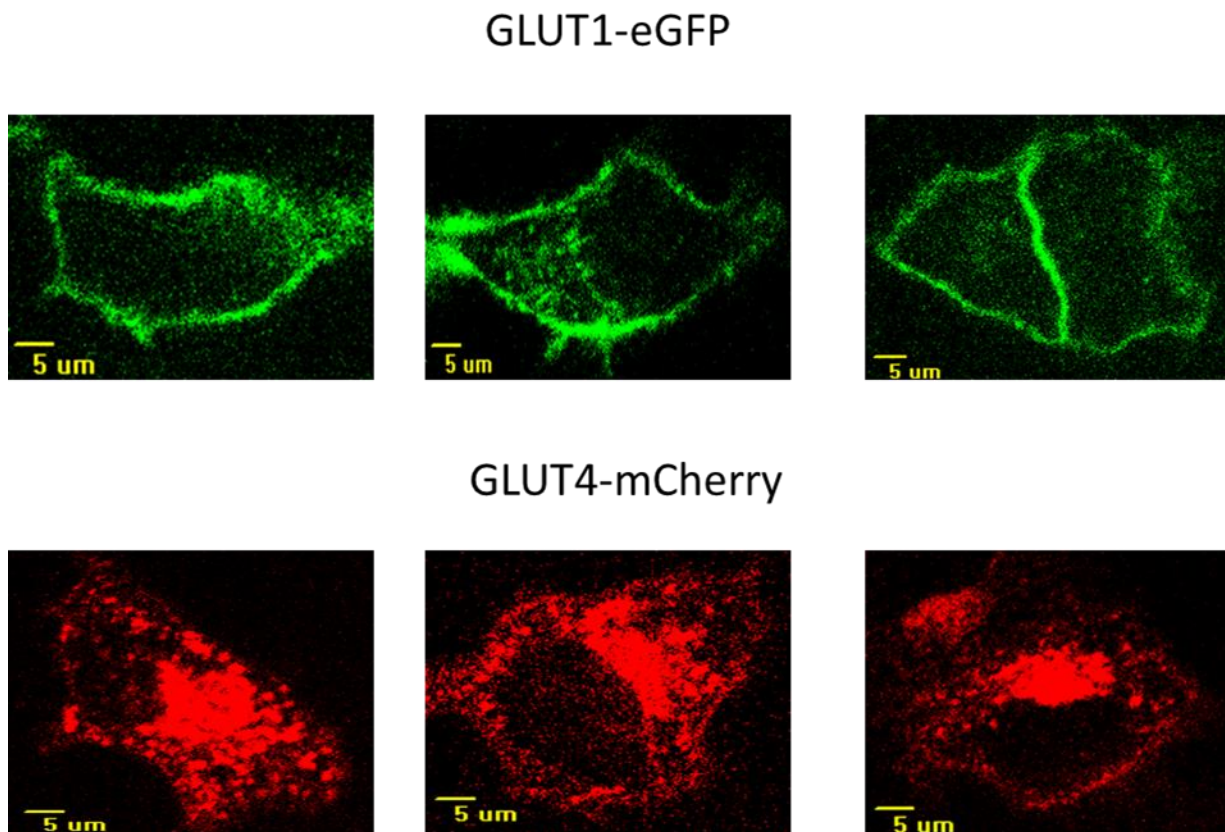


Figure 5.2: GLUT Imaging on CHO Cells. The clustering of GLUT1 (labeled with eGFP) and GLUT4 (labeled with mCherry) on CHO cells prior to the addition of albumin, C-peptide, and Zn^{2+} . Picture from Geiger et al.

The next step in this collaboration would be to incubate the cells in varying conditions at 0.5 mL for 2 h at 37 °C before looking at total fluorescence. The CHO cell

conditions include albumin, albumin and Zn^{2+} , albumin and C-peptide, plus a combination trio of albumin, C-peptide, and Zn^{2+} . In addition, some cells would remain untouched to act as a control.

5.5 Future Albumin Binding Studies

The experiments discussed in Chapter 2 can be furthered with several other experiments. To effectively compare the effect of glycation percentage on albumin binding, the 11% nBSA saturation experiments should be repeated without C-peptide or Zn^{2+} . Once this is completed, the albumin binding to RBCs with and without C-peptide and Zn^{2+} can be analyzed at 11%, 14% (from chapter 2), 17%, 23%, and 45-48% glycation. It would also be helpful to analyze RBC C-peptide uptake in the presence of varying albumin glycation percentages. Studies here analyzed C-peptide uptake in 12% and 46% glycated albumin, while additional studies at 17% and 23% would be helpful. Also, after the 11% nBSA without C-peptide or Zn^{2+} data is collected, the MS data without C-peptide or Zn^{2+} would have a control to compare to. A future experiment comparing MS RBCs and control RBCs on the same day with C-peptide and Zn^{2+} would give a faster approach to analyze more samples (meaning a potential diagnostic).

It would also be interesting to conduct Zn^{65+} binding studies to RBCs with gBSA and C-peptide present because data indicates that Zn^{2+} has a lower affinity to gBSA than nBSA.³³ Studies here analyzed albumin binding and C-peptide uptake with gBSA but did not directly analyze the Zn^{2+} binding. In these experiments 20 nM radioactive Zn^{65+} would be placed in samples containing 20 nM C-peptide, 7% RBCs, and PSS. The PSS would contain varying albumin glycation percentages (11-48%). From this data, it could be

determined if the binding of Zn^{65+} to RBCs is statistically different when in the presence of nBSA or gBSA.

To emphasize the importance of healthy albumin for T1D therapies involving C-peptide and Zn^{2+} , a competitive radiolabeled experiment could be conducted. RBCs previously incubated with varying percentages of gBSA (11-48%) would be exposed to our proposed complex (nBSA, C-peptide, and Zn^{2+}) to determine if the nBSA will kick-off the gBSA from the RBC. The nBSA would be labeled with a ^{99m}Tc tag to analyze through the gamma counter. If the nBSA removes the gBSA and effectively causes downstream effects (analyze ATP to determine), this would be a huge step in understanding T1D complications and provide the concept for a new therapeutic.

REFERENCES

REFERENCES

- (1) Rosenfeld, L. Insulin: Discovery and Controversy. *Clin. Chem.* **2002**, *48* (12), 2270–2288.
- (2) Brostoff, J. M.; Keen, H.; Brostoff, J. A Diabetic Life before and after the Insulin Era. *Diabetologia* **2007**, *50* (6), 1351–1353.
- (3) Huo, L.; Harding, J. L.; Peeters, A.; Shaw, J. E.; Magliano, D. J. Life Expectancy of Type 1 Diabetic Patients during 1997–2010: A National Australian Registry-Based Cohort Study. *Diabetologia* **2016**, *59* (6), 1177–1185.
- (4) Forbes, J. M.; Cooper, M. E. Mechanisms of Diabetic Complications. *Physiol. Rev.* **2013**, *93* (1), 137–188.
- (5) Steiner, D. F. The Proinsulin C-Peptide - a Multirole Model. *Exp. Diabetes Res.* **2004**, *5* (1), 7–14.
- (6) Wahren, J.; Foyt, H.; Daniels, M.; Arezzo, J. C. Long-Acting C-Peptide and Neuropathy in Type 1 Diabetes: A 12-Month Clinical Trial. *Diabetes Care* **2016**, *39* (4), 596–602.
- (7) Sjöberg, S.; Gjötterberg, M.; Berglund, L.; Möller, E.; Östman, J. Residual C-Peptide Excretion Is Associated with a Better Long-Term Glycemic Control and Slower Progress of Retinopathy in Type I (Insulin-Dependent) Diabetes Mellitus. *J. Diabet. Complications* **1991**, *5*, 18–22.
- (8) Johansson, B. L.; Borg, K.; Fernqvist-Forbes, E.; Kernell, A.; Odergren, T.; Wahren, J. Beneficial Effects of C-Peptide on Incipient Nephropathy and Neuropathy in Patients with Type 1 Diabetes Mellitus. *Diabet. Med.* **2000**, *17*, 181–189.
- (9) Sjoquist, M.; Huang, W.; Johansson, B. L. Effects of C-Peptide on Renal Function at the Early Stage of Experimental Diabetes. *Kidney Int.* **1998**, *54* (3), 758–764.
- (10) Samnegård, B.; Jacobson, S. H.; Jaremko, G.; Johansson, B. L.; Ekberg, K.; Isaksson, B.; Eriksson, L.; Wahren, J.; Sjöquist, M. C-Peptide Prevents Glomerular Hypertrophy and Mesangial Matrix Expansion in Diabetic Rats. *Nephrol. Dial. Transplant.* **2005**, *20* (3), 532–538.
- (11) Pierson, C. R.; Zhang, W.; Sima, A. A. F. Proinsulin C-Peptide Replacement in Type 1 Diabetic BB/Wor-Rats Prevents Deficits in Nerve Fiber Regeneration. *J. Neuropathol. Exp. Neurol.* **2003**, *62* (7), 765–779.
- (12) Sima, A. A. F.; Zhang, W.; Sugimoto, K.; Henry, D.; Li, Z.; Wahren, J.; Grunberger, G. C-Peptide Prevents and Improves Chronic Type I Diabetic Polyneuropathy in the BB/Wor Rat. *Diabetologia* **2001**, *44* (7), 889–897.

- (13) Samnegaård, B.; Jacobson, S. H.; Jaremko, G.; Johansson, B. L.; Sjöquist, M. Effects of C-Peptide on Glomerular and Renal Size and Renal Function in Diabetic Rats. *Kidney Int.* **2001**, *60* (4), 1258–1265.
- (14) Sjöberg, S.; Gunnarsson, R.; Gjøtterberg, M.; Lefvert, A. K.; Persson, A.; Ostman, J. Residual Insulin Production, Glycaemic Control and Prevalence of Microvascular Lesions and Polyneuropathy in Long-Term Type 1 (Insulin-Dependent) Diabetes Mellitus. *Diabetologia* **1987**, *30*, 208–213.
- (15) Zerbini, G.; Mangili, R.; Luzi, L. Higher Post-Absorptive C-Peptide Levels in Type 1 Diabetic Patients without Renal Complications. *Diabet. Med.* **1999**, *16*, 1048–1049.
- (16) Johansson, B. L.; Sjöberg, S.; Wahren, J. The Influence of Human C-Peptide on Renal Function and Glucose Utilization in Type 1 (Insulin-Dependent) Diabetic Patients. *Diabetologia* **1992**, *35*, 121–128.
- (17) Yosten, G. L. C.; Kolar, G. R.; Redlinger, L. J.; Samson, W. K. Evidence for an Interaction between Proinsulin C-Peptide and GPR146. *J. Endocrinol.* **2013**, *218* (2), B1–B8.
- (18) Kolar, G. R.; Grote, S. M.; Yosten, G. L. C. Targeting Orphan G Protein-Coupled Receptors for the Treatment of Diabetes and Its Complications: C-Peptide and GPR146. *J. Intern. Med.* **2017**, *281* (1), 25–40.
- (19) Liu, Y.; Chen, C.; Summers, S.; Medawala, W.; Spence, D. M. C-Peptide and Zinc Delivery to Erythrocytes Requires the Presence of Albumin: Implications in Diabetes Explored with a 3D-Printed Fluidic Device. *Integr. Biol.* **2015**, *7*, 534–543.
- (20) Ockner, R. K.; Weisiger, R. a; Gollan, J. L. Hepatic Uptake of Albumin-Bound Substances: Albumin Receptor Concept. *Am. J. Physiol.* **1983**, *245* (1), G13–G18.
- (21) Wright, T. L.; Lysenko, N.; Ockner, R. K.; Weisiger, R. A. Interaction of Natural and Synthetic Albumin Polymers with Hepatocytes. *Hepatology* **1987**, *7* (2), 294–301.
- (22) Lockwood, S. Y.; Summers, S.; Eggenberger, E.; Spence, D. M. An In Vitro Diagnostic for Multiple Sclerosis Based on C-Peptide Binding to Erythrocytes. *EBioMedicine* **2016**, *11*, 249–252.
- (23) Letourneau, S.; Hernandez, L.; Faris, A. N.; Spence, D. M. Evaluating the Effects of Estradiol on Endothelial Nitric Oxide Stimulated by Erythrocyte-Derived ATP Using a Microfluidic Approach. *Anal. Bioanal. Chem.* **2010**, *397*, 3369–3375.
- (24) Minagar, A.; Alexander, J. S. Blood-Brain Barrier Disruption in Multiple Sclerosis. **2003**, *9*, 540–549.
- (25) Smith, K. J.; Lassmann, H. The Role of Nitric Oxide in Multiple Sclerosis. *Neurology* **2002**, *1*, 232–241.

- (26) ThermoFisher Scientific. M-270 Amine Protocols www.thermofisher.com (accessed Sep 24, 2020).
- (27) Wahren, J.; Kallas, Å.; Sima, A. A. F. The Clinical Potential of C-Peptide Replacement in Type 1 Diabetes. *Diabetes* **2012**, *61* (4), 761–772.
- (28) Luensmann, D.; Jones, L. Impact of Fluorescent Probes on Albumin Sorption Profiles to Ophthalmic Biomaterials. *J. Biomed. Mater. Res. - Part B Appl. Biomater.* **2010**, *94* (2), 327–336.
- (29) Verchere, C. B.; Paoletta, M.; Neerman-Arbez, M.; Rose, K.; Irminger, J.-C.; Gingerich, R. L.; Kahn, S. E.; Halban, P. A. A Novel Secretory Product of the Rat Pancreatic Beta Cell Produced by the Truncation of Proinsulin Connecting Peptide in Secretory Granules. *J. Biol. Chem.* **1996**, *271* (44), 27475–27481.
- (30) Gruppuso, P. A.; Susa, J. B.; Sehgal, P.; Frank, B.; Schwartz, R. Metabolism and Placental Transfer of 125I-Proinsulin and 125I-Tyrosylated C-Peptide in the Pregnant Rhesus Monkey. *J. Clin. Invest.* **1987**, *80* (4), 1132–1137.
- (31) Limbird, L. E.; Motulsky, H. Receptor Identification and Characterization. In *Handbook of Physiology- Cellular Endocrinology*; Wiley-Blackwell: Hoboken, 1998; pp 49–67.
- (32) Geiger, M.; Janes, T.; Keshavarz, H.; Summers, S.; Pinger, C.; Fletcher, D.; Zinn, K.; Tennakoon, M.; Karunaratne, A.; Spence, D. A C-Peptide Complex with Albumin and Zn²⁺ Increases Measurable GLUT1 Levels in Membranes of Human Red Blood Cells. *Sci. Rep.* **2020**, *10* (1), 1–9.
- (33) Jacobs, M. J.; Pinger, C. W.; Castiaux, A. D.; Maloney, K. J.; Spence, D. M. A Novel 3D-Printed Centrifugal Ultrafiltration Method Reveals in Vivo Glycation of Human Serum Albumin Decreases Its Binding Affinity for Zinc. *Metallomics* **2020**, No. 12, 1036–1043.